Master thesis : Voltage conditioner: possibilities and limitations

Auteur : Dumont, Antoine

Promoteur(s) : Van Cutsem, Thierry

Faculté : Faculté des Sciences appliquées

Diplôme : Master : ingénieur civil électricien, à finalité spécialisée en "electric power and energy systems"

Année académique : 2018-2019

URI/URL : http://hdl.handle.net/2268.2/6763

University of Liege
Faculty of Applied Sciences

Mitigation of voltage sags by a voltage conditioner

Master Thesis

Master thesis advisors : Pr. Thierry Van Cutsem - Dr. Patrick Scarpa

DUMONT Antoine [s142239]

Graduation studies conducted for obtaining the Master Degree in electrical engineering

Academic year 2018-2019

Abstract

These days, the interest in Power Quality problems increases due to the higher sensitivity of electronic and electrical devices. Among these, voltage dips, also called voltage sags, are one of the most critical problem. They can occur for several reasons, e.g. a fault far in the network causes a voltage dip at a distant load terminal. Even if this fault occurs very far from the observation terminal, a voltage dip would be observed. Then, these occurs very often in power system. They can affect factories, data centres and sensitive loads. It can disturb the process or sometimes, yield to the complete shutdown of the system. This causes huge financial losses to the company.

In order to protect the sensitive equipment, several solutions of various types have been developed. Euro-Diesel has been implemented for several decades a solution called *No-Break KS*®. This one is composed of a synchronous machine, an accumulator, a diesel engine and a decoupling self (called *choke*). At steady-state, only the synchronous machine is used and the accumulator stores energy. The grid is present and provides active power while the synchronous machine produces or absorbs reactive power (power factor compensation). When a perturbation occurs, the accumulator releases its energy in order to feed continuously the critical loads. The load voltage is also maintained in a given interval. If the perturbation is too severe, the diesel engine starts and provides mechanical power to the machine.

The main drawback of this method is that it is expensive and space consuming. The goal of this thesis is to analyse the behaviour of the equipment if the diesel engine and the accumulator are removed. Only the synchronous machine and the self are present.

This work can be divided in several parts. The first one is constituted of the bibliographic part. It explains the basic properties of a voltage dip, the state of the art concerning the load sensitivity and the existing mitigation techniques.
Afterwards, the model of the studied equipment is derived and explained. This one is implemented in the software *ERACS* from RINA company. It allows to model electrical power systems and to perform load-flow, transient, fault,... studies. The equivalent schematic comprises the choke model, the synchronous machine, the utility side and the loads. Concerning these, it has been chosen to model a data centre. This one is a typical example faced by Euro-Diesel every day. Then, 20% are asynchronous machines and 80% are constant power loads. These model respectively the cool down system and all the power electronics. The Automatic Voltage Regulator of the synchronous machine is also derived based on the one used by Euro-Diesel.

In a third part, the simulations are performed. Several dips of different characteristics are simulated in order to obtain the limit cases, i.e. cases where the device can not deal with the dip. These are plotted on curves called "Power Acceptability Curves". These are standard curves that represent the maximal dip duration sustainable by the equipment for a given dip depth. Two types of fault are analysed: the three-phase and the single-line-to ground faults. These have been chosen because they represent respectively the most severe and the most frequent fault. For the first one, the influence of all dip parameters on the machine stability and on the load voltage is assessed. At the end, the results are drawn on the Power Acceptability Curves. For the second type, less severe, only the results on the Power Acceptability Curves are shown.

The last part of this work studies the impact of different load types on the results. These are shown to have a strong influence. Two additional types of loads have been analysed: motors and real constant power loads. The second one is different from the initial case because, in the transient module, the shunt

called "constant power" loads by ERACS are modelled as constant admittances. Again, the limit cases are extracted for all dips.

Acknowledgements

I would like to thank all the people that helped me directly or indirectly during the redaction of this thesis. They have been given me a lot of their time, tons of advice and positive criticism.

I would first like to express my sincere acknowledgement to my thesis advisors, Professor Thierry Van Cutsem and Doctor Patrick Scarpa for the time they have dedicated to me, their patience and their knowledge. They have followed me all along the process and have been always present to answer my questions.

Afterwards, I would like to acknowledge the team of Euro-diesel for their welcome, their support and their help. I would like to express my profound gratitude to Vincent Defosse. Its door was always open whenever I ran into a trouble spot or had a question about my research or writing. I also thank Quentin Dejace and my office neighbour Luc Thiteux for their support. Finally, Christopher Petit also helps me a lot concerning the Automatic Voltage Regulator model. I express my gratitude to the Euro-Diesel company in general for providing me the tools to realise this thesis.

I would also like to thank Mr. Kevin Davey, from RINA company, for all his answers about the software ERACS.

My sincere thanks also go to all the Professors of Faculty of Applied Sciences, especially Professors Patricia Rousseau and Christophe Geuzaine who agreed to be part of my jury.

Then, I also thank the other students present at Euro-Diesel, Luis Izquierdo, Julie Potier, Valentin Dubisy and Jean-François Lizin. They shared general information about the company and support me all along the process.

Finally, I also express my gratitude to my girlfriend, my mother, my father and all my friends for their support and the encouragements they gave me.

Summary

List of Figures

List of Tables

Chapter 1

Introduction to voltage dips

1.1 First definition and characterisation

According to IEEE Std.1159-2009 [3], a voltage dip is a drop of the RMS voltage magnitude between 10% and 90% of the nominal value lasting from half a cycle (at the supply frequency) to 1 min. An example of voltage dip is shown in figure 1.1. This one represents a single-phase voltage evolution and its sudden decrease; after some time, the voltage recovers and goes back to its initial value. In general, the voltage dip can affect three-phase systems and the effects can be different in each phase. In this case, the dip is said "unbalanced". Otherwise, it is said "balanced". [11]

One must be careful that the reference voltage used to define the voltage sag is the RMS voltage as advised in [7]. The difference between the words "voltage sag" and "voltage dip" is the following as explained in [26]:

- A voltage sag refers to the remaining voltage, e.g. a voltage sag of 60% means that 60% of the RMS voltage remains.
- A voltage dip refers to the amount by which the voltage has dropped, e.g. a voltage dip of 60% means that 40% of the RMS voltage remains.

These can be characterised using different parameters as explained hereafter.

1.1.1 Magnitude

According to [7], in several simulations of voltage sags studies, the parameter called magnitude of the sag is the remaining RMS voltage during the events. If the voltage waveform is recorded in samples, the RMS can be computed thanks to:

$$V_{rms}(k) = \sqrt{\frac{1}{N} \sum_{i=k-N+1}^{k} v_i^2}, \tag{1.1}$$

Where discreet samples of the voltage v_i are recorded (N is the number of samples per period).

This definition can easily be used when a single-phase fault or a three-phase fault occurs. In the first case, it is equal to the magnitude of the faulted phase and in the second case, it is equal to the voltage drop in all the phases. However, a problem occurs when characterising unbalanced voltage sags due to phase-to-phase fault (with or without the ground) or non-trivial dips. Other problems are pointed

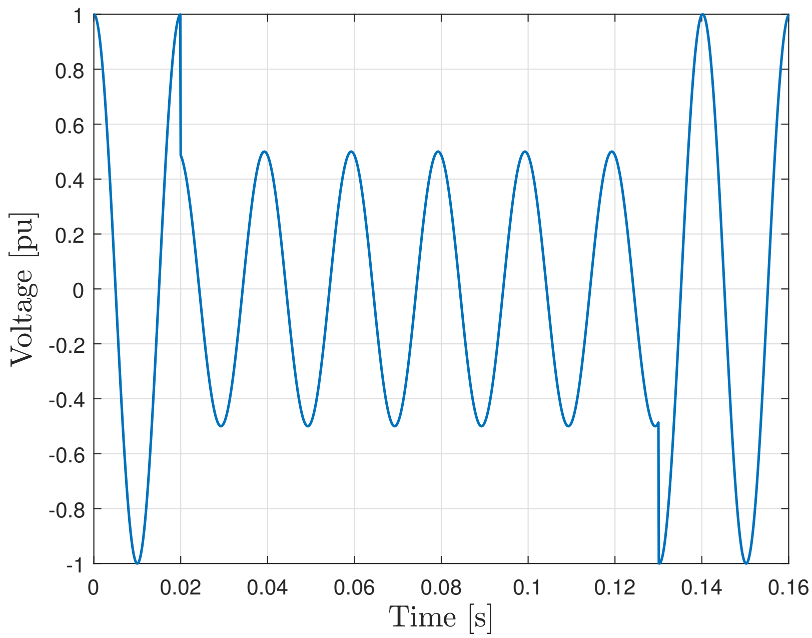

Figure 1.1
Example of voltage dip

out in [11]. For example, a voltage sag in one phase has the same "magnitude" as the one if the voltage sag would have occurred in the three phases. Then, these can be classified with both the same severity.

To counteract these problems, the authors in [11] introduce two quantities, the characteristic voltage and the so-called PN-factor. These are defined by the searchers using the positive- and negative- sequences of the voltage. However, these words suit better when the goal is to classify precisely the different dips. In this study, the goal is to simulate the behaviour of the dips and analyse their influence on loads. Moreover, the voltage waveforms are going to be accessible for all the dips. Therefore, the "magnitude" as called previously is sufficient in the scope of this work. More generally, the magnitude is the lowest remaining voltage between the three phases. It is also called "depth" in some cases when referring to the voltage drop. This term is more used with the word "dip".

This magnitude depends upon various factors, e.g. the fault impedance, the line impedance, the transformer connections between the observation point and the fault location, ...

An example of magnitude is given using the voltage divider model shown in figure 1.2. If a three-phase fault (without impedance) is applied at point F, if the pre-fault voltage is 1 pu, the generator voltage is 1 pu and the current going in the load are neglected, the remaining voltage at the PCC (point of common coupling) is given by:

$$\bar{V}_{sag} = \frac{Z_L}{Z_s + Z_L} \tag{1.2}$$

With $Z_L = R_L + jX_L$, the feeder impedance and $Z_s = R_s + jX_s$, the source impedance.
The magnitude of the voltage is the norm of this phasor.

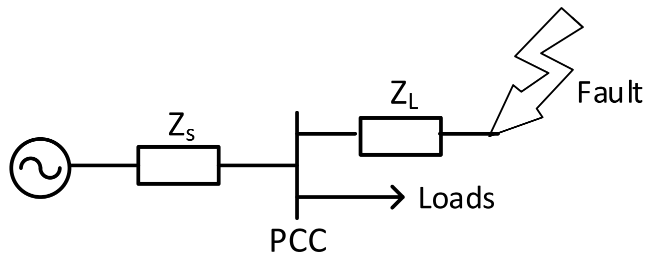

Figure 1.2
Voltage divider model

1.1.2 Duration

As explained in [7], the duration is the time interval between the starting time and the ending time. These two are referred as the time at which the voltage goes under or go back up a given threshold. Usually, this threshold is set to 0.9 (in pu). The duration depends on the initiation time of the fault and of the time taken by the circuit breakers to clear the fault. [9]

Then, different names can be given to power quality problems depending on their durations and their magnitudes. These are given in [3] and assembled in figure 1.3.
This figure gives the classification for the dips and for other power quality problems linked to the change in voltage (e.g. swell,...). For all these, the same principle as for voltage dips can be applied and their parameters are the same (magnitude, duration,...).

1.1.3 phase angle jump (PAJ)

This characteristic is sometimes not taken into account but it is of prior importance as shown in [34]. Indeed, it becomes essential due to the increase use of power electronic equipment. In fact, these usually use the phase of the signal as reference for their firing angle. It is also important when studying synchronous machine as shown in [5]. Thirdly, the system NO-BREAK KS®of EURO-DIESEL uses this PAJ to detect the dips and starts the diesel engine.

The voltage divider model shown in figure 1.2 can be used to illustrate this PAJ. The dip is expressed in equation 1.2.
The change of argument (phase shift compared to the pre-fault argument) of this voltage is called the phase angle jump. This one is given by:

$$\varDelta\varPhi = \arctan\left(\frac{X_L}{R_L}\right) - \arctan\left(\frac{X_L + X_s}{R_L + R_s}\right) \tag{1.3}$$

From this expression, one can remark that the phase angle jump is different than zero if the feeder impedance ratio X_L/R_L is different from the source impedance ratio X_s/R_s. This phase angle jump occurs during the dip but it can also occur after the dip. For example, if the network topology has been changed due to the fault (e.g. a line has been tripped to eliminate the fault and it is not reclosed), the voltage phase angle at the studied bus would have been changed. In this study, the term "phase angle jump" refers to the jump occurring during the dip.

An important remark can be pointed out, the PAJ can be different in the three-phases if the fault is unbalanced.

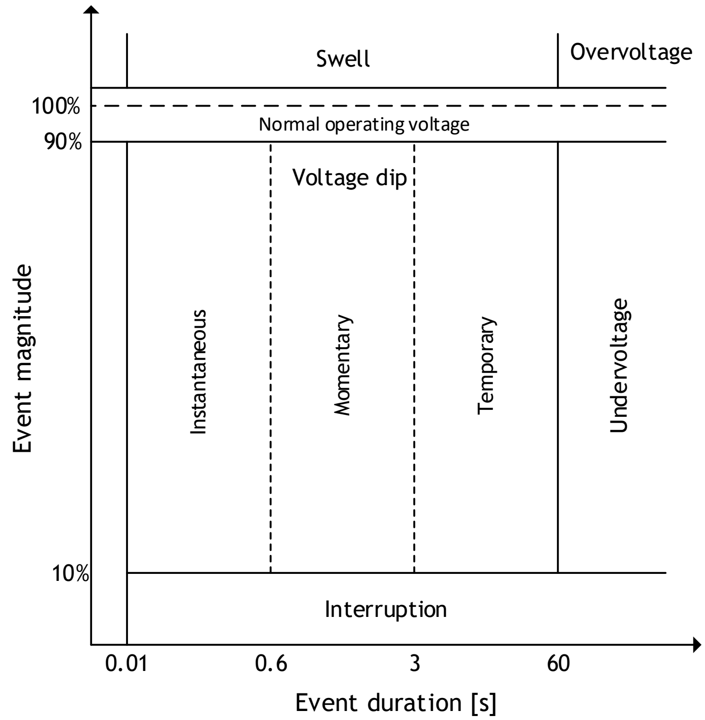

Figure 1.3
Classification of different types of voltage Power Quality problems according to their duration and magnitude

In theory, the phase angle jump can be positive or negative. However, in general, the X_s/R_s ratio of the feeder is bigger than X_L/R_L. This yields to a negative phase angle jump [22]. In the scope of this study, only these ones are going to be considered.

1.1.4 Point-on-wave

The point-on-wave is not always used as a characteristic for voltage dips. However, as shown by several papers [5], [14], [23] and [4], this is of interest when studying the behaviour of synchronous machines subjected to sags. Sometimes, the stability of the machine depends on this factor. In fact, this one influences the behaviour of the machine for unbalanced sags only.

The point-on-wave can be defined as the arbitrary angle ψ_i where the fault occurs. It is equal to the angle on the voltage sine waveform when the fault occurs. [5]

However, in this study, the software ERACS uses the phasor approximation. This one consists, among other things, in neglecting some terms in the dynamic equations of synchronous machines (the so-called "transformer voltages"). This results in neglecting the dynamics shorter than one cycle. Then, whatever the initial point-on-wave, the results are not going to change. In order to observe the influence of this parameters, a software using the full dynamic equations and called "Electromagnetic transient simulation" software should be used.

1.2 Origin of Voltage Dips

Following the definition, one can remark that several phenomenons can yield to voltage dips. These have all different characteristics and evolutions in time. Modelling in several software has already been carried out, for example, in MATLAB in [31] and in EMTP in [32]. These can be used as reference to identify the different origins.

1.2.1 Faults

These can be of several origins like lightning on overhead lines (the most frequent cause), snow, ice,... accumulating on conductors and yielding to short-circuits, trees, civil engineering vehicles or animals touching the phases, or internal failures of components. [28]

These faults can be of several types: three-phase, two-phase, two-phase-to-ground and single-phase-to-ground faults. Then, depending on the transformer connections between the measurement and the fault location, the voltage dip seen by the load will be different. A typical representation is shown in the voltage divider model in figure 1.2.

The voltage dips due to faults are characterised by short transition periods (nearly rectangular) and can be very deep in some cases. These can go up to 100% of depth if the fault occurs just next to the measurement location. It often represents the worst case of voltage dip. As the different levels of the power system have different characteristics (impedances, protections, transformer connections, ...), the characteristics described before (e.g. magnitude and duration) will strongly depend on the fault location and on the measurement location.

Examples are shown in figures 1.4 and 1.5 respectively for a single-phase-to-ground fault and a three-phase fault. For these, the starting time is 0.1s and the ending time is 0.3s. The pre-fault magnitude is 1 pu and the voltage dip has a depth of 0.5 pu. The phase angle jump is -45°. It is quite high but these cases are just examples for illustration.

1.2.2 Transformer energising

This phenomenon occurs when a transformer is switched on. This moment occurs at random instant and the voltage is not the same as at the time it has been turned on. Then, the location on the saturation curve is not the same, the core can saturate and inrush currents of high magnitude are created. This results in a voltage sag in the power system. [12]

An example of RMS voltage (line voltage) evolution at a 11kV bus is shown in figure 1.6 from [32]. It can be observed that the resulting voltage sag is unbalanced. The transition when the transformer is switched on is sharp and the recovery is gradual until the nominal level of the line. One can also remark that the dip magnitude is not very deep (2% in the case of figure 1.6 but it can go up to 15%). [12]

This phenomenon also introduces harmonics of even order in the voltage waveform as explained in [31].

1.2.3 Large induction motor starting

When started, induction motors draw several times their rated current, and thus, create a voltage dip in the power system. An example of such a voltage dip is presented in figure 1.7. [32]

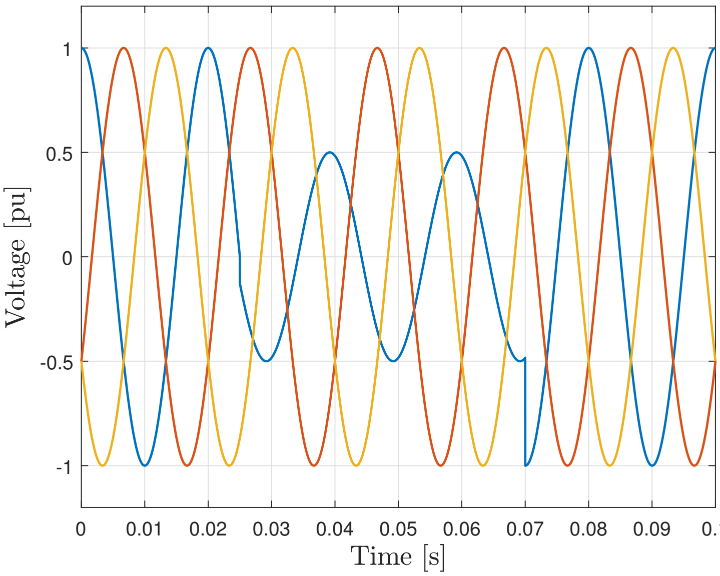

Figure 1.4
Single-phase-to-ground fault in a three-phase power system

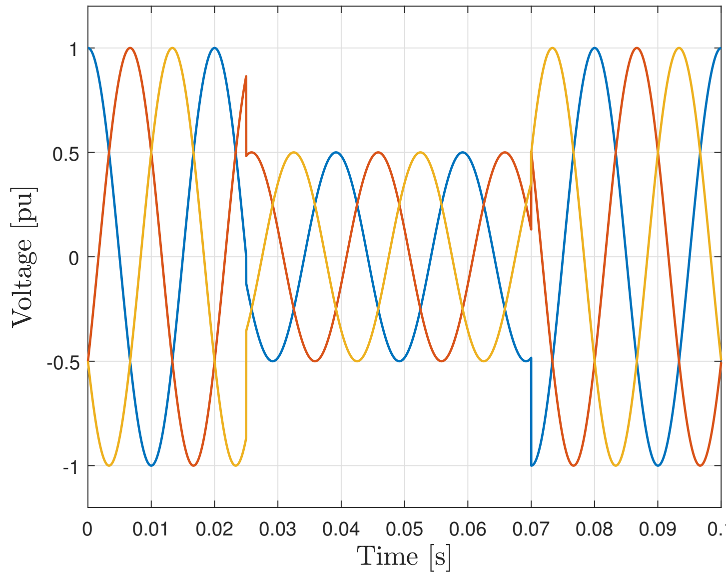

Figure 1.5
Three-phase fault in a three-phase system

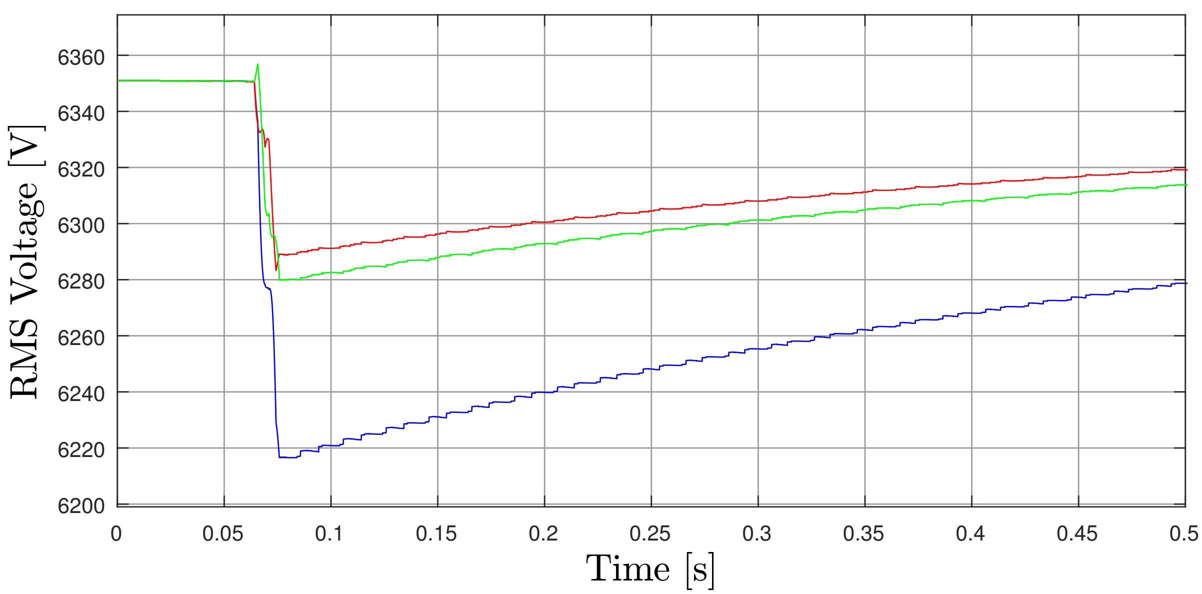

Figure 1.6
Voltage evolution for a voltage dip due to a transformer energising [32]

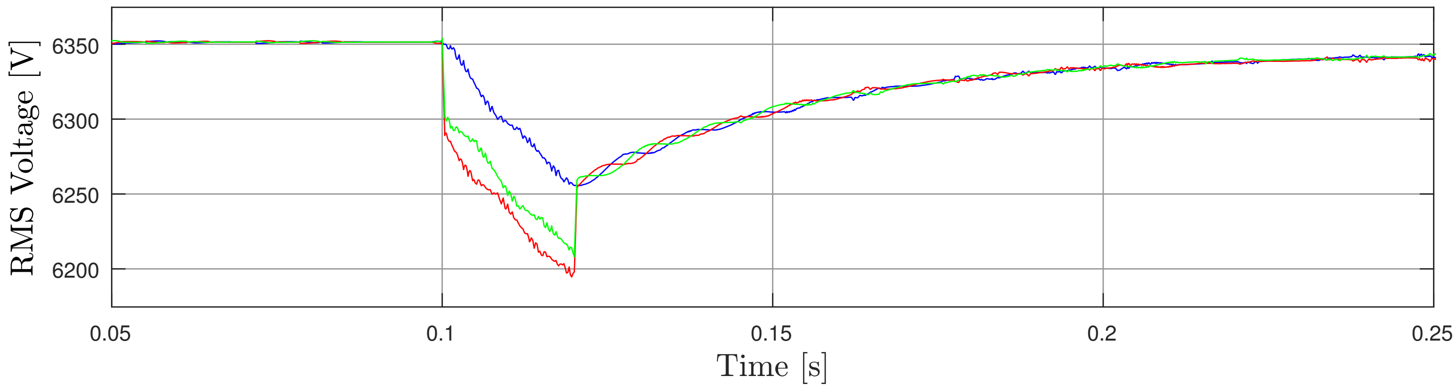

Figure 1.7
Voltage evolution for a voltage dip due to motor starting [32]

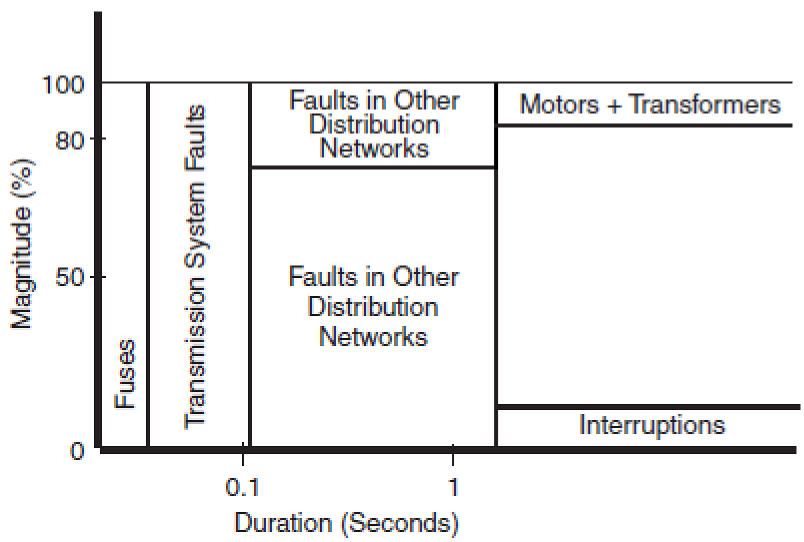

Figure 1.8
Classification of the voltage sags origin according to their duration and magnitude [8]

As shown in the figure, the dip is balanced and is not very deep. Like for the transformer energising, the recovery is gradual. [32]

1.2.4 Classification according to the origin

As pointed out in [8], the voltage dip origins can be classified according to their duration and their magnitude. For example, motors and transformers cause voltage dips that are smaller in magnitude than those initiated by faults. However, these are usually longer. Then, the protection in the transmission system acts generally faster than in the distribution system, resulting in shorter dips. A classification depending on the duration and the magnitude of the voltage dips is done in figure 1.8. In this one, the magnitude in ordinate is the remaining magnitude.

1.3 Classification of voltage dips

The classification explained here suits better to dips due to faults. The two additional types (transformer energising and motor starting) are treated separately.

First, the difference between the two type sets introduced has to be pointed. Fault types refer to the fault in itself (single-phase, two-phase, ...) and dip types refer to the voltage dips as seen from the loads or the measurement devices.

In fact, as pointed out in [11], all the dips resulting from faults can be classified in seven categories. These categories are such that the dips seen by a load is comprised is this set, whatever the connections (transformer types) between the fault position and the load.
The phasor diagrams and expressions of these seven types are shown in table 1.1. The phasor diagrams are shown in rows 2 and 6. The expressions of these phasors are given in rows 3 and 7. In the expressions, $\bar{V}$ is a phasor. This one can be used to build the dip knowing the expressions. In fact, depending of the fault type used, it corresponds to the line voltage of the faulted phase (single-phase-to-ground or three-phase faults) or the phase voltage between the faulted phases (phase-to-phase faults with or without the ground).

Nevertheless, the types shown in the table 1.1 refer to "special" types where there are no phase angle jump. In reality, the types refer more to a movement of the phasors with respect to their pre-fault value. This is the reason why rows 4 and 8 are present. These two explain these relative movements for all the dips.

The three possible locations of observation are shown in figure 1.9. The correspondence between the fault type, the location of observation and the dip type is shown in table 1.2. The way to understand these is the following, if a two-phase fault at location I is observed at location II, the resulting observed dip is of type D. This artificial way to see voltage enables to limit clearly the set of dips that can be met in the network.

In fact, the transformers can be of three types. The first one is constituted of all the transformers of type Dy, Yd and Yz. Then, the second type regroups Yny, Yyn, Yy, Dd and Dz transformers. The last type is made of the Ynyn transformers. The last type does not modify the type of dip. The two other types change the dip type. However, new types are not generated. All the seven cases are obtained using Dy transformers. Other types could have been used (Yd, ...) but the results would have been similar.

Another advantage of this method is that, by simulating all of these types, the connection of the load (star or delta) does not need to be simulated. For example, a single-phase fault results in a type B for a star connected load. For the same fault, a delta connected load sees a different type of dip. However, this types is comprised in the set. It corresponds to type C. The same reasoning can be applied for all the possible faults. [8]

For example, a type B dip arrives at a substation. This one comes from a single-phase fault in the network and its phasor diagram is shown in the first column of table 1.3. One can remark that the phase angle jump on the faulted phase is present. At a substation, a Dy transformer is present. The phasor diagram of the secondary side voltage is shown in the second column of the same table. It corresponds to a type C. It is further "transmitted" in a lower level and after a second Dy transformer, it becomes a type D as illustrated in the third column of the table. In all this example, the losses in the transformers and in the lines are neglected because the goal is to show the evolution when going through transformers.

In this case, phase A is considered as the reference phase. Considering the other phases would yield to

Type A	Type B	Type C	Type D
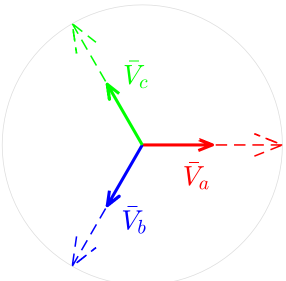	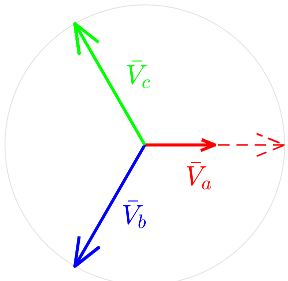	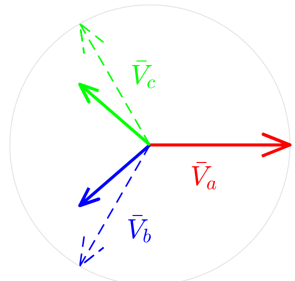	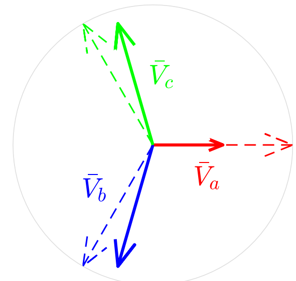
$\bar{V}_a = \bar{V}$ $\bar{V}_b = -\frac{1}{2}\bar{V} - \frac{\sqrt{3}}{2}j\bar{V}$ $\bar{V}_c = -\frac{1}{2}\bar{V} + \frac{\sqrt{3}}{2}j\bar{V}$	$\bar{V}_a = \bar{V}$ $\bar{V}_b = -\frac{1}{2} - \frac{\sqrt{3}}{2}j$ $\bar{V}_c = -\frac{1}{2} + \frac{\sqrt{3}}{2}j$	$\bar{V}_a = 1$ $\bar{V}_b = -\frac{1}{2} - \frac{\sqrt{3}}{2}j\bar{V}$ $\bar{V}_c = -\frac{1}{2} + \frac{\sqrt{3}}{2}j\bar{V}$	$\bar{V}_a = \bar{V}$ $\bar{V}_b = -\frac{1}{2}\bar{V} - \frac{\sqrt{3}}{2}j$ $\bar{V}_c = -\frac{1}{2}\bar{V} + \frac{\sqrt{3}}{2}j$
Same magnitude drop and phase angle jump for the three phasors	Magnitude drop and phase angle jump in one phase only	Magnitude drop and phase angle jump in two phases(tend to come closer)	Magnitude drop in all the phases but phase angle jump in two phases only (tend to move away)

Type E	Type F	Type G
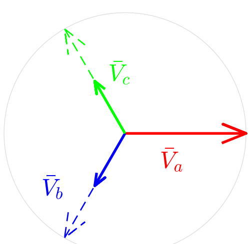	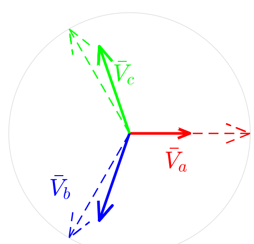	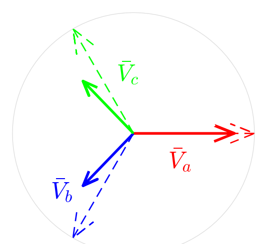
$\bar{V}_a = 1$ $\bar{V}_b = -\frac{1}{2}\bar{V} - \frac{\sqrt{3}}{2}j\bar{V}$ $\bar{V}_c = -\frac{1}{2}\bar{V} + \frac{\sqrt{3}}{2}j\bar{V}$	$\bar{V}_a = \bar{V}$ $\bar{V}_b = -\frac{1}{2}\bar{V} - \frac{\sqrt{3}}{2}j\left(\frac{2}{3} + \frac{1}{3}\bar{V}\right)$ $\bar{V}_c = -\frac{1}{2}\bar{V} + \frac{\sqrt{3}}{2}j\left(\frac{2}{3} + \frac{1}{3}\bar{V}\right)$	$\bar{V}_a = \frac{2}{3} + \frac{1}{3}\bar{V}$ $\bar{V}_b = -\frac{1}{2}\left(\frac{2}{3} + \frac{1}{3}\bar{V}\right) - \frac{\sqrt{3}}{2}j\bar{V}$ $\bar{V}_c = -\frac{1}{2}\left(\frac{2}{3} + \frac{1}{3}\bar{V}\right) + \frac{\sqrt{3}}{2}j\bar{V}$
Magnitude drop and phase angle jump in two phases (same phase angle change)	Magnitude drop in all phases and phase angle jump in two phases only (tend to move away)	Magnitude drop in all phases and phase angle jump in two phases (tend to come closer)

Table 1.1
Phasor diagrams and corresponding expressions for the seven dip types

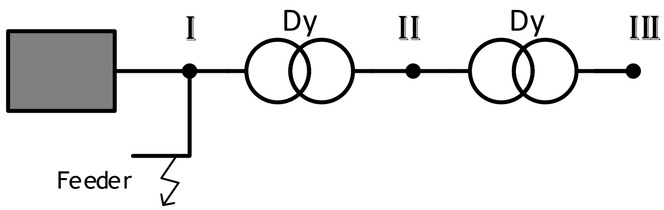

Figure 1.9
Transformer connections between the fault location and the measurement bus [11]

Fault type	Measurement location		
	I	II	III
Three-phase	A	A	A
Two-phase-to-ground	E	F	G
Two-phase	C	D	C
Single-phase	B	C	D

Table 1.2
Relation between the types of fault, the fault location and the resulting voltage dip types [11]

First level	Second level	Third level
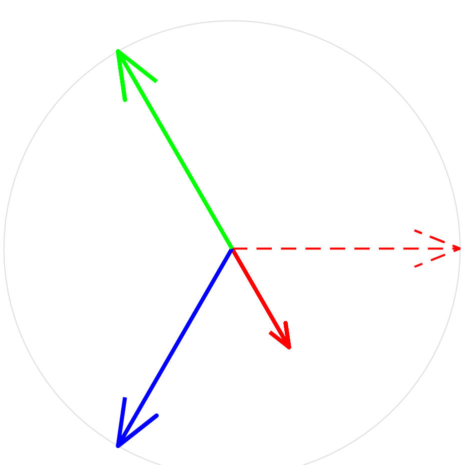	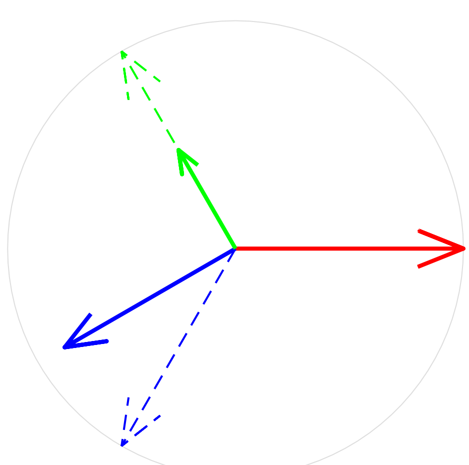	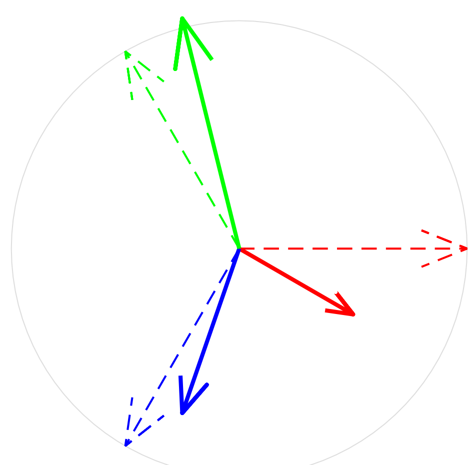

Table 1.3
Phasor diagram corresponding to the example

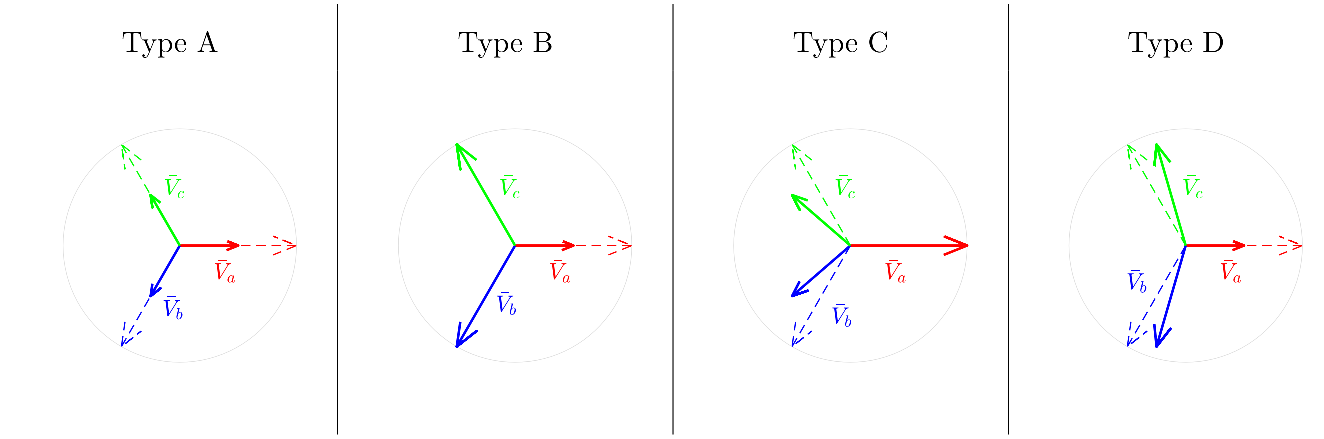

Table 1.4
Phasor diagram for the four dip types

twelve additional voltage sag types (type A is the same whatever the reference phase). However, the situation is similar and phase A is going to be considered as the reference phase in all cases in this study.

Thanks to this method called "ABC classification", all the transformations resulting from transformers are taken into account. Another method, classifying in four types using a "characteristic voltage" and a term introduced previously, the "PN-factor", is also pointed out in [11]. In fact, this PN-factor allows to take into account the influence of the fault on the non-faulted phase(s). The advantage of this last method is that it takes into account the fact that the positive, negative- and zero-sequence impedances are sometimes not the same. This simplification is used to derive the first approach detailed previously. Nevertheless, the ABC classification is more suitable for the simulations, which is the case here. The other method is more complex but is more suitable when the goal is to classify these. As this is not the goal of this study, the first approach is followed here. [11]

The second method is used in several situations. In this one, type A refers to a drop in the three phases. Type B and C refer to a main drop in one phase and in two phases respectively. The type D is also a drop in the three phases but this one is unbalanced. The "drop" used to characterise the type is referred as the "main" drop. The other phases can also see a drop in their magnitudes but this one is smaller. Table 1.4 represents the corresponding phasor diagram. Like for the first classification introduced, transformer connection does not yield to new types. [10]

Other characterisation methods have been derived by searchers. For example, [19], [6] and [18] introduce an approach called "Space vector methodology". Its main advantage is that it uses only a phasor and the zero-sequence voltage to characterise the dips. It is based on the Clarke transformation. This one can be written:

$$\begin{pmatrix} x_\alpha(t) \\ x_\beta(t) \\ x_0(t) \end{pmatrix} = \frac{2}{3} \begin{pmatrix} 1 & -1/2 & -1/2 \\ 0 & \sqrt{3}/2 & -\sqrt{3}/2 \\ 1/2 & 1/2 & 1/2 \end{pmatrix} \begin{pmatrix} v_a(t) \\ v_b(t) \\ v_c(t) \end{pmatrix} \tag{1.4}$$

The third component is the zero-sequence. The first two components are used to form a phasor called "space vector":

$$\bar{x}(t) = x_\alpha(t) + jx_{beta}(t) \tag{1.5}$$

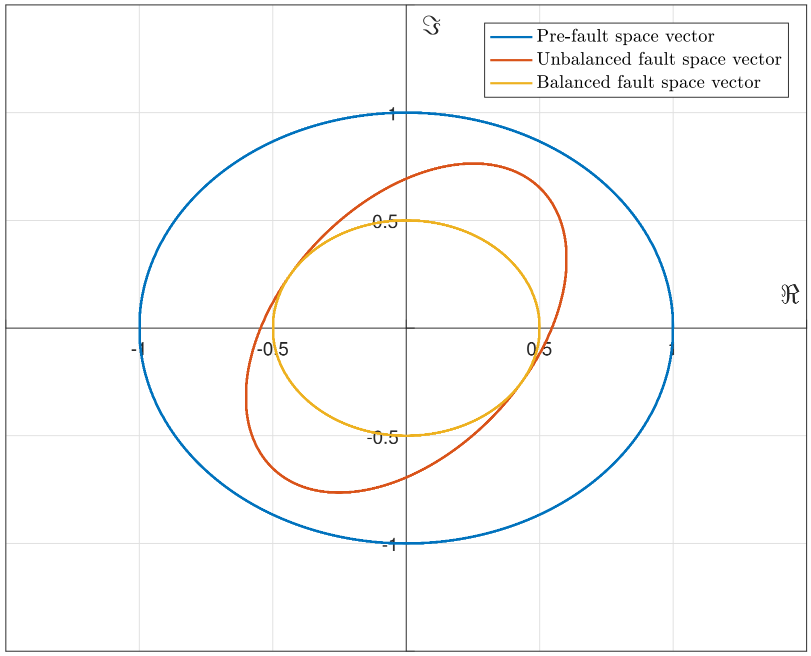

Figure 1.10
Space vector representation of voltage dips (pre-fault, unbalanced and balanced cases)

Then, the idea is to plot this phasor in the complex plane and to analyse the obtained shape. It can be shown that in the base case (no dips), it represents a circle of radius equal to the voltage and of centre (0,0). If a balanced fault is present, the representation is also a circle but of smaller radius. In the case of an unbalanced voltage sag, the shape becomes an ellipse.
The three cases are shown in figure 1.10. In this particular example, the pre-fault voltage is 1 pu (blue space vector). This one is represented by a circle of radius equal to 1 pu. The unbalanced dip (red) consists in a drop in phase a and b without PAJ. This results in an ellipse. The balanced dip (yellow) is represented by a circle of radius equal to the remaining voltage. In this case, this value is 0.5 pu.
Afterwards, the parameters of the obtained shape are used to classify the dip. The studied parameters are: the shape, the radius (for a circle), the inclination of the major axis and the length of the major and minor axes (for an ellipse). [19]

Again this last method is more suitable for detection and classification of voltage dips (monitoring). Then, it is more complex than the "ABC classification" and the first classification explained is kept for this study.

Chapter 2

Sensitivity of the equipment

As already mentioned, several types of equipment are sensitive to voltage dips. The study of the behaviour of equipment subjected to dips is called the immunity analysis.

A usual way to represent the load sensitivity is by using curves function of the duration and the magnitude. Then, sustainable dips are represented above the curve. The lower part represents too severe dips that can yield to tripping or malfunction of the equipment. The same principle can be applied to the upper part of the curve (for voltage swells). These curves are called "voltage tolerance curve" or "power acceptability curve". They are determined by testing the equipment. An example can be shown in figure 2.1. [7]

2.1 Existing standards and power acceptability curve

The first useful standard is the IEC 61000-4-11 and the IEC 61000-4-34. These ones describe a method to be used for the characterisation of the equipment sensitivity. They concentrate on the description of the equipment needed to assess the test and make sure every tests are similar, whatever the place. These applied to equipment with rated current respectively below and above 16 A. [17]

Obviously, the power acceptability curves are different for all the equipment. However, some important ones, used many times as reference, are described hereafter:

- The CBEMA curve, stating for "Computer Business Equipment Manufacturers' Association", was created in 1977 to identify the performance of computers. It was created by ITIC (Information Technology Industry Council). Afterwards, it was taken by IEEE as a standard immunity against voltage sags. [7]
- The ITIC refreshed the curve in 2002, yielding to the so-called "revised CBEMA curve" or "ITIC curve". This one was created in 2002. [7]
- Another curve called "SEMI F47-0706" was created by the semiconductor industry. This one focuses on sustainable dips for semi-conductor processing equipment. [16]

The three curves described above are shown in figure 2.2. As can be seen, the two CBEMA curves do not only focus on voltage dips but also take into account the voltage swells (over-voltage). The SEMI curve only focuses on voltage dips.
In 1997, another important standard was published by IEEE, the IEEE std. 493, also called "golden book". It presents standards to apply to commercial and industrial power systems. It also gives the number of times that a particular piece of equipment can fail to operate. This number is function of the

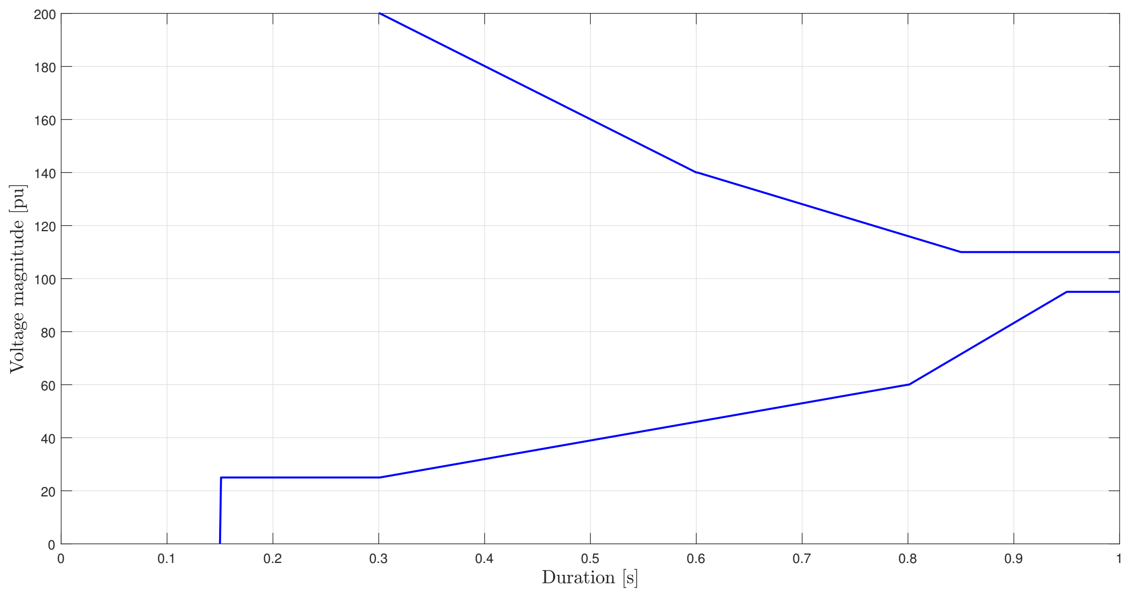

Figure 2.1
Example of voltage tolerance curve

power system and of the work condition. Then, knowing this standard number, the sensitivity of the device has to be adjusted. [13]

An important remark can be made concerning these curves. They do not take into account two important parameters of the voltage: the point-on-wave and the phase angle jump. If these are very important, the curves are not strictly valid. Then, the analysis can lead to false conclusions. [15]
Another way to characterise the sensitivity of an equipment is described in [15]. It does not constitute a standard but it is more a new way to represent the curves. In this one, the voltage dip is transformed in the dq0-space using the Park transformation. Then, the sensitivity to various types of voltage dips can be represented in this three-dimensional space and in the dqt-space (similar to the space vector classification approach but using the Park transformation). An example is shown in figure 2.3 where the sensitivity for a single-line-to-ground fault is drawn. A curve in the dqt-space is represented in figure 2.4. This one corresponds to a line-to-line fault. Then, for each curve, several variants can be drawn depending on the phase angle jumps.

The sensitivity is assessed by drawing the observed voltage dip in the 0dq-space or in the dqt-space. Then, if the obtained curve is contained inside the 3D curve plotted before (corresponding to the standard), the event can yield to malfunction of the machine. This volume has a similar meaning as the curve under the previous standard curves. The same reasoning can be applied on the dqt-curve. [15]

The main improvement of this method is the fact that it can take into account all the important parameters of sags. These are the magnitude, the duration, the point-on-wave and the phase angle jump. [15]
However, in practice, this method is difficult to use and it remains mainly theoretical.

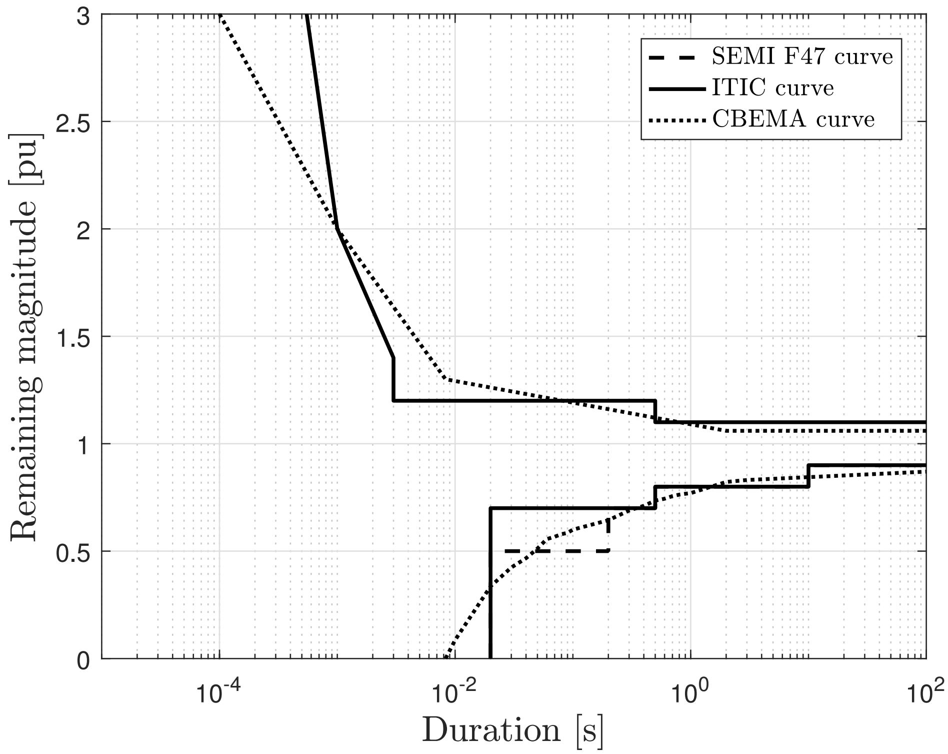

Figure 2.2
Initial (1977), revised (2002) CBEMA and SEMI F47-0706 curves

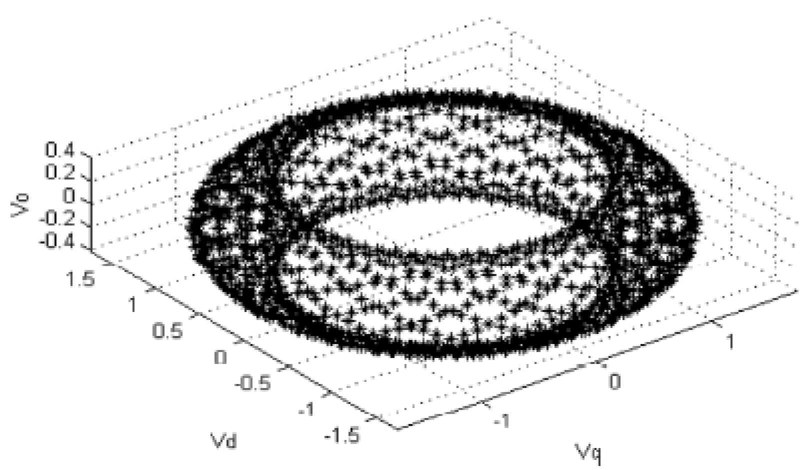

Figure 2.3
Sensitivity of an equipment for single-line-to-ground fault in 0dq components [15]

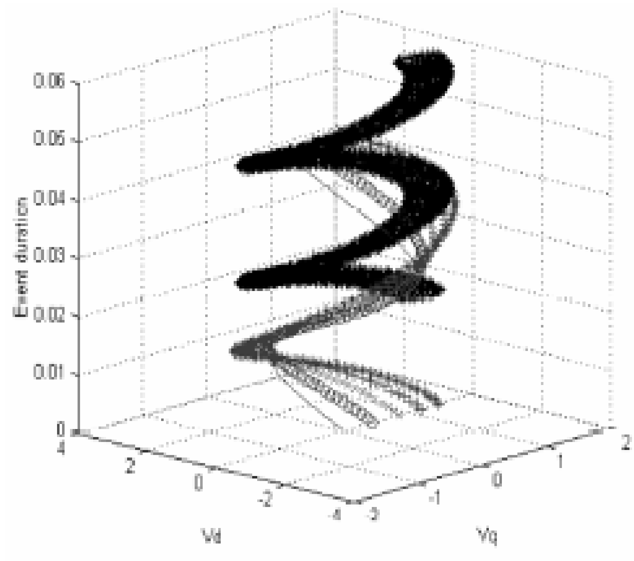

Figure 2.4
Sensitivity of an equipment for a line-to-line fault in the dqt-space [15]

2.2 Method to access the equipment sensitivity

The practical method for accessing the equipment sensitivity is given in the IEC 6100-4-11 as explained before. It defines for example test levels to apply to a given kind of element. Then, following [7], its goal is to "establish a common reference for evaluating the immunity of electrical and electronic equipment when subjected to voltage dips, short interruptions and voltage variations". Then, it concentrates on the practical tests and it needs to use sag generators to simulate different behaviours and models the different possible origins. [7]

The approach here is different and uses simulation and a software to assess this immunity.

2.3 Sensitivity considered for this study

In this section, the threshold values of the voltage and of the duration have to be defined for all the equipment. During the simulation, if load voltage values under these thresholds are found, the equipment would be considered to have tripped. This means that the particular dip is not covered by the studied equipment.
Several studies have been carried out to assess the sensitivity of crucial equipment used in the industry. Among the equipment, some of them are critical for the process. They can be classified according to [21]:

- Motors, heating elements and other three-phase loads that are connected directly to the feeders.
- Adjustable-speed drivers and power electronic elements also use three-phase voltage. They are connected directly or through an isolation transformer.
- Lighting are usually connected through single-phase connections.
- Control devices such as computers,... use single-phase connections.

Obviously, the sensitivity is going to be different for all these elements. This one can also be different within the same category. For example, two motors can have different responses depending on their parameters. Therefore, accessing the sensitivity of a particular equipment is nearly impossible. This is the reason why standard known values have to be considered.

In the scope of this study, the CBEMA standard is used as reference value. This one is taken because it is more continuous and physical than other curves.

Concerning the influence of the point-on-wave and the phase angle jump, the same curves are considered for all the point-on-waves and phase angle jumps studied. In fact, for all studied cases, the phase angle jump will be found and used. Concerning the point-on-wave, as already mentioned, its influence can not be accessed with ERACS.

Chapter 3

Mitigation techniques

As explained, voltage dips are sometimes critical as they can yield to tripping or malfunction of equipment. Depending on the equipment, this can yield to the complete shutdown of the factory and in some cases, these equipment can not be started before several hours. Then, it yields to high financial losses for companies. Then, if some areas are exposed or are critical, the sensitivity should be improved. This can be done using several techniques. These are classified in four categories based on the location where they take place as illustrated in figure 3.1. Generally, it is less expensive to act at lower level than in the utility side. [24]

3.1 Utility side mitigations

This consists in improving the power system reliability and decreasing the number of fault by acting on the origin of the faults. For example, one can prevent faults due to trees by increasing the trimming. One can also improve the insulation between lines, ... [24]

Another way to act is through the duration of the dips. This one can be lowered by improving the circuit breakers. The dips become shorter and, therefore, less severe [24].

A last way to mitigate sags is through topology change:

- Installing a distributed generation source.
- Splitting bus and supplying via an express feeder.
- Using series reactors at strategic points. This decreases the dip at the point-of-common coupling by increasing the impedance between the fault location and the point at which the dip is observed.

These three ways to modify the topology have been investigated in [25]. It appears that the best solution is to use express feeder. However, at the end, the results are mitigated and these solutions remain very difficult to use and very expensive. Moreover, these are independent of the customer.

3.2 State of the art in protective equipment

First, these equipment act in a different manner on the voltage. They can be classified in three groups [33]:

- An external energy source is used. The load is supplied by this source and all voltage sags can be countered. UPS and flywheels are typical examples of this category.

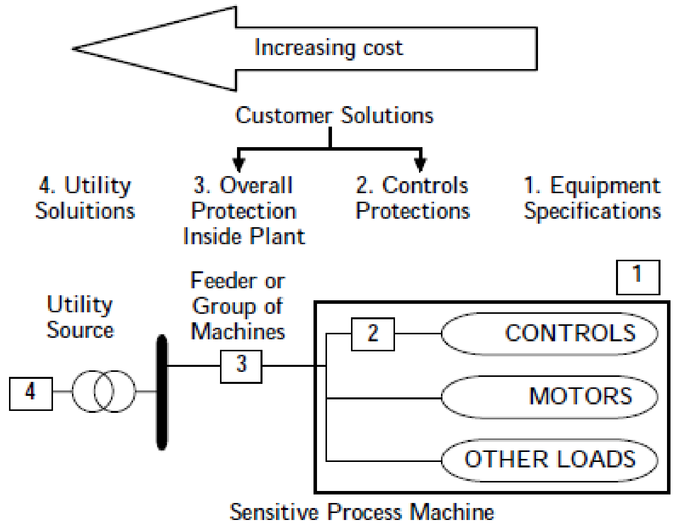

Figure 3.1
Different levels where the sensitive can be improved [24]

- The missing voltage is added in series to the remaining voltage. These can also contain a power source. They have limitations on the manageable depth.
- The compensation of the missing voltage is done by drawing more power from the supply. It increases the power coming from the grid (through an increase in current). This does not necessitate an internal energy source.

There are a lot of different types of mitigation equipment. The most remarkable ones are the tap changing transformers, the dynamic voltage regulators, the flywheels and motor-generator sets, the ferroresonant transformers, the magnetic synthetizers, the Uninterruptible Power Supply (UPS), Static Var Compensator (STATCOM) and shunt connected synchronous machines.

First, tap changing transformers act on the voltage in a similar way than the one used in power systems. A fast response can be achieved thanks to thyristors (one cycle). The main drawback is that the number of thyristors needed becomes gigantic if a good resolution is needed. Moreover, the manageable depth is not very big. [24]

Then, Dynamic Voltage Regulators (DVR) are devices connected in series with the supply through a transformer. It is used to add the missing voltage [33]. These can be used with very big loads and they can provide active power to the loads during the dip [24]. These are of two types [33]:

- First type: No energy storage is present. Then energy comes from the supply (increase of the current). They can not operate if the voltage drop is too big.
- Second type: An energy storage is present. This allows to ride through deeper voltage sags but the duration is sometimes limited (depending on the energy storage).

The main advantage of the first type is its smaller size and purchase cost. It also does not require a lot of maintenance and it can provide reactive power to the load. For the second type, the device is generally bigger, more expensive and has a lower efficiency (due to the energy storage). However, it can filter out the harmonics and can deal with more severe dips as expressed after. An example of a second type device is shown in figure 3.3. [33]
The mitigation capacity depends on the type of device and on the load. The second type is better than

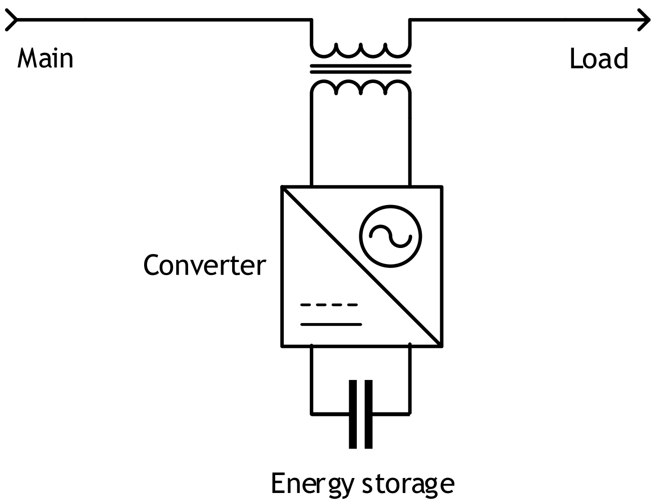

Figure 3.2
Schematic of a Dynamic Voltage Regulator (type 2)

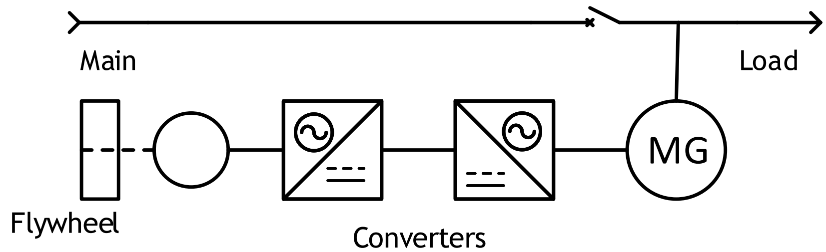

Figure 3.3
Example of flywheel connection [33]

the first one. In general, this capacity decreases if the load increases (for the same device). Dips of depth up to 30% can be mitigated by the first type. The second one can mitigate 50% depth dips. [33]

Third, flywheels and motor-generator sets can be used. It consists of a rotating mass used to store energy. It is spun thanks the grid energy and when a dip occurs, energy is taken back and injected to supply the load. Sometimes, a DC interface is present after the flywheels. This one is converted back in AC after. This is done because otherwise, the frequency would decrease when the kinetic energy of the flywheel is converted in electricity (decrease in speed). Two types of flywheels exists: traditional and advanced flywheels. The first ones are made of steel and can rotate at limited speed (a few thousands RPM). The advanced ones are made of carbon fibre. Then, these can reach very high speeds in the vacuum (up to 60000 RPM). They can be used as intermediate supply before a back-up system starts. [24]
They can mitigate drops of 100% (depth). The maximal duration can go up to 30s in some cases. Their main advantages are their size (compared to battery or other energy storage), their filter capability and their capability to provide reactive power. These two parts are detailed later in the study. However, these are generally very expensive and require a lot of maintenance. Moreover, the global efficiency is sometimes low. The schematic of this device is shown in figure 3.3. [33]

Another type of equipment is the ferroresonant transformer. It is also called Constant Voltage Transformer (CVT). It consists of a transformer and a capacitor (designed according to the particular situation). The secondary is designed in such a way that the magnetic core operates in saturation and in resonance with the capacitor. Then, if the voltage on the primary changes, the voltage in the secondary stays approximately constant. It works only in a defined range and for small voltage drops. [24]
The main drawbacks of this method are that there are many problems when the load is not linear. Moreover, lot of harmonics are present in the signal and the mitigation is sensitive to the value of the capacitor and of the power supply frequency. Indeed, the value of the capacitor is computed for a given value of the power supply frequency. If this one is different, the mitigation changes. It has also a high output impedance. Nevertheless, the response time is quite good (up to 1.5 cycles) and the reliability is good. It does not require a lot of maintenance and it is relatively cheap. [33]
To conclude, this device works very well for small loads without motor.

The magnetic synthetizers is similar to CVT but suits better for big loads. It consists of iron core reactors, transformers, capacitors and an energy storage. There is no electrical connection between the

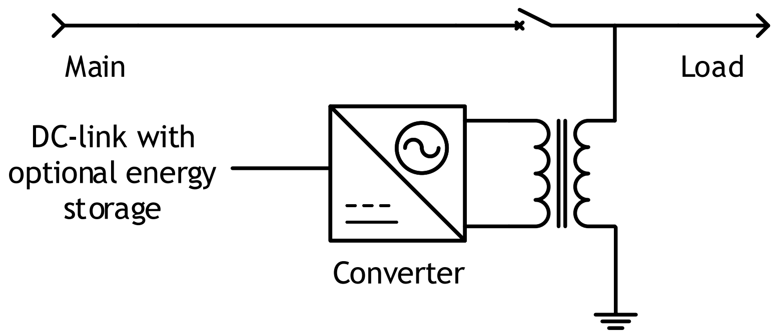

Figure 3.4
Schematic of a Static Var Compensator [33]

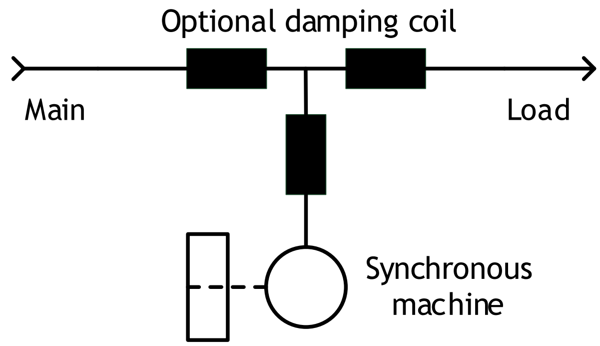

Figure 3.5
Shunt connected synchronous machine [33]

output and the input of the device and it provides a three-phase sine wave voltage at the output whatever the form of the input voltage. Its main advantage is that the output is independent of all electrical parameters (except of the order of rotation of the phasor and of the frequency). Its drawback is its price. [24]

The Static Var Compensator (STATCOM) injects a current in parallel with the load. It can provide reactive power into the system. Its capacity can be increased by adding an energy storage. It can mitigate depth of 60%. The drawbacks of such method are that it is quite big and that the reaction time is quite long. A schematic of a STATCOM is provided in figure 3.4. [33]

The last solution consists of a shunt connected synchronous machine. The principle is similar to a STATCOM but there is no need of power electronic here. It can take voltage drops up to 60% for 6s. It has the advantage to be smaller than other devices. It can also filter the harmonics and provide reactive power. However, sometimes the efficiency can become low. A schematic is shown in figure 3.5. [33]

It is important to mention that several variants to these devices exist. Then, for example, the connections can differ in the series compensation (with a transformer or with power electronics). Afterwards, the energy storage can be different. One can use batteries, Compressed Air Energy Storage (pressurised air), Supercapacitors, Superconducting Magnetic Energy Storage,... The study of all these is not in the scope of this work. The elements can also be different if they are used as intermediate before an energy source like a diesel engine is started.

3.3 Characteristic of the studied device

The studied device consists of a synchronous machine connected through a three-point choke. The diagram is shown in figure 3.6. This machine consists of a synchronous machine that is free to spin. This one has an exciter that can be controlled to increase or decrease the reactive produced/absorbed. As it is not connected to a turbine or a mechanical source of energy, it can not provide active power. Then, the only parameter that one can tune is the reactive power absorbed of produced. This one is controlled thanks to the internal EMF of the machine. The control is done automatically thanks to the Automatic Voltage Regulator (AVR) that keeps the load voltage around 1pu.

The two essential elements of the equipment are:

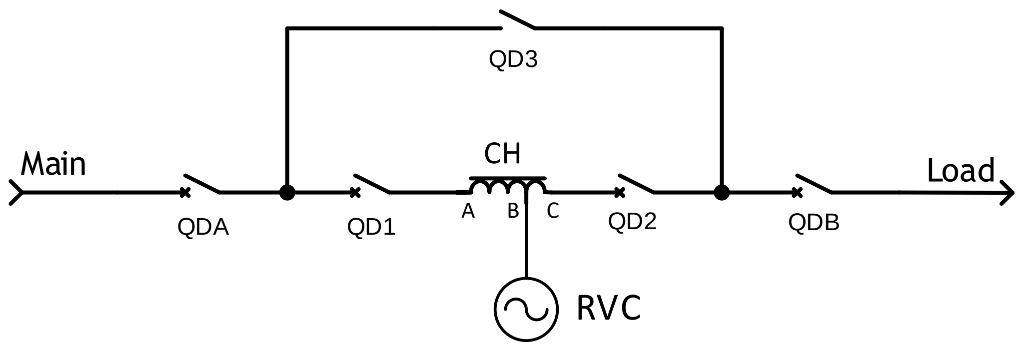

Figure 3.6
Studied shunt connected synchronous machine

- A high impedance choke: this enables to isolate the machine from the network and enables the correction of the voltage.
- A low impedance synchronous machine: it provides the reactive power needed to control the voltage. It does not provide any active power except during small voltage variations. Then, it decelerates and injects this active power to help the networks. It comes back at equilibrium immediately after.

As briefly explained, the equipment has three main functions. First, it helps the network and releases active power in the case of a voltage sag (resulting in a loss of power coming from the network). Then, it acts as a filter of the harmonics coming from the network (voltage harmonics), from the load (current harmonics), the zero-sequence current (load neutral current) and the voltage harmonics created by the load harmonic current. At the end, it helps compensating the reactive power produced or absorbed by the load. Thanks to this, it improves a lot the power factor seen by the network.

The Choke is in this case a three-point self. In smaller UPS machine produced, this one is a simple choke. In this case, as there are no energy storage or diesel engine, the system can be improved thanks to this. It helps improving the voltage on the load side. In fact, it acts as an auto-transformer that boost a little bit more the load voltage when a sag is present. The ratio between the number of turn in the left (AB portion) and in the portion BC needs to be much higher than 1 to have a bigger impedance in the left and ensure the filtering property. Generally, in Euro-Diesel's product, it is set to a ratio of 5:1 or 6:1. The higher figure is related to the left part of the choke.

The different elements present in the diagram and labelled "QD" are relays and circuit breakers. In practice, they have several functions like by-passing the equipment, ... These have been kept to show the full equipment used by the company. In the scope of this study, these are not used and are not modelled in the software.

3.3.1 Voltage support in case of dip

The first thing to mention is that, electrically speaking, the loads are closer to the alternator than to the network. Therefore, the voltage seen by the loads is "cleaned" by the alternator. This phenomenon is reinforced by the big reactance of the left part of the choke. For example, during dips, the alternator can maintain the terminal voltage around the nominal. Due to its proximity, the voltage seen by the loads is closer to this voltage and is better.
This property is the main function studied here as it occurs when the voltage from the main decreases. Then, the power coming from this side decreases too. The resulting unbalance of power is going to be compensated by the synchronous machine. As this machine is not connected to an external source of

energy, it provides this energy by decelerating.
As a reminder, If the choke resistance is neglected, the power equation is given by:

$$P_{12} = \frac{V_1 V_2 \sin(\theta_1 - \theta_2)}{X} \tag{3.1}$$

In this equation, the power goes from BUS-1 to BUS-2, $\bar{V_1} = V_1 \angle \theta_1$ and $\bar{V_2} = V_2 \angle \theta_2$ are the phasor voltages at bus 1 and 2. X is the reactance through which the active power flows. Similar quantities can be used to define the reactive power entering the reactance (for side 1):

$$Q_{12} = \frac{V_1^2 - V_1 V_2 \cos(\theta_1 - \theta_2)}{X} \tag{3.2}$$

In the case of a step decrease in the main voltage, the machine provides active power to supply the load by decelerating. Then, the power flow through the machine reactance induces a change in phase angle at the point B of the choke. Following equation 3.2, this increases the reactive power produced by the machine. This reactive power flows between portion AB of the choke and goes to the main. A similar behaviour is observed when the voltage from the main increases. In this case, the synchronous machine accelerates and absorbs active power.

Obviously, the amount of active power that the machine can absorb or release is limited. Then, the machine is not able to cope with all the sag magnitudes and durations. If the sag is too severe, the machine can become unstable. This is going to be further analysed in the next chapters.

This function is mainly used in the existing equipment to cope with small voltage variations. In this one, an accumulator helps the machine by providing it additional energy at constant frequency. If the dip is too severe, a diesel engine is started and supply the synchronous machine with mechanical power. Then, this equipment can deal with all voltage dips.

3.3.2 Filtering of the harmonics

All this part is described in a Technical Information provided by the company for their customers [1].

First, a definition needs to be introduced. The homopolar currents or voltages are current and voltage harmonics that generate a current in the neutral. It corresponds to the zero-sequence voltage and current. It can be shown that, in terms of harmonics, it is constituted of the 3^{rd}, 6^{th}, 9^{th},... The non-homopolar components are the positive- and negative-sequence of the voltage and the current. In term of harmonics it corresponds to the 1^{st}, 2^{nd}, 4^{th}, 5^{th}...
The association of a low reactance synchronous machine (obtained by over-sizing the machine) and a high impedance choke behaves as a filter for the harmonics. The main principle is explained hereafter for the filtering of the voltage harmonics coming from the network. The behaviour is similar for the filtering of the current harmonics coming from the loads, of the zero-sequence currents from the loads (load-neutral current) and of the voltage harmonics from the loads due to the current harmonics.

Consider the simplified circuit of the equipment when the circuit breaker QD1 and QD2 are closed (QD3 is open) and using only a simple choke as shown in figure 3.7. This one focuses on the behaviour against harmonics coming from the main. The principle with a three-point choke is similar as the impedance on the left section is much bigger than the one of the right portion (AB portion in the diagram).

In this figure, X_{ch} is the reactance of the choke and X_e is the subtransient reactance of the machine. The synchronous machine can be simplified in this subtransient reactance because only the non-homopolar

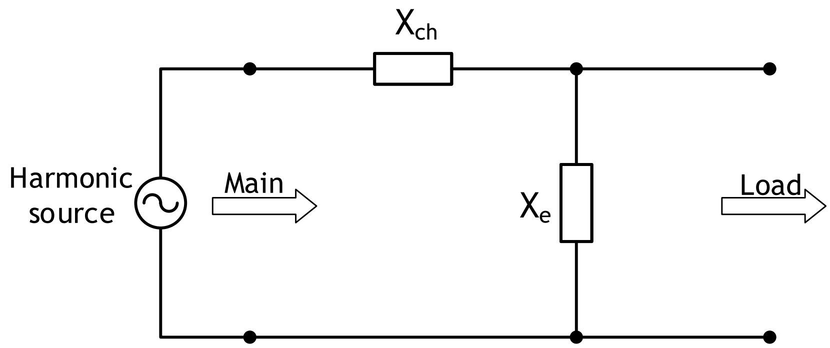

Figure 3.7
Simplified circuit considering harmonics from the main

harmonics are considered. This reactance can be noted X''_d. Then, the voltage divider formula can be used. If the voltage seen by the load is U_{load} and the one coming from the main is U_{main}:

$$\frac{U_{load}}{U_{main}} = \frac{X''_d}{X''_d + X_{ch}} \tag{3.3}$$

As one can see, the formula is independent of the considered harmonic. Then, if the reactance X_{ch} is very big and the subtransient reactance of the machine is very small, the resulting voltage will be very small. When considering the homopolar harmonics, the same principle can be applied but the reactance X_e is now equal to the zero-sequence reactance of the machine. This one is also small and the results are the same.

The set machine-choke also enables the filtering of:

- Non-homopolar harmonic currents from the load
- zero-sequence currents from the load
- Voltage harmonics due to current harmonics from the load

Each time, the same diagram (with correct reactances) can be used and the results are found using either the voltage divider or the inductive shunt model.

3.3.3 Power factor compensation

All this part comes from a Technical Information [2] made for customers by the company.

In this part, a simple choke is used because the focus is made on the left portion of the diagram. The results are similar with a three-point choke.

Usually, a load consumes active power and produces or absorbs reactive power. This results in a certain power factor $\cos\phi$. An increase in reactive power yields to an increase in the current from the main and in additional costs. Then, in steady-state, the machine can improve this power factor. This is done by supplying or absorbing the reactive power required or produced by the load. The machine performs this thanks to the control of the voltage at the load terminal. The voltage is maintained around 1pu at this point. Moreover, the grid also maintain the voltage around 1pu. Then, following equation 3.2, if the voltage on both side of the choke is at 1pu and that the phase angle difference across the choke remains small, the reactive power flowing through the choke remains very small and the power factor remains

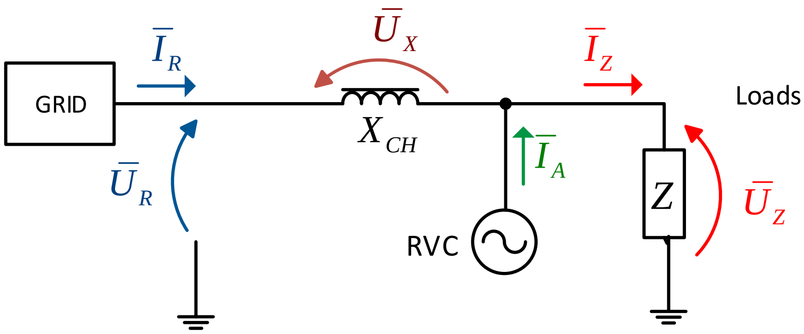

Figure 3.8
Diagram in steady-state

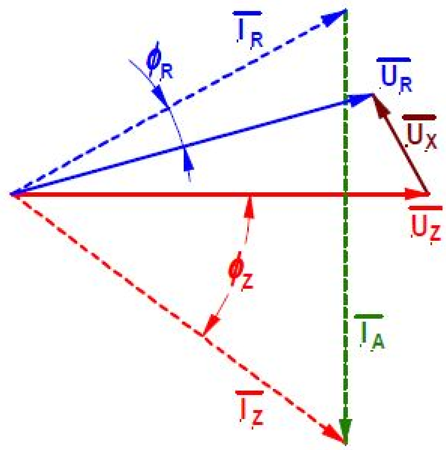

Figure 3.9
Power factor compensation when $U_{main} = 0.9pu$

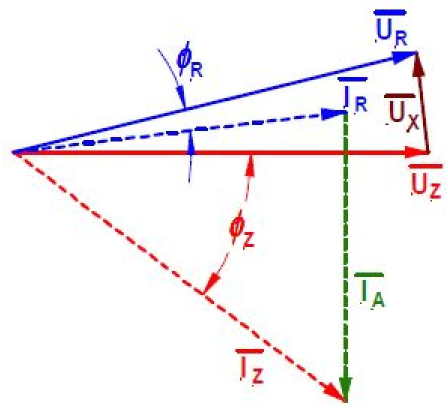

Figure 3.10
Power factor compensation when $U_{main} = 1pu$

close to 1. In fact, the machine acts as a synchronous compensator.

This compensation can be achieved whatever the voltage of the main. The behaviour is explained hereafter when this voltage is equal to 1 pu and to 0.9 respectively. The quantities used here are defined in figure 3.8.

As the system is in steady-state, it is governed by the following set of equations:

$$\bar{U}_R = \bar{U}_X + \bar{U}_Z \tag{3.4}$$
$$\bar{I}_R = \bar{I}_Z - \bar{I}_A \tag{3.5}$$
$$\bar{U}_X \perp \bar{I}_R \tag{3.6}$$
$$|\bar{U}_X| = X|\bar{I}_R| \tag{3.7}$$
$$|\bar{U}_Z| = U_{nom} \tag{3.8}$$

The first two equations are second and first Kirchhoff's laws. The third one expresses that there is a 90° phase lag between the current in the choke and the voltage across this one. The fourth one is Ohm's law applied to the choke and the last one expresses that the load is running at its nominal voltage. If one assumes a standard load power factor equal to 0.8, the phasor diagrams corresponding to this set of equations can be drawn. This gives the diagrams shown in figures 3.9 and 3.10.

At the end, the power factor can be computed. It is higher than 0.9 in both cases and is higher than without the machine. In fact, the machine provides the reactive power to the load. For the first case, it also provides reactive power to the grid due to the smaller voltage. The reactive power consumed by the choke is produced by the machine in this case. When $U_{main} = 1pu$, it can be shown that half of the reactive power consumed by the choke is produced by the machine and half is produced by the main.

The behaviour is similar for other main voltages and if the load produces reactive power. At the end, the power factor is better in all cases provided than the load consumes enough active power (not too small loads).

To conclude on the requirement of the system:

- The synchronous machine needs to have a subtransient and zero-sequence reactance as small as possible. This is obtained by over-sizing the machine. However, there is a limit due to the increase in the losses with the machine size.
- The choke reactance (portion AB) has to be high enough. However, this one has to stay in a reasonable range in order to not consume too much reactive power and to not induced a too big phase shift across the choke when the active power flow.
- A three-point choke is used in order to improve the voltage compensation.

Chapter 4

Modelling of the network

The basic diagram of the equipment is shown in figure 3.6. This chapter aims at introducing the modelling of the different parts of the studied system in ERACS. The principle diagram is shown in figure 4.1. This one shows the total circuit and can be divided in three main parts, from the left to the right: the utility side, the voltage conditioner and the loads. These three parts are detailed hereafter separately.

4.1 ERACS

ERACS is an electrical power system analysis software. This one belongs to the group RINA. It consists of several modules called Loadflow, Fault, IEC 909, Harmonic injection, Harmonic impedance, Protection co-ordination, Transient stability, G5/4 and Arc Flash Risk Assessment.

A full description of the software and its module can be found in the ERACS technical manual [20]. This section aims at giving a slight overview of the implemented procedure behind the software interface.

Several projects can be created in Database. In these, several networks can be created to model the different studied situations. Inside these networks, several situations can be stored. These illustrate the change in the parameters. The diagrams are built on a plane linking elements together. There are, for example, transmission lines, bus, cables, synchronous machines (generators or motors), induction machines, loads, ... A library is associated to the project and contains all the data for the elements. This one can be shared between projects,... These elements are called keys and each element of the diagram is linked to a key.

Two modules are going to be used in this study, the loadflow and the transient stability modules. These

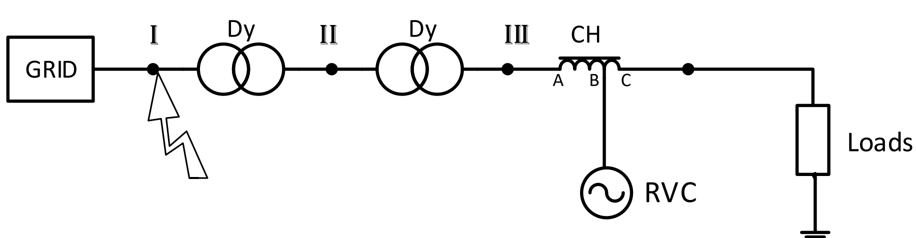

Figure 4.1
General diagram of the studied situation

are described briefly hereafter.

4.1.1 Loadflow module

The loadflow module consists in computing the steady-state configuration of the system. It gives the voltage profiles, the power flows, the current flows, the power productions,... ERACS uses an iterative procedure to solve the system of equations driving the system. The procedure is the following:

1. Interpretation of the system data (element parameters, ...).
2. Equivalent representation of the non-linear elements present in the system (synchronous machine, variable impedance shunt, load tap changing transformer and induction machine). These are represented as a fixed admittance device. During this step, a voltage profile of 1pu is assumed.
3. Construction of the admittance matrix **Y** and its inverse, the impedance matrix **Z**.
4. Computation of the injection currents related to the non-linear elements (machines). These are computed assuming a 1pu profile and assembled in the vector of injection current **I**.
5. Computation of the voltage profile by solving $\mathbf{V} = \mathbf{ZI}$.
6. Adjustment of the vector of injection current **I** to get the expected conditions at the terminal of each element (knowing the voltage profile **V**).
7. Testing of the convergence by computing the difference between the voltage profile and the network elements behaviour: if it is smaller than the convergence, the next step is step 8. If it is not good, step 5 is repeated.
8. Getting the final admittance matrix knowing all the voltages **V** and the injection currents **I**.
9. Computation of the final matrices (**Z** and **Y**) and post-processing of the results.

The modelling using the injection current is illustrated hereafter with an example. Let a constant power load consumes 0.5pu of active power and 0pu of reactive power.
In general, it is first modelled, assuming $V = 1pu$ at its terminal, by an admittance of $0.5 + 0j$. It corresponds to step 2 of the process. The corresponding injection current is 0pu (step 4). These values are put respectively in the admittance matrix and the injection current vector.
Then, the system terminal voltages are computed as stated in step 5. This can give a load terminal voltage different from 1pu. The value of the admittance has to be changed to keep a constant consumed power. For example, if V becomes 1.1 pu, it has to be set to 0.41322pu. In this case, the input current is equal to 0.4545pu ($0.4545 * 1.1 = 0.5pu = P$).

Instead, in ERACS, the Norton equivalent is used. This one dissipates the same power as the original circuit by keeping the same input current but varying the current source. The admittance of this one is the same as the initial value ($0.5pu$) and the current source is set to correct the power. In this case, this equivalent current source is equal to $-0.1367pu$ (entering the source). Then, the current entering the equivalent admittance is equal 0.4545+0.1367 = 0.55. The current adjustment corresponds to step 6. Then, the next iteration is started if the convergence is not good.

At each step, the non-linear element behaviours are adjusted using the controlled injection currents. Then, only this vector is modified. The admittance matrix is therefore not modified and both speed and convergence are improved.
Concerning the voltage terminals of PV machines, the angle of the slack machine or the voltage hold by

grids, these can be modified using the injection currents (at step 6). For example, to obtain a zero phase for the slack bus angle, all the current phases can be shifted.

4.1.2 Transient stability module

This module enables the time analysis of the network. Several types of disturbances can be applied to the element of the system (fault, failure of generator,...) and the time evolution of the system is studied. This software uses the phasor approximation but is able to divide the different sequence. Therefore, unbalances can be considered.

Two basic hypotheses are made in this module. The first one states that the electromechanical devices (motor and generators) and their controllers control the dynamic evolution of the system. This is equivalent to stating that the time constants of the network are big. Then, there are no transport delays. The second main hypothesis states that the positive sequence dominates. Therefore, the two other sequences are used only when needed (computation of fault current).

The procedure used is the following:

1. Read values obtained from loadflow and the additional informations of the motor(s) and the generator(s).
2. Construct the admittance and impedance matrices **Y** and **Z** of the system.
3. Initiate the state variables of the machines and of their controllers.
4. Start the procedure:
   (a) Check event schedule
      - Yes: Execute it and calculate network flows.
      - No: Go to step (b).

   (b) Compute the state variables by solving the differential equations (Trapezoidal integration method).

   (c) Inject the resulting current to get the voltage profile (same as loadflow).

   (d) Check the tolerance:
      - OK: Go to step (e).
      - Not OK: Go to step (b).

   (e) Update the vector of results, update the time and adapt the step size.

   (f) Go to step 5 if the time is finished or repeat step 4.
5. Post-process of the results.

ERACS automatically adjusts the integration step used during the resolution of the differential equations. The computation is then quicker than otherwise. If nothing happens, it detects it and increases this step. Otherwise, it decreases it.

Nominal power [MVA]	$V_{nom,1}$ [kV]	$V_{nom,2}$ [kV]	R [pu on rating]	X_l [pu on rating]
2.5	11	0.4	0.005	0.07

Table 4.1
Data of the distribution transformer between locations II and III

4.2 Utility side

ERACS allows us to apply events in the module called "Transient stability" and to explore the response in the time domain. These events can be of several types. For example, it can be faults, switched on of synchronous machines or starting of motors. These faults can be of four types: single-phase-to-earth, phase-to-phase, two-phase-to-earth and three-phase. As seen in the chapter on voltage dips, there are seven types of dips. These can be obtained using two or one Dy transformers between the fault and the observation location. This principle is used here to create "artificially the different types". Thanks to this, all the possible voltage dip types due to faults can be studied.

The grid model holds a voltage of 1 pu. It has a short-circuit power equal 100 MVA and a X/R ratio of 10 (for all sequences). It corresponds to an impedance equal to 0.1 + 0.995j pu (on its own base).

The transformer between the locations I and II (between high and medium voltage) is there only to model the possible change of fault. Then, it is modelled using a transformer with a very small resistance (almost zero) and a zero leakage reactance (for both sides). The nominal voltages are 36 and 11 kV for side I and II respectively. This one is going to be changed into a Ynyn transformer depending on the expected type. The second transformer is set to realistic values because it models the one at the entry of the company. This one is usually present and influences the results. Then, it has to be modelled. It is of type Dyn and the nominal voltages are 11 and 0.4 kV respectively for locations II and III. The data entered in ERACS for this equipment are given in the table 4.1.
ERACS uses the approximation that the magnetising reactance of the equivalent transformer is very big and can be neglected.

Concerning the fault, it will always be applied at location I. The magnitude and the phase angle jump of the voltage during the fault are going to be adjusted using the fault impedance Z_g. This one is the impedance between the ground and the faulted phase(s). The expression of the remaining voltage can be obtained for the various types of fault. The development for the three-phase and single-phase faults are given in appendix D.

In this study, it is assumed that the voltage at BUS-1 comes back at its initial value when the fault is cleared. It is, for example, a case where the line has not been tripped or has been reclosed. In fact, due to the way the fault is modelled, ERACS does not allow to have a different voltage after the dip.

A remark can be emitted concerning the voltage dip types B and E. These are obtained by observing the fault at the same location as the application point. In practice, the distribution transformer is going to stay of Dyn type. There will be at least one transformer between the location of the fault and the observation point. Then, these can not be observed in this system and are not going to be studied. In practice, these corresponds to type where a zero sequence is present. In fact, the majority of the loads are either connected in delta or through a Dy transformer. This one suppresses the zero sequence and the types B and E are not common.

$T_{f,N}$	$T_{f,D}$	SC	ΔU^2_{max}	$K_{p,s}$	$K_{i,s}$	$v_{f,max}$ [V]	$v_{f,min}$	T_f [ms]
2.4e-4	3.7e-3	0.0364	29,1	73,6	50	44	0	10

Table 4.2
Parameters of the controller in the s-domain

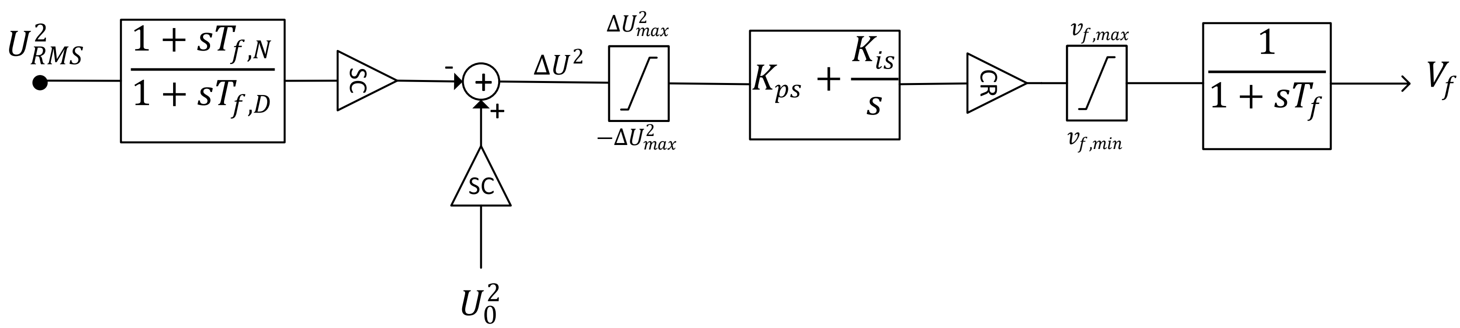

Figure 4.2
block diagram of the final Automatic Voltage Regulator

4.3 Voltage conditioner part

The principle diagram has already been discussed. The two elements to model for this part are the synchronous machine and the three-point choke.

The synchronous machine is modelled using the model of a synchronous generator given in ERACS. This one allows to enter the data using the Park equations. The data of the studied machine are given in the Appendix A. This machine is assumed to be directly connected to the choke (no cable or transformer).

The software allows to link an Automatic Voltage Regulator (AVR) and a governor to the machine. These can be built using the module called *UDM*. In the studied case, the AVR is going to be the same as the one used by EURO-DIESEL for their machine. In practice, this one is implemented in a micro-controller. Therefore, it is implemented in the discrete domain while ERACS uses a continuous system. Then, the coefficients have to be converted using a transformation. The "bi-linear transformation" is used here. The discrete controller and more details about the transformation are given in the appendix F.
After simplification, the controller of the AVR in the s-domain is given in figure 4.2. The values of the parameters are given in table 4.2. In this controller, the first block is the filter and the second one is the PI controller. This AVR is linked to the load bus. The input, the set point entry and the output are all in pu.

As the machine does not provide active power to the system (except through kinetic energy conversion), there are no turbines or diesel engines linked to it. Then, no governors are attached to the synchronous machine modelled.

The data corresponding to the three-point choke are given in the Appendix B.
For this element, an equivalent schematic has to be derived. The general schematic is given in figure 4.3. L_1, L_2 and M are respectively the inductance of the AB and AC part and the mutual inductance between the two parts. The equivalent schematic can be obtained by using short-circuit and open-circuit tests. This gives the schematic shown in figure 4.4. In this equivalent schematic, a negative value should be given to the B winding.
The problem is that ERACS does not allow to assign negative values to inductances. A capacitor could

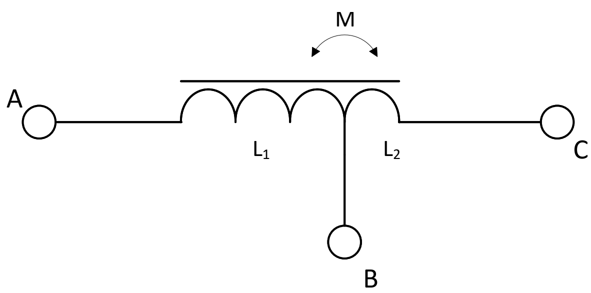

Figure 4.3
General schematic of a three-point choke

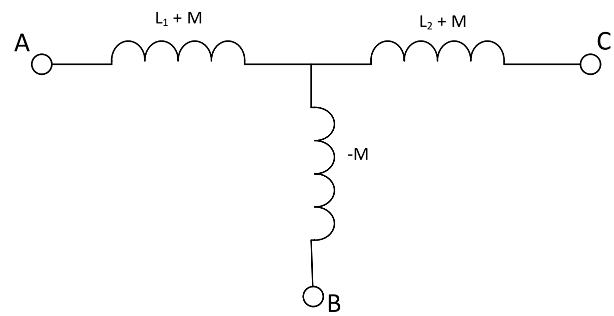

Figure 4.4
Equivalent schematic of a three-point choke

have been used to model this but this works only in static. Then, a different way is to use a three-winding transformer because ERACS allows to set negative values to their leakage reactances. Then, the equivalent leakage reactances are set to the corresponding values of the schematic. The transformer ratios are equal to 1:1 because the three-point inductance does not transform the nominal voltage.
For the total wire resistances (for both parts), these are computed knowing the total losses (given in Appendix B). The ratio of the number of turn is equal to 6 between the parts AB and BC. Then, the total resistance obtained is multiplied by 5/6 and by 1/6 respectively for the side AB and BC. The corresponding equation are:

$$P_{losses} = 3R_{total}I_{nom}^2 \tag{4.1}$$

The factor 3 comes from the fact that the nominal current is a one-phase current. All the values are in natural units. This gives a total resistance equal to 0.42 mΩ. This gives that the resistances on both sides are equal to $R_{AB} = 0.35\ m\Omega$ and $R_{BC} = 0.07\ m\Omega$. For the third wire (from B to the synchronous machine), the resistance is assumed to be negligible.
The last thing to add to the transformer is the ground. The inductance does not modify the zero-sequence element and does not represent an open-circuit to this sequence. The transformer should to have a similar behaviour. Then, the way to model that is to use a star transformer with all three grounds connected. The impedance to the ground is equal to zero in each winding.
Concerning the zero-sequence impedance of the transformer model, this one depends on the choke type. As the choke used by the company is a shell type, this impedance is set to the same value as the positive- and negative-sequence impedances.

4.4 Load side

The total load is assumed to consume 80% of the nominal apparent power of the machine. The equipment has a nominal power of 2500 kVA. Then, the load consumes 2000 kVA.
The load can be modelled in ERACS using different elements depending on its nature. The load studied is a typical load encounter by the company. It consists of a data centre and is composed of two parts:

- A part absorbing a constant power and functioning at a constant power factor (set to 0.95). This models the power required for the servers, ... It constitutes 4/5 of the load or 1600 kVA.
- Induction motors used to model the fans, ... that cool down all the IT equipment. Its consumption is set 320 kW. Then, it consumes the last 1/5 of active power provided.

The constant power part consumes 1600 kVA with a power factor equal to 0.95. Then, it absorbs 1520 kW and 525.89 kvar. The motor set consumes 320 kW. In fact, it is constituted of three smaller motors

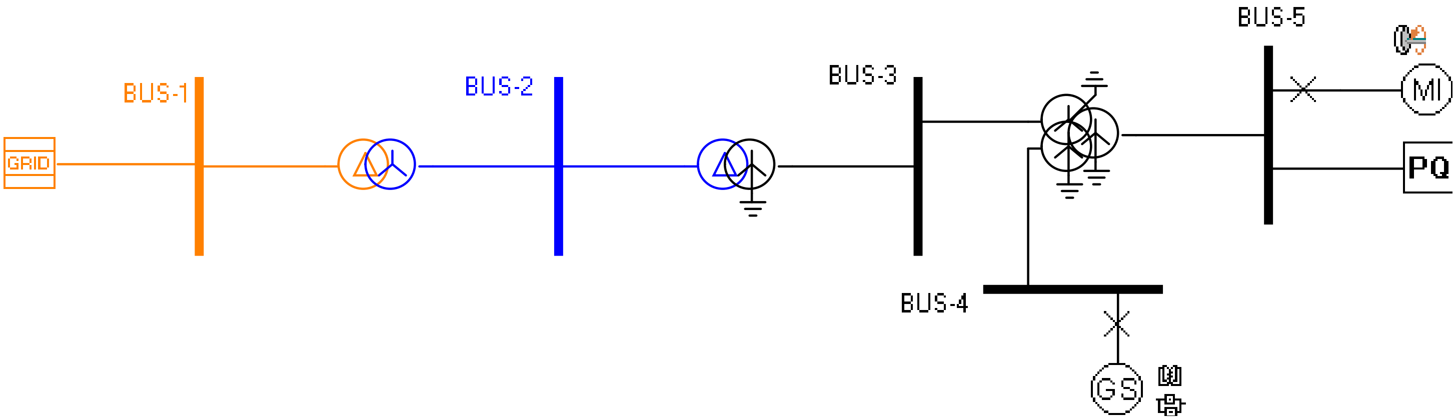

Figure 4.5
Final diagram used to model the system

(nominal power 145 kVA). All the loads have a nominal voltage of 0.4 kV. The data of the motors are provided in Appendix C. These come from the ERACS reference library.
ERACS provides a way to model the mechanical load of the motor. Then, in this case, it is modelled using the equation 4.3 from [27]. In this case, T_{m0} is the load at synchronous speed ($\omega_r = 1$), A, B and C are three constants respectively equal to 1, 0 and 0 and ω_r is the rotor rotational speed. This relation is typically used for fans. This type has been chosen because it suits the best to the model of a cooling system a system. The inertia constant H corresponding to this load is equal to 0.7s. The motors are assumed to be two-pole machines. The nominal power taken to convert is the one of the machine (given in C). This gives:

$$H = 0.7s = \frac{0.5J\omega^2}{S_N} \Longleftrightarrow J = \frac{0.7S_N}{0.5\omega^2} = 2.0568kg\ m^2 \tag{4.2}$$

$$T_m = T_{m0}(A\omega_r^2 + B\omega_r + C) \tag{4.3}$$

The final diagram studied here is given in figure 4.5.
An important remark has to be made concerning the constant power loads in ERACS. In the transient module, these ones are implemented as constant admittance loads. The value of these is computed based on the loadflow results. This means that the powers (active and reactive) vary greatly with the voltage during transient. In practice, the voltage is going to decrease during the dip. Then, the power is going to decrease too. This yields to a less severe case because the active power that the machine will have to produce is smaller.
It is interesting to study the case with a real constant power load. For this, another way to model it has to be found. This is further explained in dedicated section.

4.5 Hypotheses and limits of the software

ERACS is a numerical tool. It can solve numerous equations but has to make some approximations and hypotheses. These add to the hypotheses made in order to model the system.

The first limit of ERACS is that it focuses mainly on the direct sequence of the network. Therefore, only the values in this sequence can be retrieved. In practice, when considering unbalanced faults, all the network has to be reconstructed. This limits the possible size and complexity of the studied network. In this case, the network is easy to reconstruct so this is not a problem but for more complex ones, it can become very difficult. This is the reason why it is not an approximation but more a limit of the software.

The first real approximation is that the controller of the synchronous machine uses the positive sequence voltage. This is a little bit different than what is done in practice (control on the real voltage). This is a strong approximation but nothing can be done about this as it can not be changed in ERACS.

Then, the next hypothesis made in the software is the phasor approximation. This one is not very strong and is discussed further in [29]. It is done in many softwares and is really acceptable for this study.

Afterwards, a simple remark can be emitted concerning the transfer of voltage through transformers. This one does not take the phase shifts into account. This is a really acceptable approximation. However, these phase shifts can be retrieved easily.

The next hypothesis is due to ERACS model of components. This applies to motors and constant power loads. For the zero-sequence equivalent network, these are modelled as open-circuit and it can not be changed [20]. In this case, it does not matter because it is behind a *Dyn* transformer that does not transmit the zero-sequence component. In practice, however, special care has to be taken on the way it is modelled.

Sixth remark, ERACS offers various ways to model loads (constant power, constant admittance, constant current, ...). However, in transient, these are all modelled as constant admittances (based on their load-flow values). Then, the choice of load becomes more limited in this module. ERACS offers a way to model these thanks the "controlled shunt" but this one is not direct and new models have to be built.

Last limit of the software, there are limited ways to model the dip. Then, the hypothesis that the network comes back at the same operating point has been made. Then, the tripping of a line or other events modifying the topology can not be modelled.

Afterwards, some hypotheses have been done when modelling the system. It concerns the dip model. This one is modelled by varying the impedance of the fault. This one has been derived using the hypothesis that the grid is the main feeder. This hypothesis is further discussed in the appendix D but it gives pretty good results.

The next hypothesis has been made during the derivation of the automatic voltage regulator and concerns the "bi-linear transformation". This is further discussed in Appendix F but the assumptions made there are usual ones.

The last thing to mention is the approximation made in order to fullfill the data of the synchronous machine. These are not exactly the same as the ones needed by ERACS. Then, the missing ones have been derived using rules of good practice given in the software technical manual [20].

Chapter 5

Simulations

This chapter describes the results obtained after the simulations of the system. Faults of different types are applied on BUS-1. The sections are organised depending on the dip type. Then, types A and B are analysed because they constitute respectively the most severe dip and the most common dip. In fact, the Type B, corresponding to a single-phase fault, is observed after a transformer *Dyn* (the distribution transformer). Therefore, it becomes a type C.
For both types, the results using the rotary voltage conditioner are compared to the standard power acceptability curves. In the base case, the system contains only the loads and the distribution transformer (and the second transformer to model the different types). In this one, the load is subjected to the dip directly and the limit accepted for the loads corresponds the power acceptability curve. This base case is shown in figure 5.1. In this one, all the data are the same as for the complete case. For each type, the maximal duration tested is 1s. This is done to focus on small dips that can happen very frequently in the network.

In all figures of this chapter, unless expressly specified, all the voltages are the remaining ones and not the depth of these.

5.1 Stability of the machine

From [30], the stability of the machine can be studied using the simple model shown in figure 5.2. The active power produced by the machine is function of its load angle δ and is given by:

$$P(\delta) = G_{eq}E'^2 - |Y_{eq}|E'E_{eq}\cos(\delta - \eta) \tag{5.1}$$

with $Y_{eq} = 1/Z_{eq} = G_{eq} + jB_{eq} = |Y_{eq}|e^{j\eta}$.

Then, if the mechanical power given to the machine is called P_m, the so-called Swing equation can be derived:

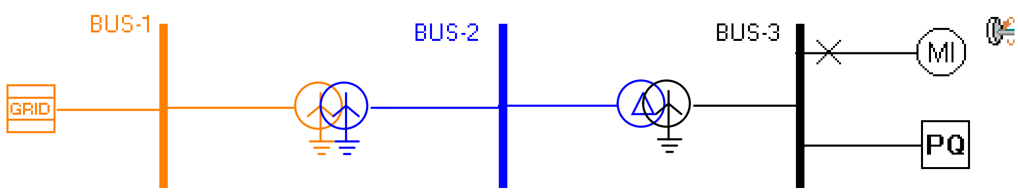

Figure 5.1
System without voltage conditioner

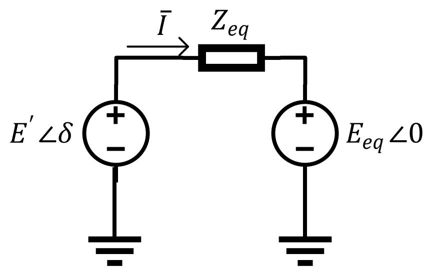

Figure 5.2
Equivalent schematic used to study the stability of a synchronous machine

$$M\ddot{\delta} = P_m - P(\delta) \tag{5.2}$$

This one traduces the energy conservation of the machine rotor. During a fault, the electrical power released to the network by the machine changes and the rotor acceleration will change following equation 5.2. From this equation, the equal-area criterion can be obtained. In figure 5.3, the mechanical power and the $P(\delta)$ curves (called P_v) are drawn. The equal-area criterion says that the system is stable if $A_{acc} - A_{dec} > 0$ (in the case illustrated on the diagram). The accelerating area A_{acc} is given by the part where the machine receives more mechanical power P_m than it can release to the network ($P(\delta)$). In this case, using the Swing equation 5.2, the acceleration of the rotor $\ddot{\delta}$ is positive. The decelerating part A_{decc} is the part where the acceleration of the rotor is negative. This means that the mechanical power is smaller than the part released in the network.

Figure 5.3 summarises the behaviour of the system when a fault occurs. In this case, the mechanical power given to the machine is constant. Before the fault, the power curve is given by $P_v(\delta)$. Then, when a fault occurs, the machine can not release the active power produced (or at least less). The curve becomes $P_d(\delta)$. It results in an acceleration of the rotor. When the fault is cleared, the system is usually weaker because the line is not in operation anymore. It results in a new curve called $P_p(\delta)$. The two areas described before depend on all these curves and are also shown in the figure.

The case of the machine considered here is a little bit different. Indeed, the mechanical power provided to this one is zero. Therefore, the machine works in the other part of the diagram. This part corresponds to negative load angle δ. The representation here is presented in figure 5.4. This curve comes directly from a simulation by taking the evolution of power of the machine and of the load angle. In this one, the initial functioning point is represented at coordinate ($-18°$; 0MW) (step 1).
Then, a fault is applied and the active power produced by the machine becomes positive (step 2). This is due to the fact that during the fault, the machine produces the active power required by the load. The $P(\delta)$ curve is changed due to the topology change in the system. This power being bigger than the mechanical power received, the rotor decelerates (according to swing equation) and follows a curve $P_d(\delta)$ (step 3), the corresponding curve during the fault. It gives the decelerating area represented in orange on the figure. The active power produced comes from the kinetic energy of the machine.

When the fault is cleared, the power produced by the machine becomes negative. In fact, the machine receives power from the grid in order to recover its released energy (step 4). At the beginning, the rotor still decelerates because of its inertia (step 5). At a moment, the value of the load angle reaches a minimum and then, starts to increase. At this time, the rotor starts to accelerate. This part is characterised by a mechanical power received bigger than the active power produced (negative) (step 6). Therefore, it corresponds to the accelerating area and is represented in green.

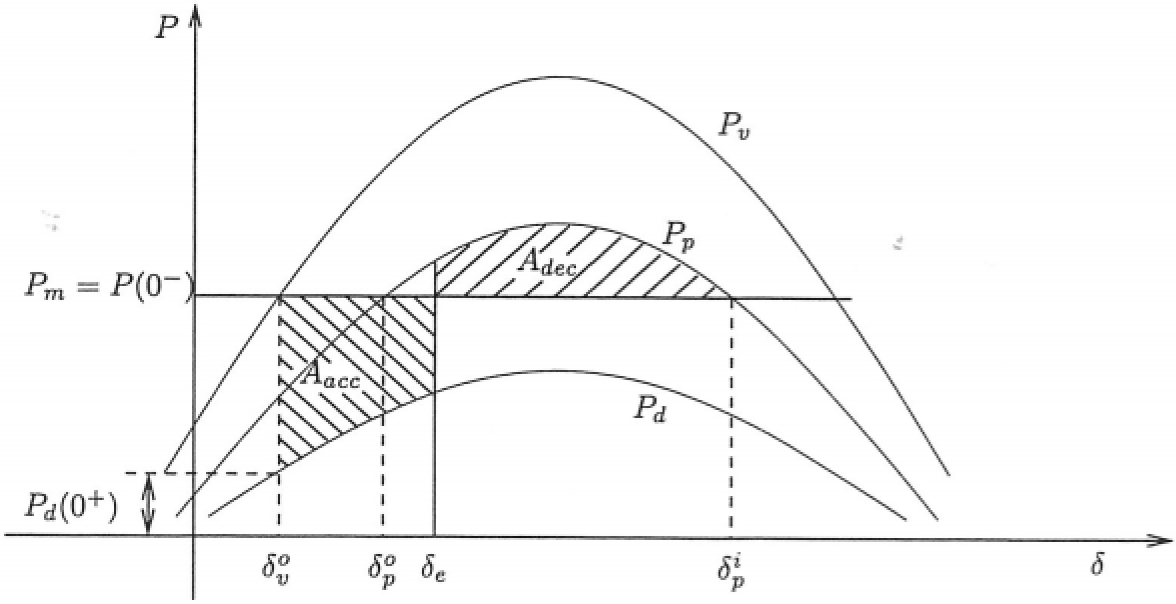

Figure 5.3
Active power as a function of the load angle δ before during and after the fault

Afterwards, the rotor starts to oscillate but stay stable. In fact, the load angle will increase due to the acceleration of the rotor. It will pass the equilibrium point due to its inertia. Its acceleration is going to decrease and the machine load angle δ will reach a maximum. At the point, its acceleration is zero and it will start to decelerate (following the swing equation). This process repeats again but the amplitudes of the oscillations decrease due to the damping of the system. When these are completely damped, the rotor is stabilised at its equilibrium point. This one corresponds to the same point as before since the $P(\delta)$ curve is the same as before the dip (no network change).
The stability of the machine is ensure if the green area (accelerating area) is bigger than the orange area (decelerating). In the other case, the load angle of the machine reaches the value corresponding to the unstable equilibrium. Then, it can not come back to its initial point. Indeed, for values of δ smaller than those of this limit case, the machine continues to decelerates. This limit value is the point where the post-fault $P(\delta)$ curve crosses the 0-axis.

All the stability study can be done on diagrams similar to figure 5.4. In fact, the areas are changed when the parameters of the dip change. This results in change in the stability.

This diagram can be found in the case where the dip is severe and an equilibrium can not be reached during the dip. In fact, as shown in figure 5.4, the $P_d(\delta)$ curve during the dip does not intercept the 0-axis (equal to the constant mechanical power line). Another situation is possible when the dip is less severe. In such a case, an new equilibrium can be found because the $P_d(\delta)$ curve intercepts the mechanical power line (equal to zero for all load angles). The same principle can be applied to find if the system is stable. If the new equilibrium exists and if the fault is applied sufficiently long enough, the new equilibrium will be reached after oscillations. The influence of these oscillations is going to be studied more precisely in the next part. Obviously, at this equilibrium, the active power produced by the machine is zero. Theoretically, the machine can operate at this point. However, in practice, the machine is going to increase its reactive power production to maintain the load voltage around 1pu. This is done by increasing the field current but in the long term, it can become too high and some limits on this one can be activated.

After the fault, when the voltage recovers, the same principle can be applied. In fact, the "initial" jump

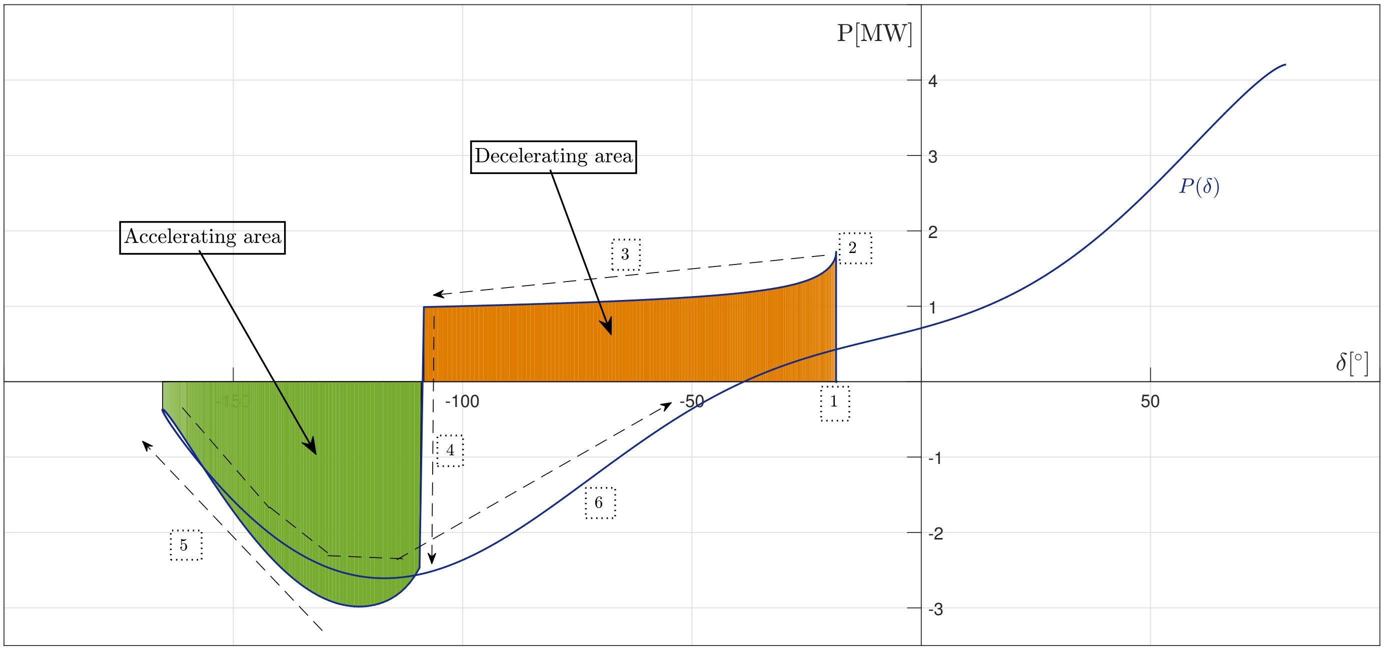

Figure 5.4
Curve $P(\delta)$ and equal area criterion in the studied case

of power will be negative like previously and will come back on the initial $P(\delta)$ curve (the system is the same as initially). The stability can again be studied using the equal-area criterion and the definition of these two areas.

5.2 Type A

The type A results from a three-phase fault. This can be observed whatever the location of the dip (I, II or III). In this case, the system used is the one with an ideal Ynyn transformer and the distribution transformer Dyn.

In this section, the parameters of the dips and their influence are going to be illustrated and analysed. To recall, these are magnitude, duration, phase angle jump and point-on-wave. As pointed out in section 1.1.4, the influence of the initial point-on-wave can not be assessed. Therefore, this one is not going to be investigated. At the end, the worst phase angle jump is going to be taken in order to plot the "new" power acceptability curve when the device is present.
This type of dip is the most severe one and the stability of the machine is not guaranteed for all these. Then, a little study of the influence of the dip parameters on the machine and its stability is useful. This one is critical because in order to be accepted, a dip has to release the machine connected and stable.

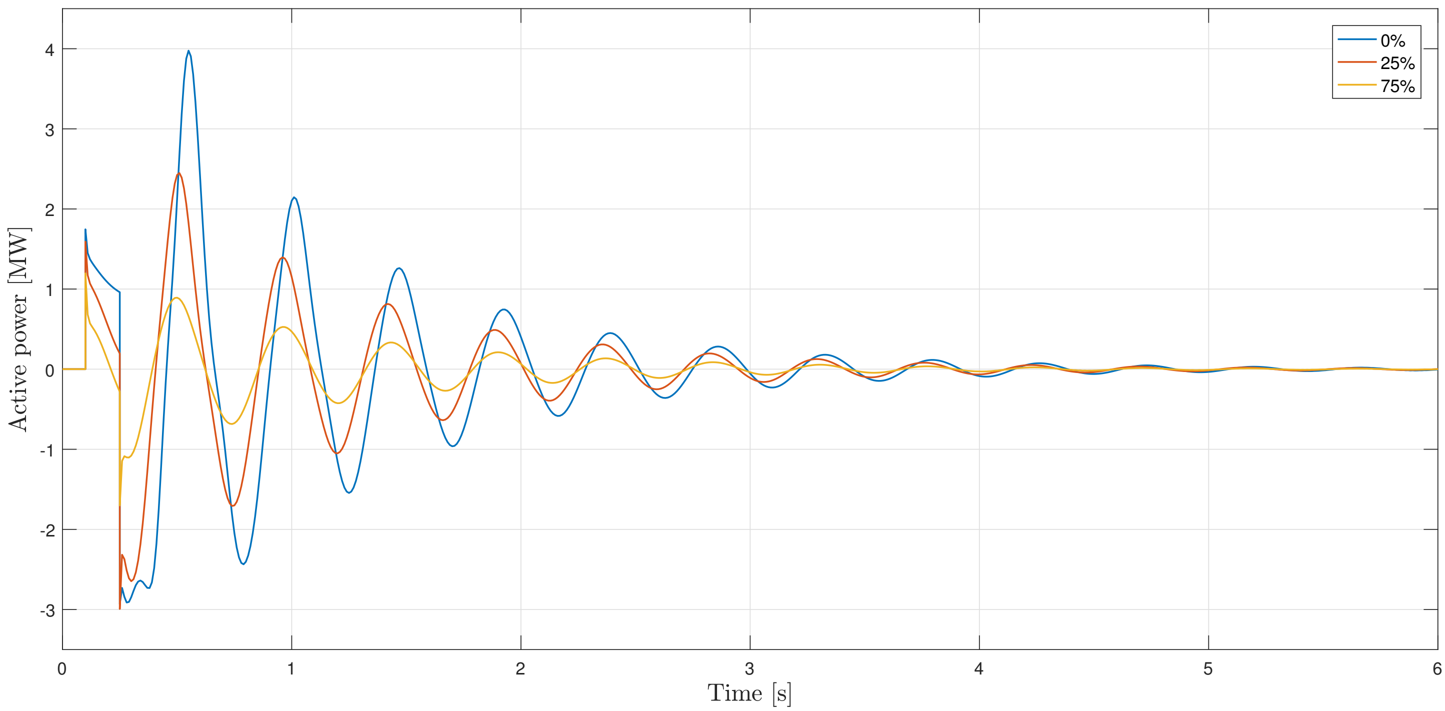

Figure 5.5
Evolution of the active power produced by the machine against time for various remaining magnitudes

5.2.1 Magnitude influence

The magnitude is the norm of the remaining voltage phasor. In this case, this one is the voltage at the fault location. Then, several simulations with varying magnitude are carried on (0, 25 and 75% of remaining voltage). In this case, the duration is maintained at 150ms and the PAJ is equal to $-10°$.

The influence of the remaining magnitude on the stability of the machine can be explained using figures 5.5, 5.6 and 5.7. Using these, the influence of the magnitude becomes clearer. In fact, decreasing this one tends to increase the amount of active power given by the machine during the dip. It has an influence on the first peak power and on the slight decrease in this power. In term of $P(\delta)$ curve, it turns on that the increase in active power production during the dip increases the decelerating area. Then, the case becomes more severe and is more susceptible to destabilise the machine.

It can be emphasised that the active power produced by the machine is due to the fact that the grid can not supply entirely the active power to the load. Then, the machine has to provide this power. This one is bigger when the dip is deeper. The oscillation phenomenon when the machine has to come back at equilibrium can be clearly shown in figure 5.6. This one shows perfectly the oscillations of the load angle due to the successive acceleration and deceleration of the rotor.

The influence on the load voltage is shown in figures 5.8 and 5.9. The simulated case is a little bit different than the previous one in order to illustrate the stability limit (the duration is extended to 200ms). This shows that the voltage decreases with time. This was expected as the active power given by the machine decreases. It shows that the magnitude of the dip influences the magnitude of the load remaining voltage. This one decreases as the dip increases.
Concerning the load angle, as seen on 5.9, the deeper the dip, the more the oscillations as explained

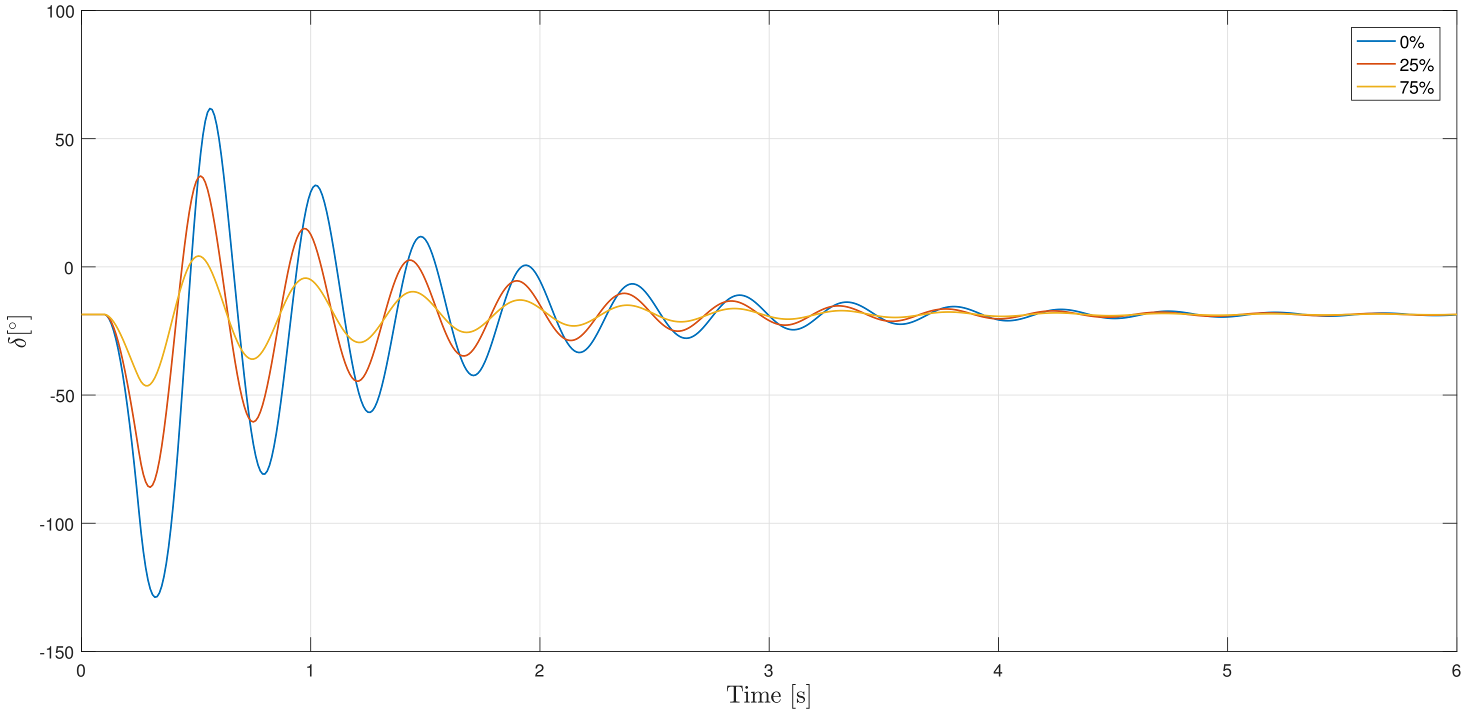

Figure 5.6
Evolution of the machine load angle δ against time for various remaining magnitudes

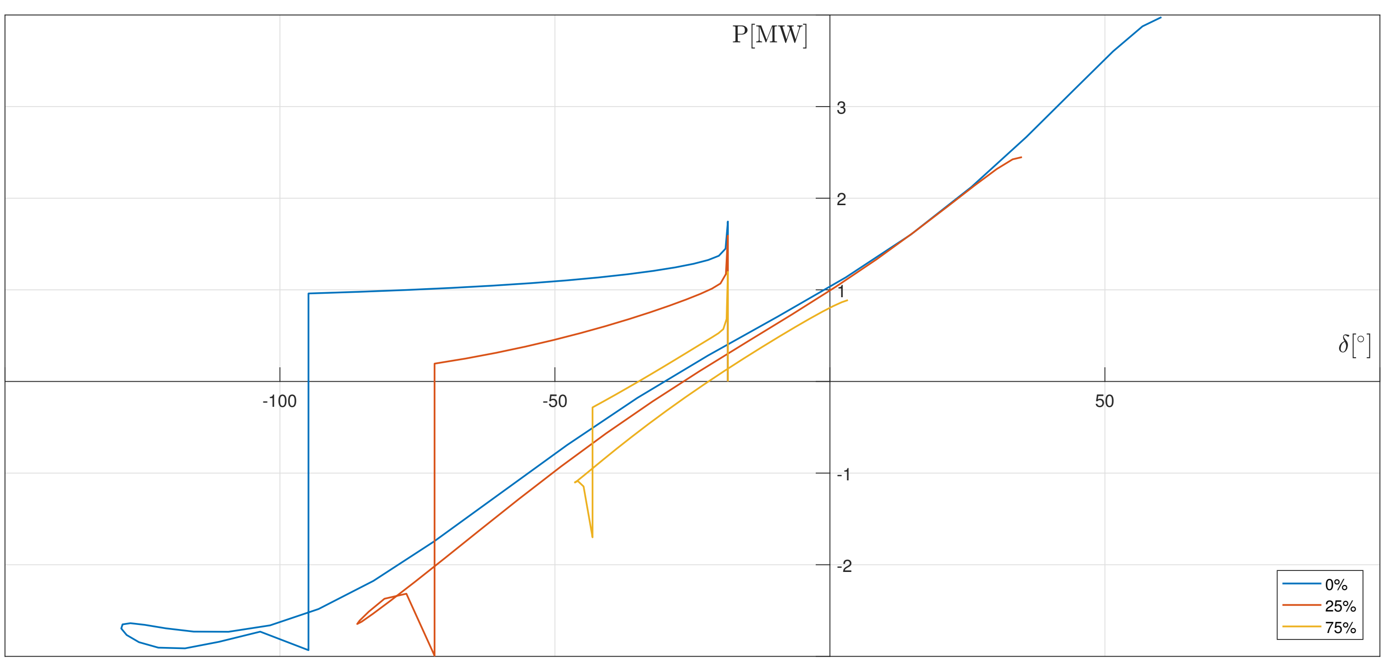

Figure 5.7
$P(\delta)$ curves of the machine for various remaining magnitudes

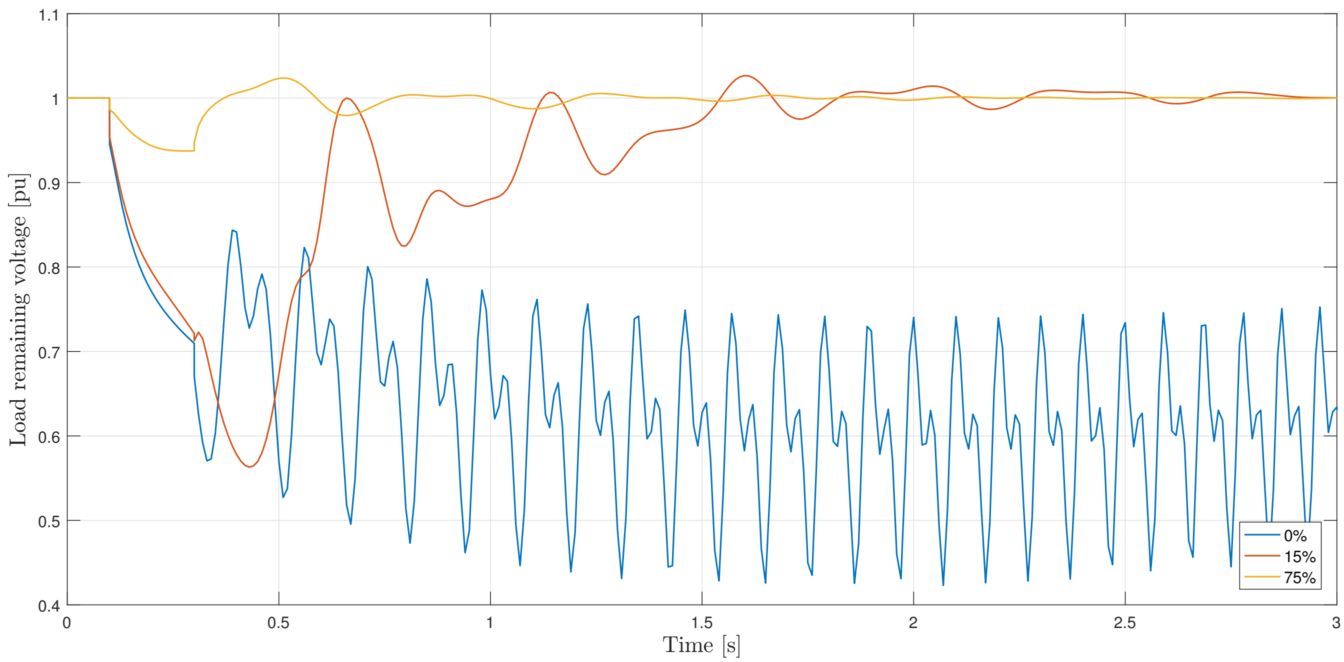

Figure 5.8
Influence of the magnitude on the remaining load voltage

before. If this dip is too severe, the machine becomes unstable. In this case, the machine should be stopped before being damaged or destroyed.

Nevertheless, in the case of a 200ms dips, the machine can take back voltage dips up to 15% (remaining) before becoming unstable. One must also be careful that the load voltage remains in the limit of the standards. Nevertheless, compared to the case without voltage conditioner (CBEMA curve), the response is well increased.

5.2.2 Duration influence

The influence of the duration can be analysed in a similar way as the magnitude. The curve of the active power produced by the machine and the $P(\delta)$ curves are shown in figures 5.10, 5.11 and 5.12. In all these cases, the duration is equal to respectively 3, 3.5 and 4 cycles (at 50Hz). The sag magnitude and the initial point-on-wave are the same and are equal to respectively 25% and $-10°$. These durations have been chosen in order to analyse the behaviour shown in [5], [14], [23] and [4]. In these, the critical duration for three-phase dips has been found to be half a period (plus any number of full period) of the supply frequency.

The impact of the duration can be explained as this: initially, the active power provided by the machine in the three cases is the same. Then, the dips end one after the other. When the duration increases, the total active power supplied by the machine increases. This tends to increase the decelerating area and thus, the limit of stability is closer. Moreover, if the machine is stable, a bigger decelerating area will yield to bigger oscillations after the dip.

The duration of the the dip is similar to the magnitude in term of impact. The longer the dip, the worst

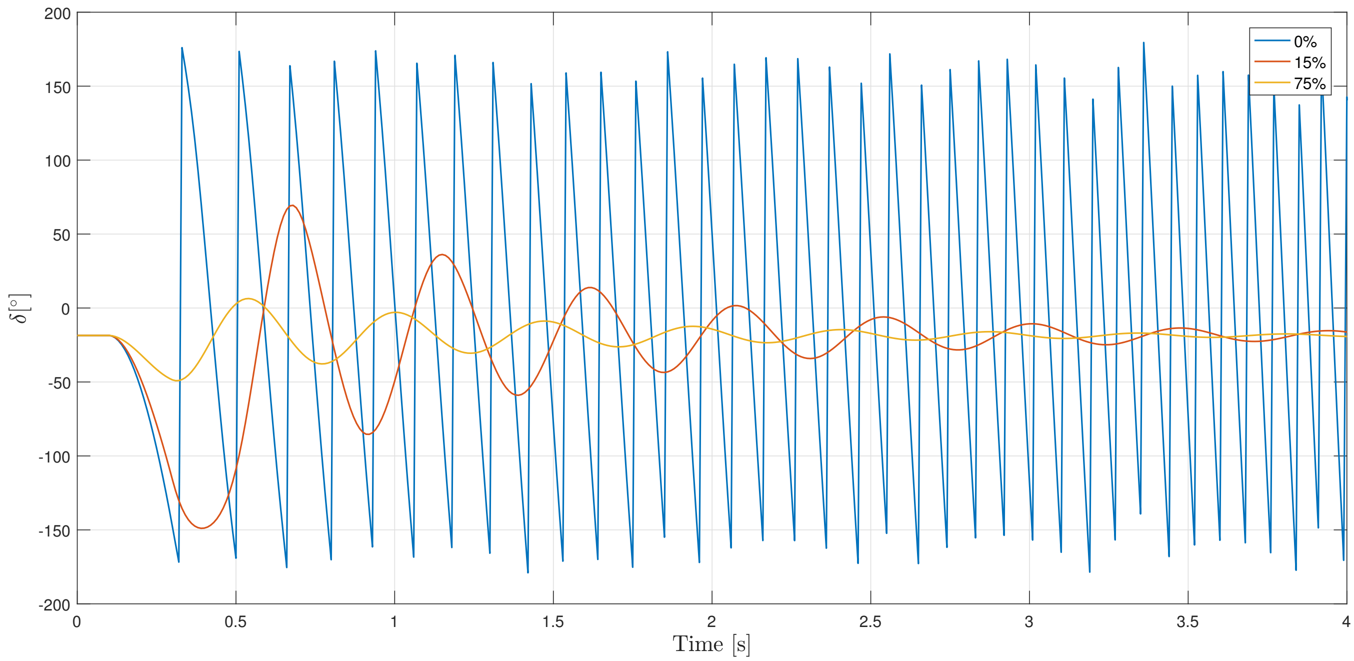

Figure 5.9
Influence of the magnitude on the load angle of the machine

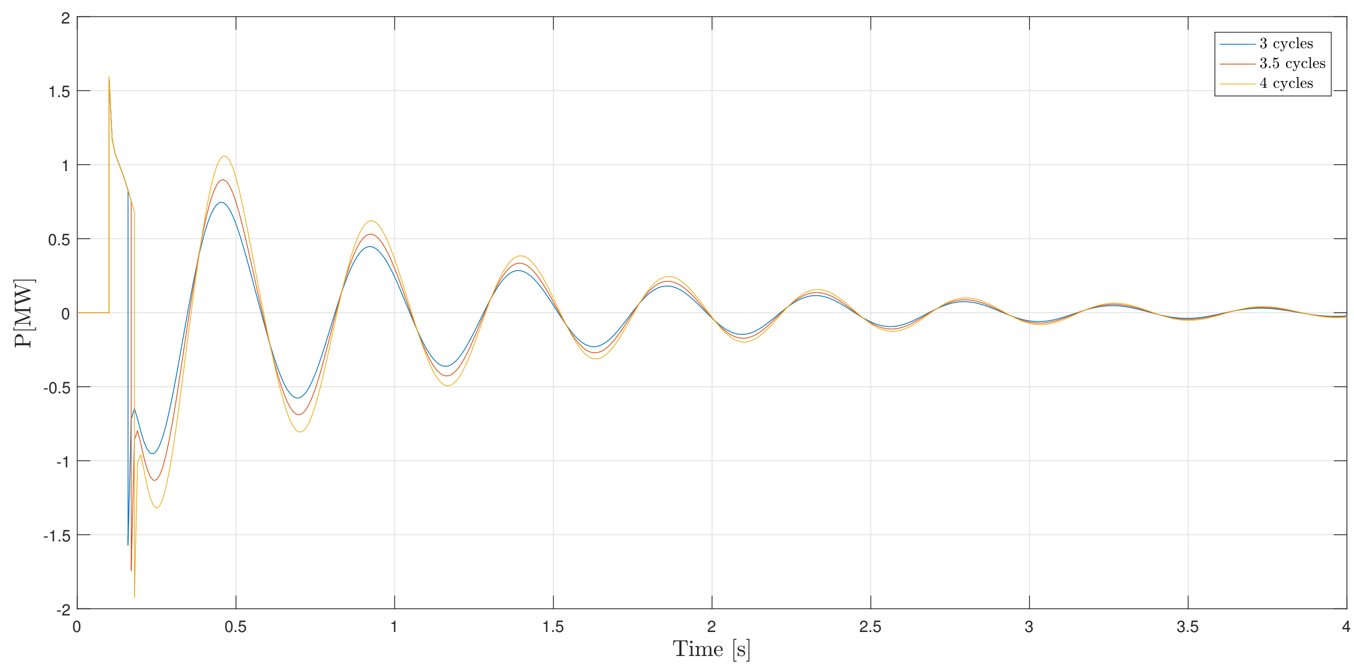

Figure 5.10
Power according to time for various durations

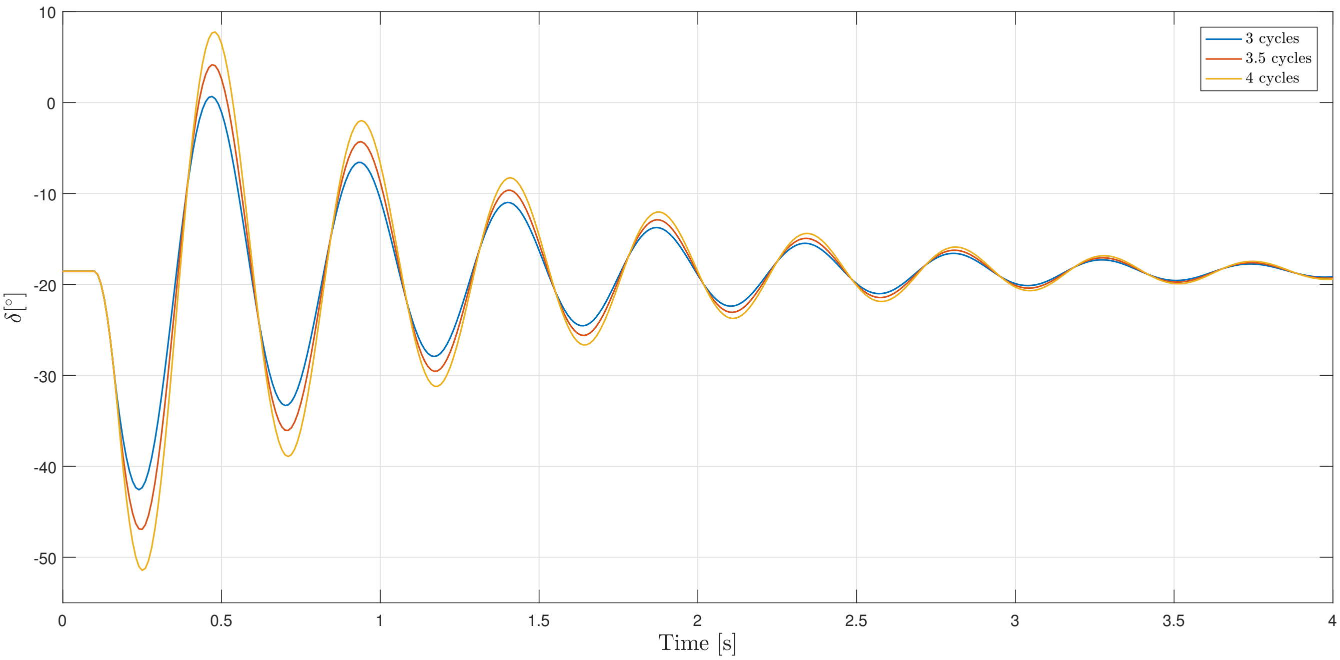

Figure 5.11
Load angle of the machine according to time for various durations

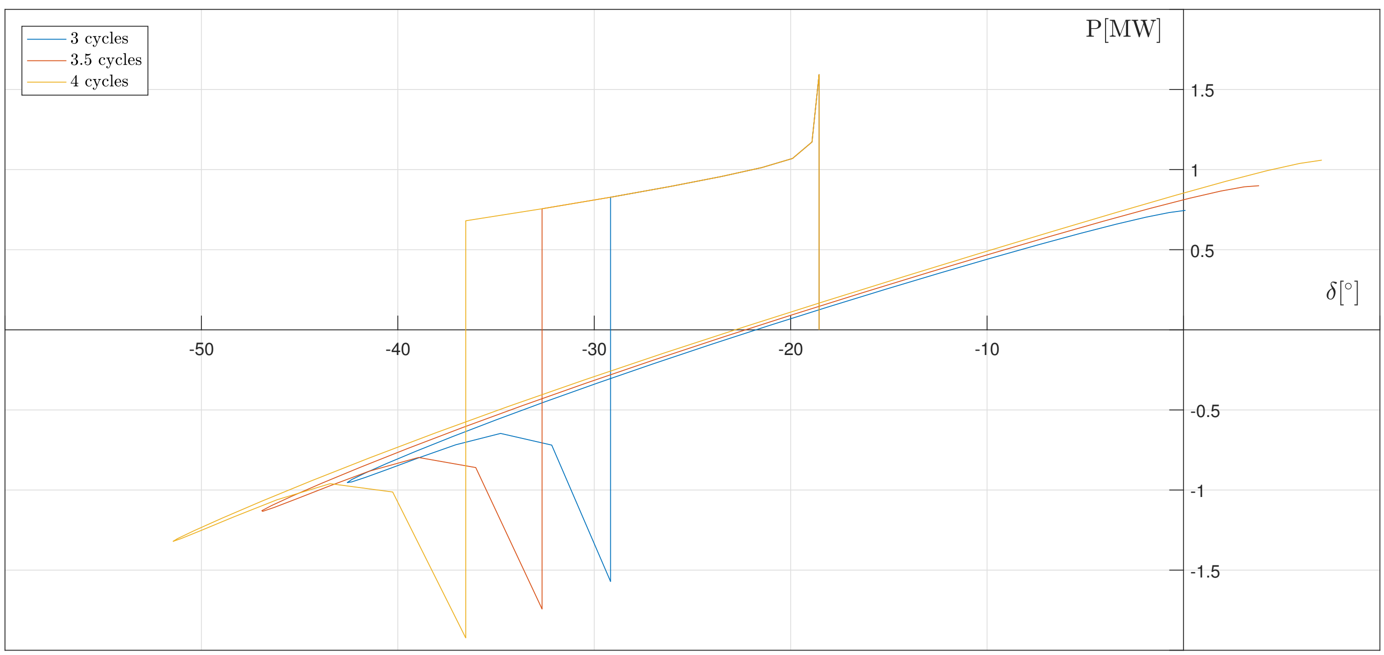

Figure 5.12
$P(\delta)$ curves for various durations

the dip. If this one is too long, the stability of the machine is not guarantied. However, the dip supported by the load will be longer than in the case without voltage conditioner. Then, the power acceptability curve will be enlarged.

As pointed out in the literature, the critical duration is equal to half the supply period (plus any number of full periods) for three-phase dips. Then, the torque peaks occurring after the recovery are the higher than can be registered. This gives also the higher current peaks. However, in this case, this phenomenon can not be observed for the same reasons as the point-on-wave (phasor approximation).

What has been said just before is valid for small duration dips. Indeed, for longer but shallower one, an additional behaviour has to be taken into account. In this case, the dip is shallow enough so that a new operating point exists (as explained before). This one can be reached for time long enough after oscillations but sometimes, this equilibrium exists but is not established before the end of the dip. This gives two extreme cases to consider. A local "maximum" is an instant at which the rotor is at a local maximum value on the $P(\delta)$ curve. A local minimum can be defined in the similar way. Then, the two extreme cases are:

- The dip ends at a local "maximum". In this case, the voltage stabilisation is very fast.
- The dip ends at a local "minimum". In this case, the voltage stabilisation is slower and a peak in the voltage response appears. This is of importance because the peak voltage can be over or under the acceptability limit.

This behaviour is illustrated in figures 5.13 and 5.14. In these, the two extreme cases explained are shown.

This behaviour can be explained again using the $P(\delta)$ curve. Figure 5.14 shows the machine load angle evolution for the case of local "minimum" and "maximum". Figures 5.15 and 5.16 show the $P(\delta)$ curve evolution for the minimum and maximum cases respectively. These were obtain in the simulations. In these, the first maximum and minimum were catch for more clarity.
For both curves, both accelerating and decelerating area can be drawn. In the two cases, a negative jump of active power is observed in order to come back on the initial $P(\delta)$ curve. In the case of a local "minimum", the jump yields to a bigger active power absorption (negative production) than in the other case. Then, the accelerating area is bigger. This yields to a more critical situation.

Another way to see the situation is to say that in the case where the end occurs at a local minimum, the jump of active power is bigger. Then, the rotor has more energy to release that in the other case. This yields to a more critical situation.

5.2.3 phase angle jump influence

To study the influence of the phase angle jump, the three other characteristics are kept constant. The magnitude and the duration are kept respectively at 25% and 150ms. PAJ of $-10°$, $-30°$ and $-45°$ are studied.

Figure 5.17 shows the evolution of the active power provided by the machine. It shows that if the PAJ increases, the initial peak of power increases. Then, at the end of the dip, the amount of power provided is the same for all three cases.
The explanation of this phenomenon is illustrated in figure 5.18. This one shows the evolution of $\Delta\theta$, the angle difference between the grid and the load voltage against time. Due to the initial phase angle jump, this difference increases at the beginning of the dip. Then, the more the PAJ, the more the difference. As angle differences induce active power transfer, the more this difference, the more the active power

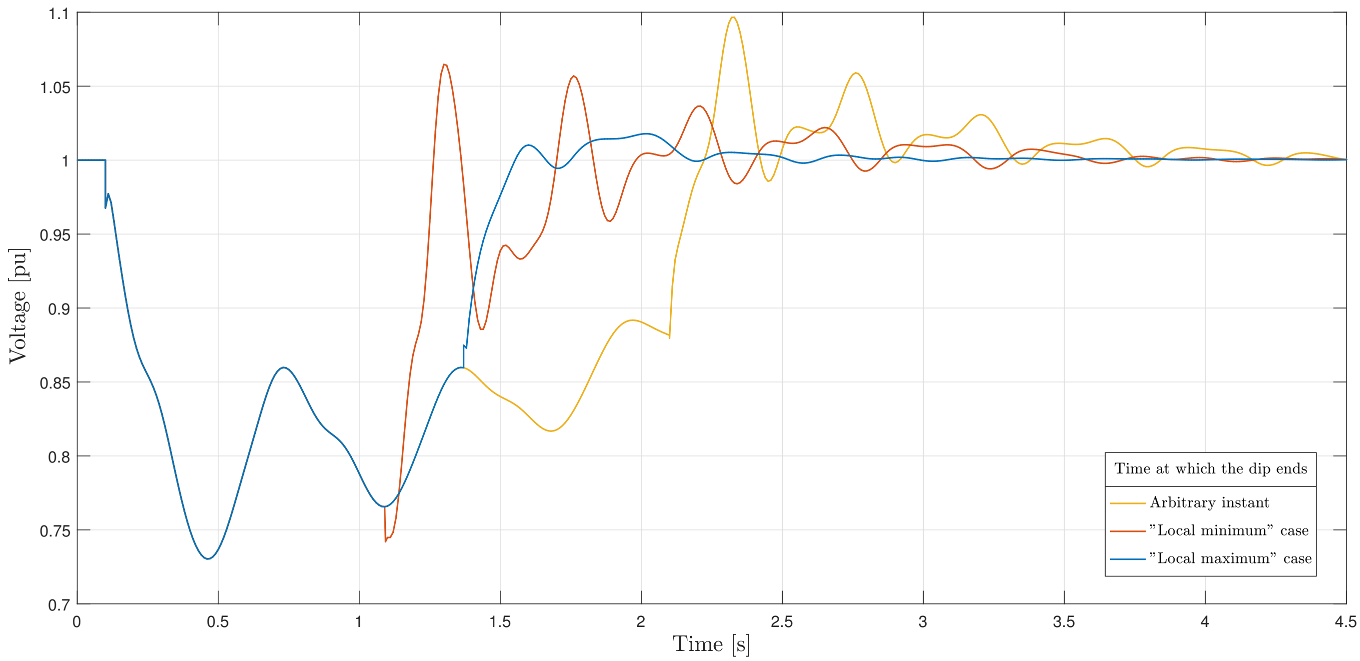

Figure 5.13
Illustration of the two extreme cases (local minimum and maximum) on the load voltage

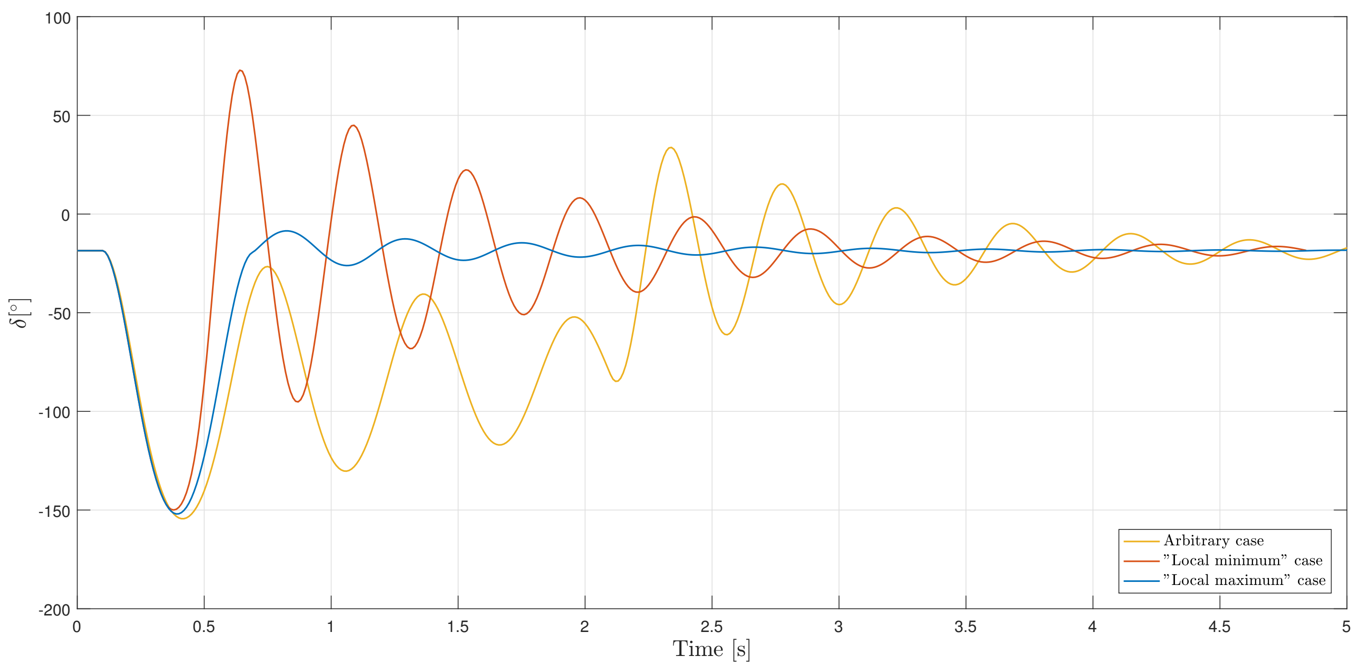

Figure 5.14
Load angle evolution for the two extreme cases (local minimum and maximum)

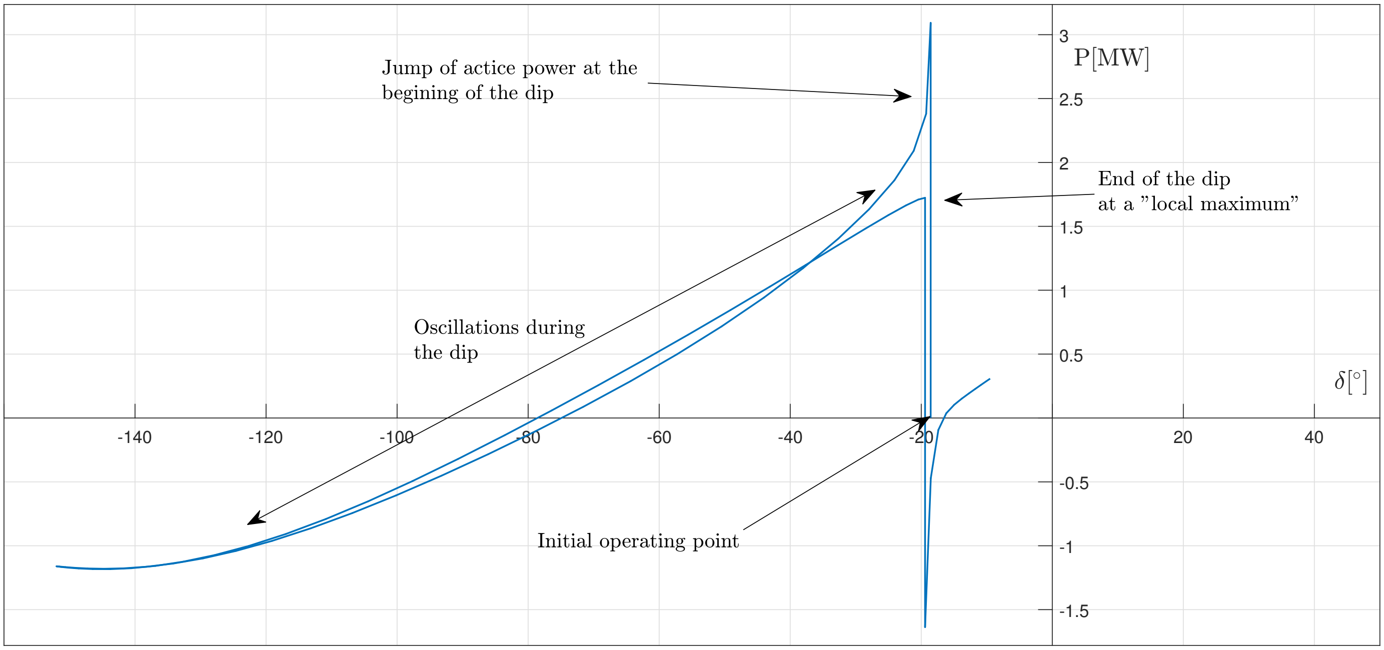

Figure 5.15
$P(\delta)$ in the case where the dip ends on a local "maximum"

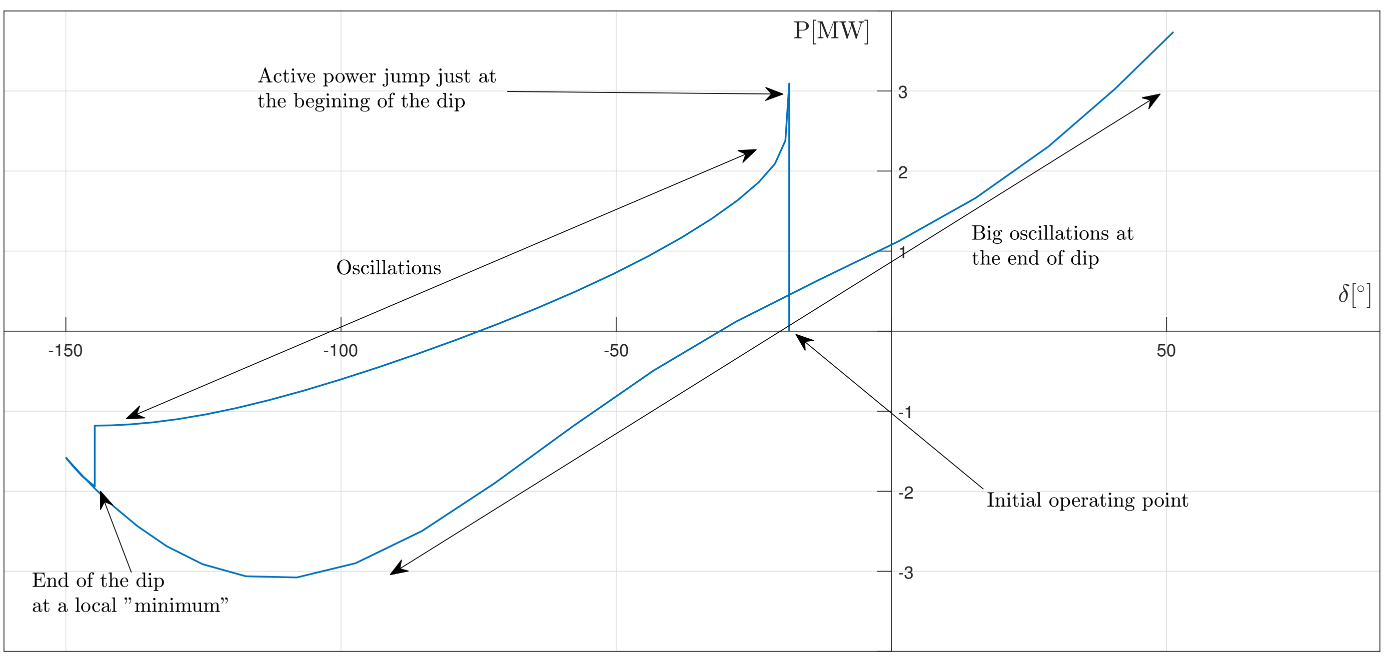

Figure 5.16
$P(\delta)$ in the case where the dip ends on a local "minimum"

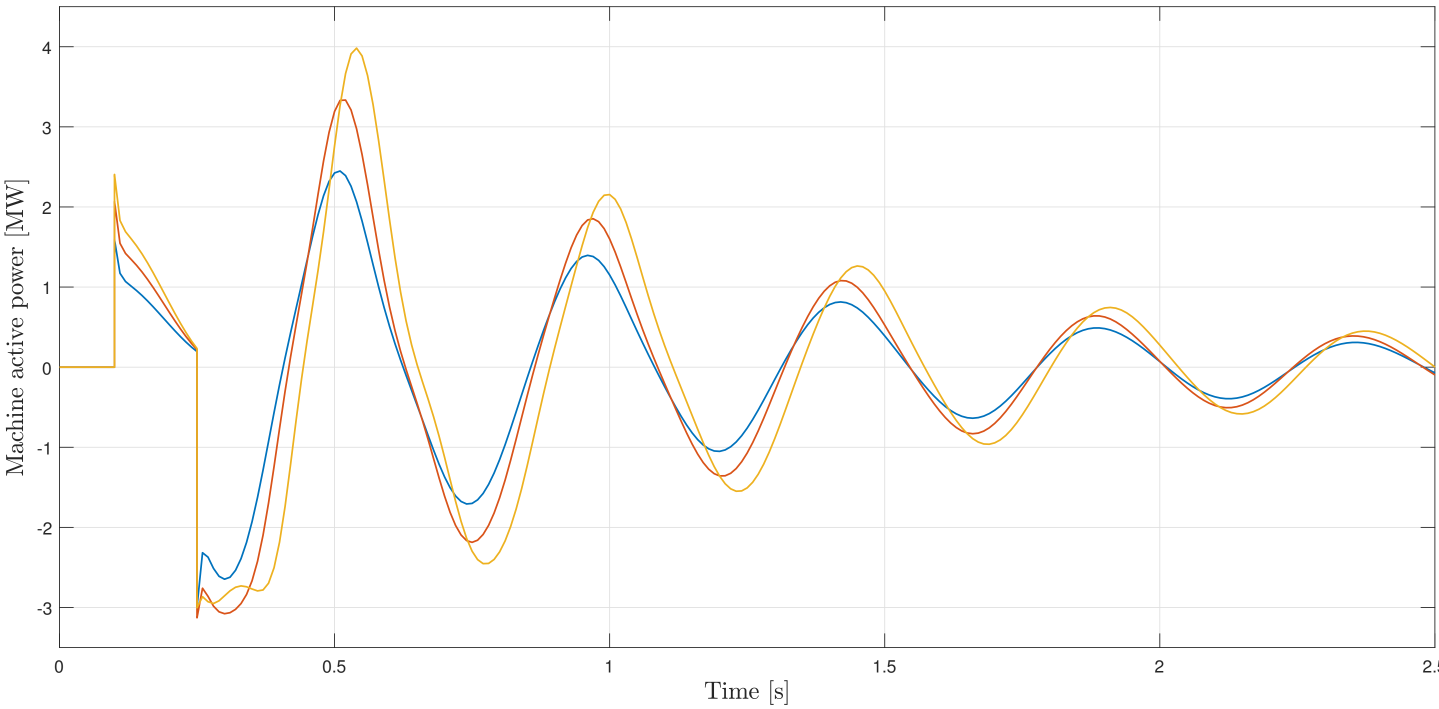

Figure 5.17
Active power provided by the machine against time for various $\Delta\phi$

transferred. This is shown in figure 5.19. This shows the power transfer from the grid to the equipment for the different PAJ. It can be observed that the power transfer (during the dip) is more pronounced when the PAJ increases. As this active power is provided by the machine, increasing the PAJ yields to an increase in the active power produced by the machine during the dip.
Afterwards, the principle is the same as before. Increasing the active power production increases the decelerating area on the $P(\delta)$ curve, thus reducing the stability limit. This is illustrated in figure 5.20.
The evolution of the remaining voltage magnitudes can be studied using figure 5.21. This one uses the same parameters as previously (only the duration has been increased up to 180ms). The voltage evolution can be divided in two main parts. These are respectively time during and after the dip. The first one is constituted of a drop in voltage magnitude and is nearly independent of the phase angle jump. This is logical as the only change for various $\Delta\phi$ is the amount of active power transferred in the fault. The voltage is independent of this jump but the machine is in a different state at the end of the dip as explained before.
After this first phase, the evolution is function of the PAJ. This is due to the different behaviour of the machine to come back to equilibrium after the dip. In this case, the stability is ensure for PAJ lower than 38° (strictly lower) in absolute value.

At the end, this study shows that bigger phase angle jump yields to worst case. Then, the bigger PAJ observable is the worst case observable. In practice, the maximum PAJ observable during a fault is −90°. However, PAJ bigger than −45° are not common and usually, they do not exceed −30° [22].

5.2.4 New power acceptability curve

Thanks to all the studies made in the previous points, the worst case has been isolated. The PAJ that yields to the worst scenario is −45°. The initial point-on-wave does not influence the results and is there-

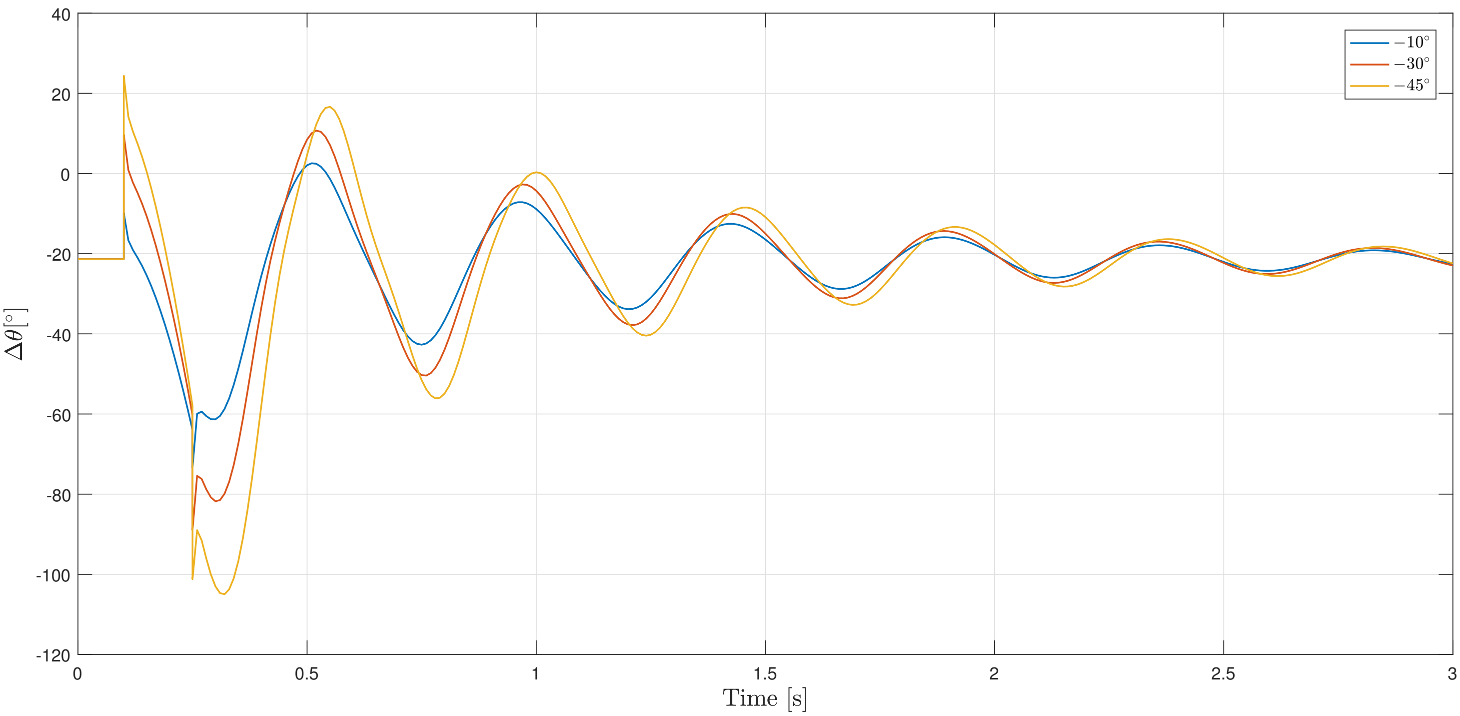

Figure 5.18
Difference between the angle of the grid and the angle of the load voltage against time for various $\Delta\phi$

fore set to 0°. Then, a new power acceptability curve can be drawn for the voltage dips of type A. This one is presented in figure 5.22. As pointed out in [22], PAJ of more than 45° are very rare and even this value is almost never reached. This is the reason why another PAJ, more reasonable is also tested. This gives another power acceptability curve also provided in figure 5.22. These new curves have the following signification: if a dip occurring at the entry can be plot in the duration-magnitude axis on the left of this curves, the load voltage will remain within acceptable limits (compared to standard). Moreover, the machine will remain connected.

There are three reasons that can yield to reject a dip. The first one is that the dip makes the machine unstable. The second and the third reasons are respectively that the dip yields to a voltage violating the lower or higher limit of the voltage. In these two cases, the voltage is not acceptable for the load (related to the CBEMA curve).
A remark can be emitted for the last reason introduced before. This one will obviously never be reached during the dip. It is going to be seen after the dip when the voltage comes back to its initial value. It usually occurs for longer dip. In the case studied here, the durations explored will not yield to over-voltage after the recovery since these are very short.

For the case where $\Delta\phi = -45°$, for dips of magnitude between 0.5 and 0.55 (remaining), the behaviour of the local optima has its importance. In fact, these are acceptable for long duration (e.g. 1s) but has to rejected for shorter durations. For example, for a dip with a remaining magnitude of 51%, the equilibrium can be found. Therefore, the dip can be sustained during 1s without any problem. However, the maximal acceptable duration is 0.208 ms because, at this time, there is a local "minimum". Due to this one, the voltage goes under limits and the dips has to be rejected. However, as it is not possible to know the length of the dip before its end, all of the longer duration has to be rejected.

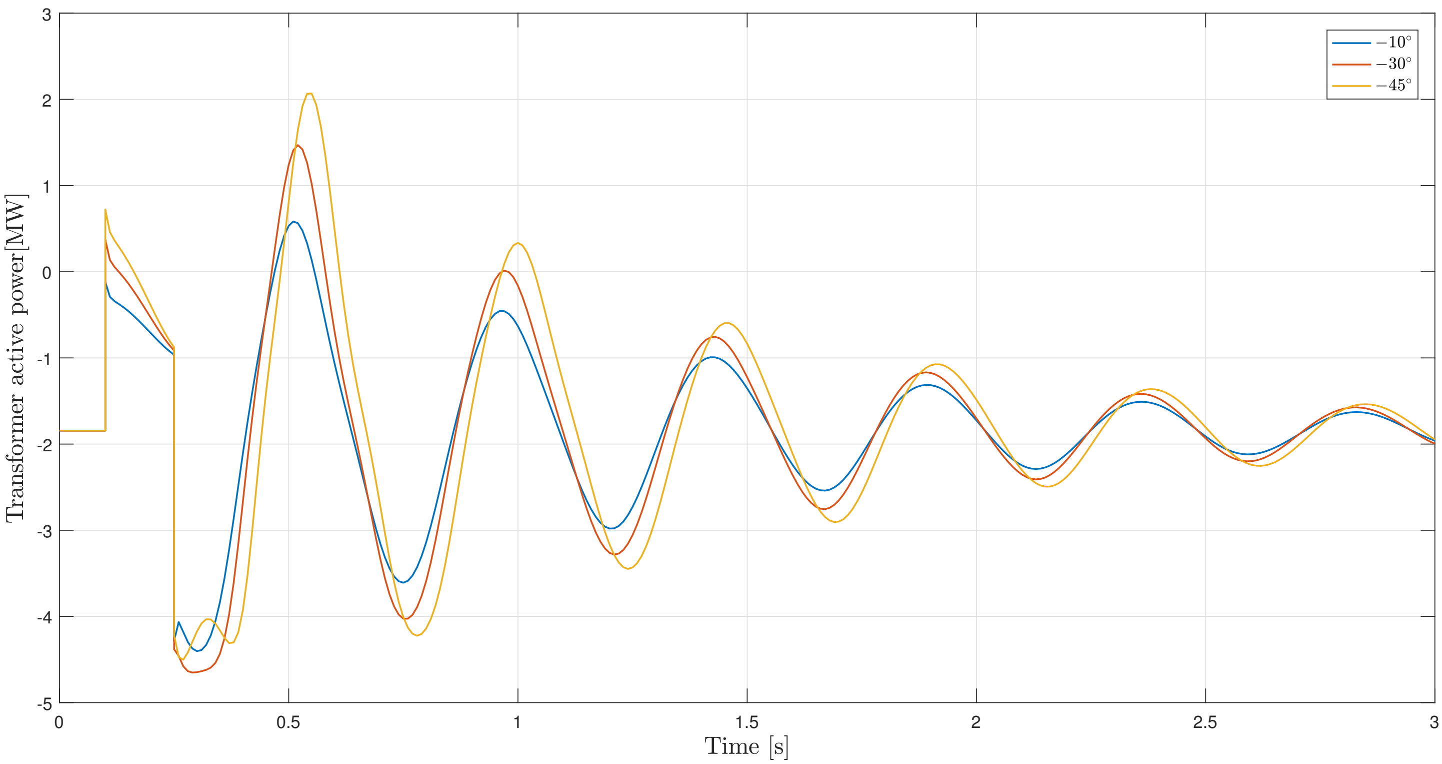

Figure 5.19
Active power transferred from the grid to the equipment for various $\Delta\phi$

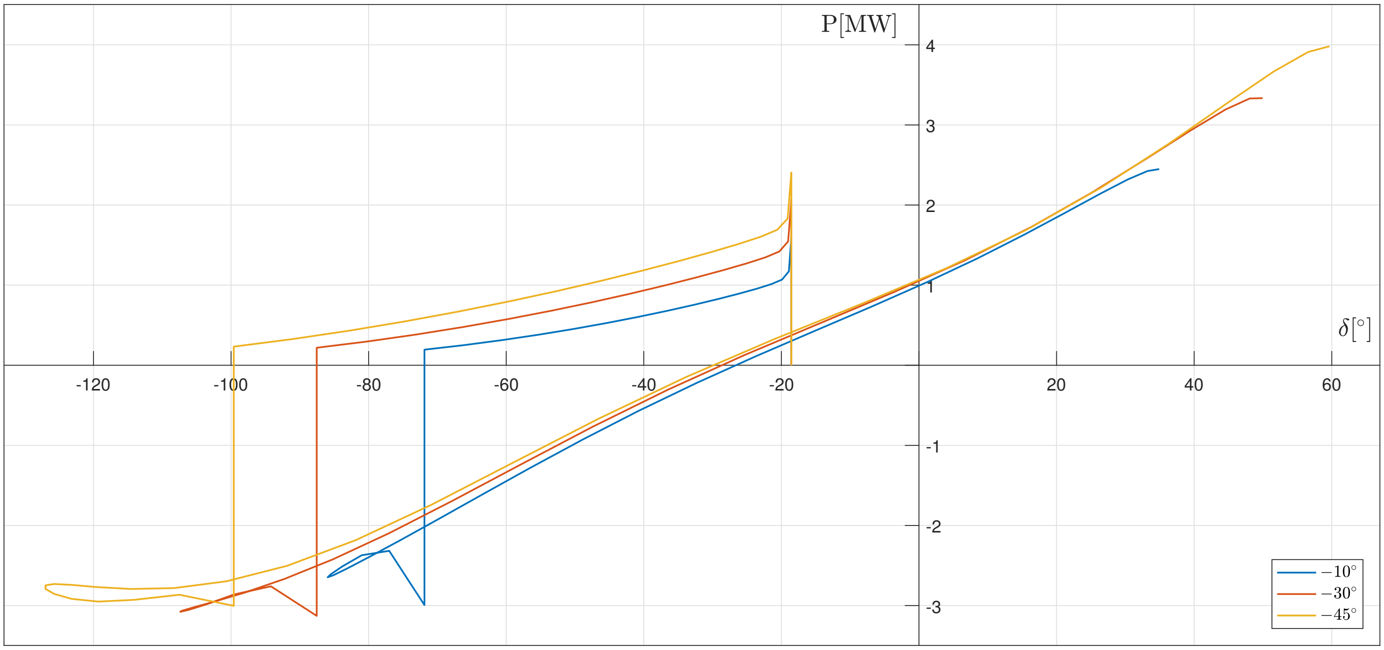

Figure 5.20
$P(\delta)$ curve for various $\Delta\phi$

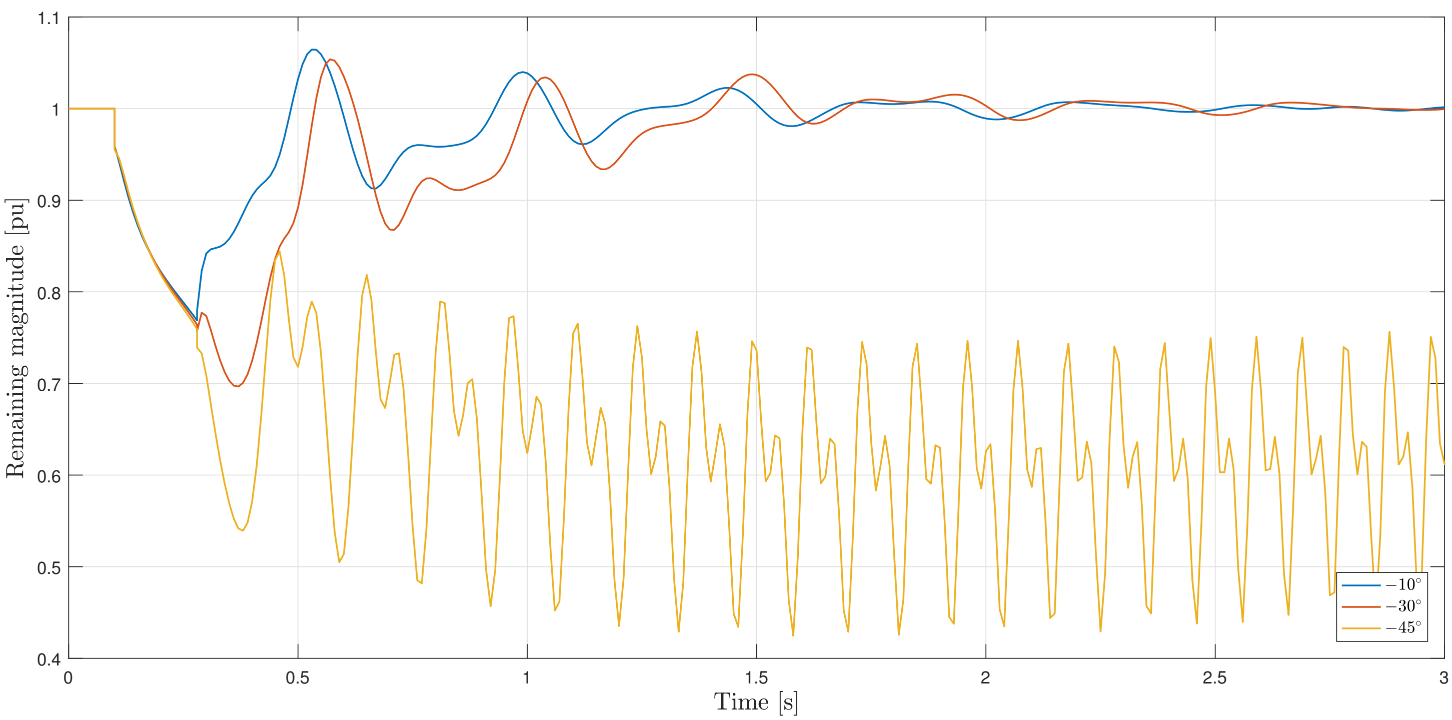

Figure 5.21
Influence of $\Delta\phi$ on the load remaining voltage

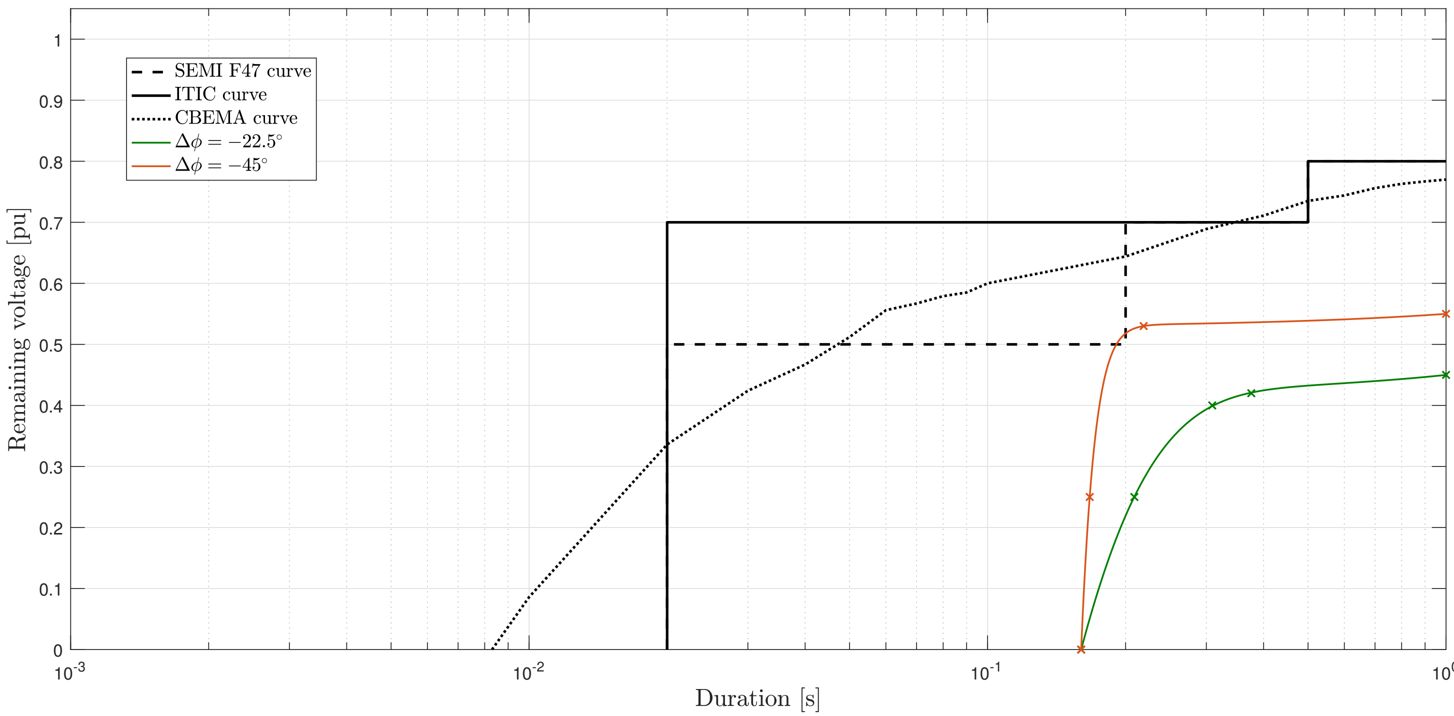

Figure 5.22
Improvements in the power acceptability curve for two phase angle jumps

This zone can be characterised as a "grey zone". In this one, one can not accept directly all dips or reject them.

Figure 5.22 shows the improvements compared to the standard curves. The figure is a focus on the useful part of the curves. The results are explored for the worst phase angle jump ($-45°$) and a more reasonable one ($-22.5°$). The main conclusion is that the reliability of the system has been improved. The remark concerning the influence of the phase angle jump can be also shown here. The results for a $\Delta\phi$ of $-45°$ are worst than the one with $-22.5°$.

At the end, a remark can be emitted concerning the current in the transformer at the entry and in the machine. These are presented in figure 5.23 in the case of a short circuit fault at the entry of the transformer. This one last 160 ms and represent the worst case possible. For the current in the transformer, it can be seen that the peak value reached is equal to 3.25 pu which is pretty huge. However, this one does not last for too long. For the machine, the current is very similar. It is a little bit higher during the dip because the machine has to supply the load. As shown in the figure, the current is higher when the dip finishes than during this one. This is due to the fact that the machine is very close to its stability limit at the end of the dip. Then, it has very big difficulties to come back at equilibrium. After this peak, the current comes back at equilibrium.

5.3 Type C

The type C can be obtained in two different ways:

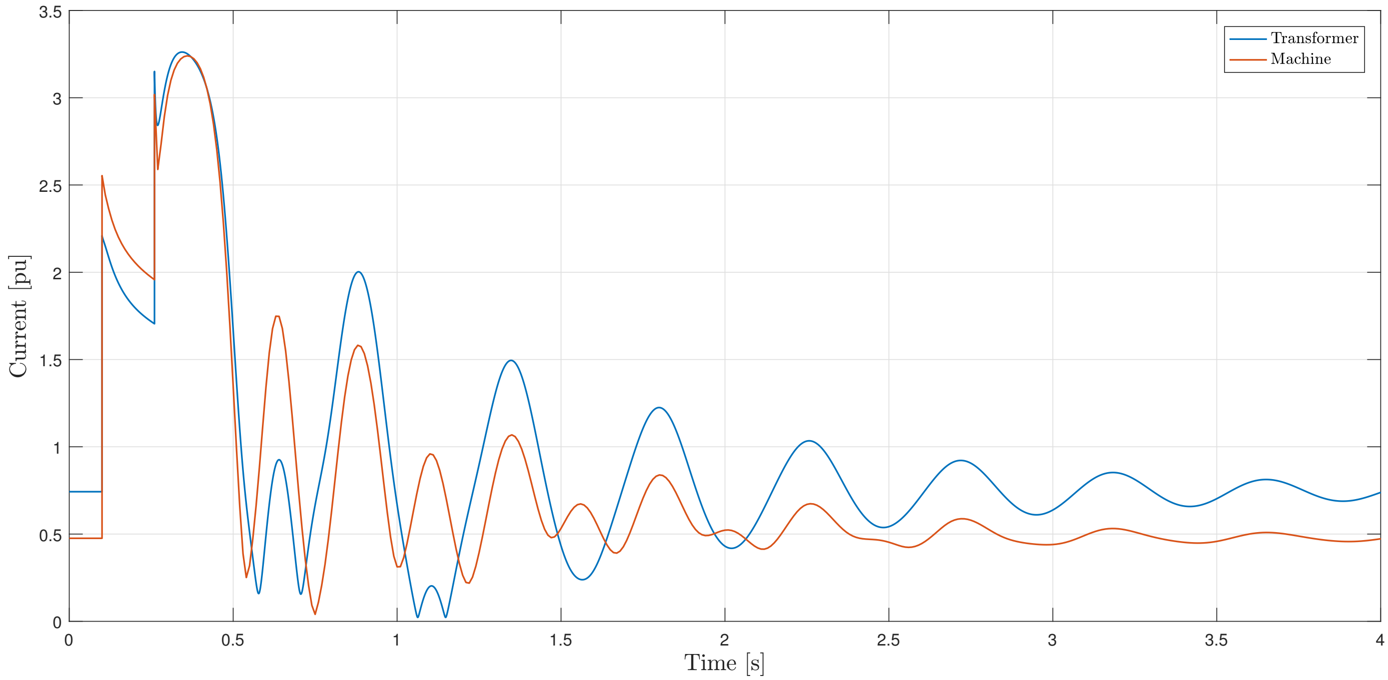

Figure 5.23
Current in the transformer and produced by the machine for a three-phase short-circuit lasting 160ms (stability limit)

- Apply a two-phase fault and observe either at location I or III.
- Apply a single-phase fault and observe at location II.

The simulation here is done applying a single-phase fault and observing it at location II. Then, the first transformer is of type $Ynyn$ and the second is kept as type Dyn. In fact, the type C is the same as a single-phase fault from which the zero sequence has been removed.
In this case, the full analysis will not be carried on. The "new" power acceptability curves are going to be obtained and shown directly. These curves are obtained for cases with and without voltage conditioner. On these, the fault plotted is the upstream one. Due to the transformer, the downstream voltage is different in the three phases (change of type). The results are not trivial and the power acceptability curve as seen from the entry of the company is different. These will show the acceptable dips at the entry of the factory (before the transformer) so that the load voltage remains within acceptable limit.

As explained previously, ERACS only provides the positive sequence results. All the sequence networks have been assembled in order to retrieve the three load voltages (see Appendix E).

5.3.1 Voltage evolution

This section aims at showing the voltage evolution along the system and illustrates the classification introduced in section 1.3. The voltage phasors evolve due to transformer type. The phasors are shown in figures 5.24 and 5.25. Those figures respectively show the evolution of the voltage magnitude and phase with time at the fault location and at the load terminals. Those two have been taken in the base case (without the synchronous machine and the choke). In fact, in the full case, the voltage across the load is

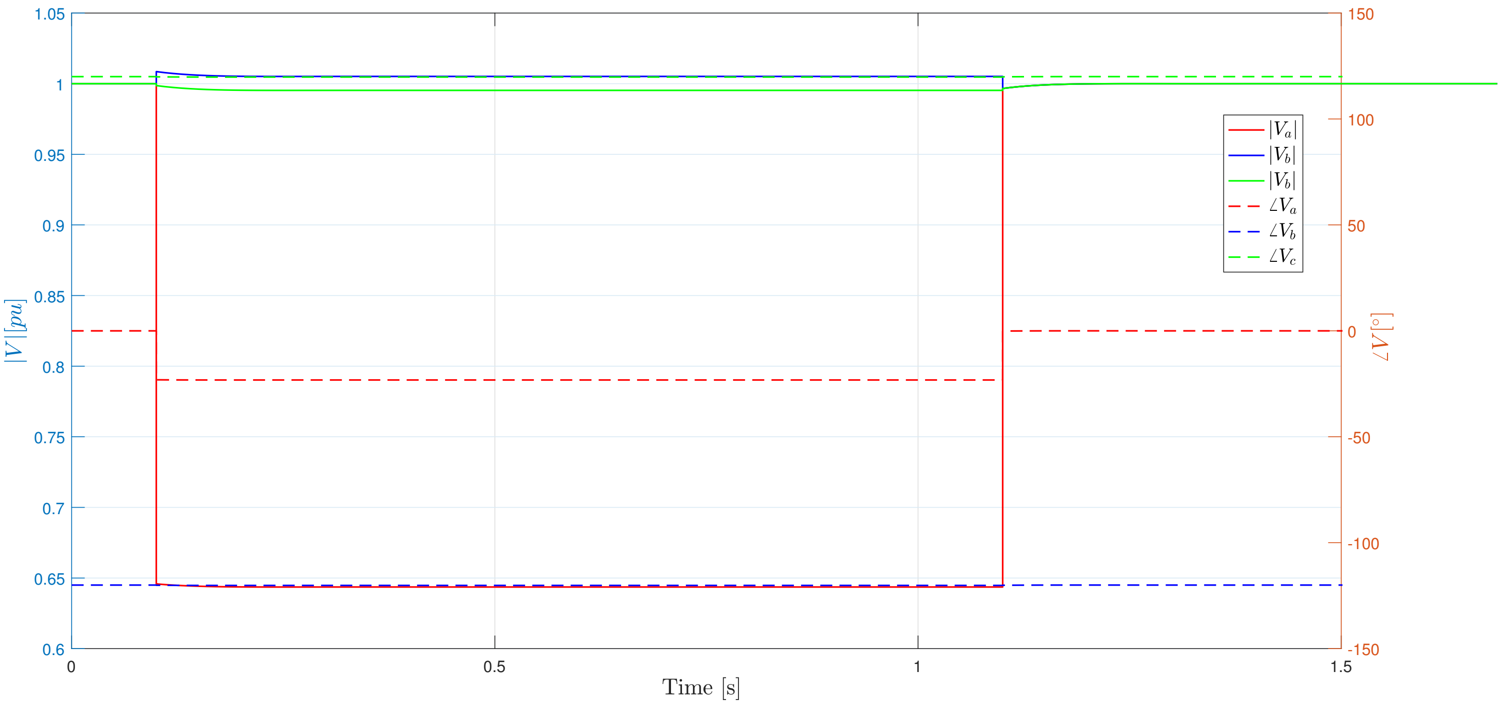

Figure 5.24
Voltage magnitude and phase angle evolution with time at the fault location (BUS-1) in the base case

controlled by the machine and the phasor evolutions are not the same.

Thanks to this, the phasors can be easily reconstruct. Then, before the transformer, at the fault location, several things can be observed:

- There is a phase angle jump in phase a during the dip but the other phase angles stay the same as before the dip.
- The magnitude of phase a is decreased a lot. This is logical as it is the faulted phase.
- Phase b and c see two opposite behaviours in their magnitudes. The first one sees a small overvoltage and the second sees a small dip. In fact, the respective increase and decrease are of same amplitude.

Thanks to all of these observations, one can confirm that the observed dip is of type B as introduced before. The only change compared to the ideal type is the movement in the two non-faulted phase. However, they are not that different and the dip can be classified as a type B.

At the load terminals, the same analysis can be done:

- The load voltage is slightly lower than $1pu$ even at steady state due to the transformer reactance.
- If the slight changes in magnitude at the beginning and at the end of the dip are ignored, phase a does not see any magnitude change. This is also true for the phase angle.
- Phase b changes in both magnitude and argument during the dip. The angle decreases and the magnitudes decreases.

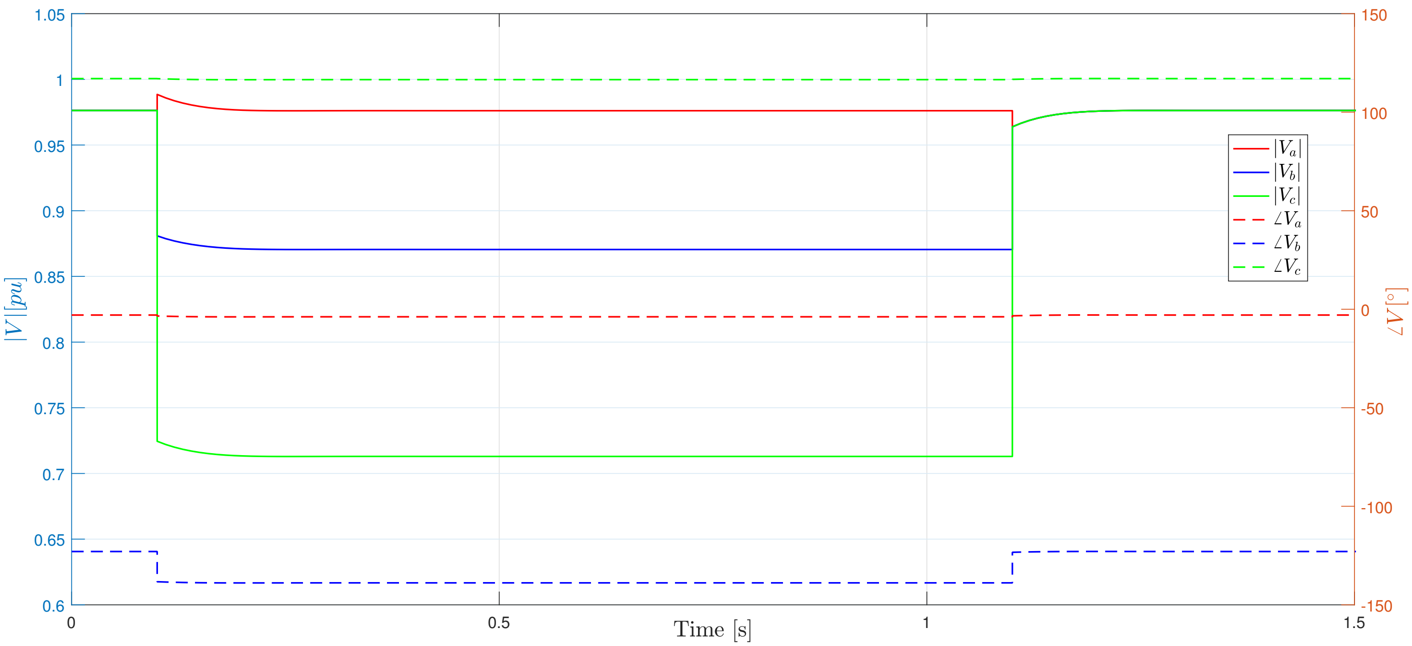

Figure 5.25
Voltage magnitude and phase angle evolution with time at the load location in the base case

- Phase c changes only in magnitude. The angle is not affected during the dip.

Then, it can be concluded that the resulting dip at the load terminal is of type C. This was expected and predicted by the classification introduced in section 1.3.

5.3.2 New power acceptability curve

In this case, like for type A, two phase angle jumps are going to be analysed. These are the same as for type A ($-22.5°$ and $-45°$).

Compared to the previous case, the voltage at the load terminals are unbalanced and the study made has to be a little bit different. Concerning the line voltages (phase-to-neutral), the three magnitudes are going to be different.
Another difference compared to before can be noticed. Due to the unbalance in magnitude and phase, the phase voltages (phase-to-phase) U_{ab}, U_{bc} and U_{ca} are going to be different. Previously, for three-phase dips, in per unit, the dips were the same when studying phase voltages or line voltages. This is not the case here and both voltages have to be studied.
As said in the introduction of this section, the case without voltage conditioner also needs its new curve. This gives two cases for each situation.

At the end, eight new power acceptability curves need to be found (2 PAJ * 2 voltages * 2 cases).
Like for the type A dips, the CBEMA curve is going to be used as standard limits.

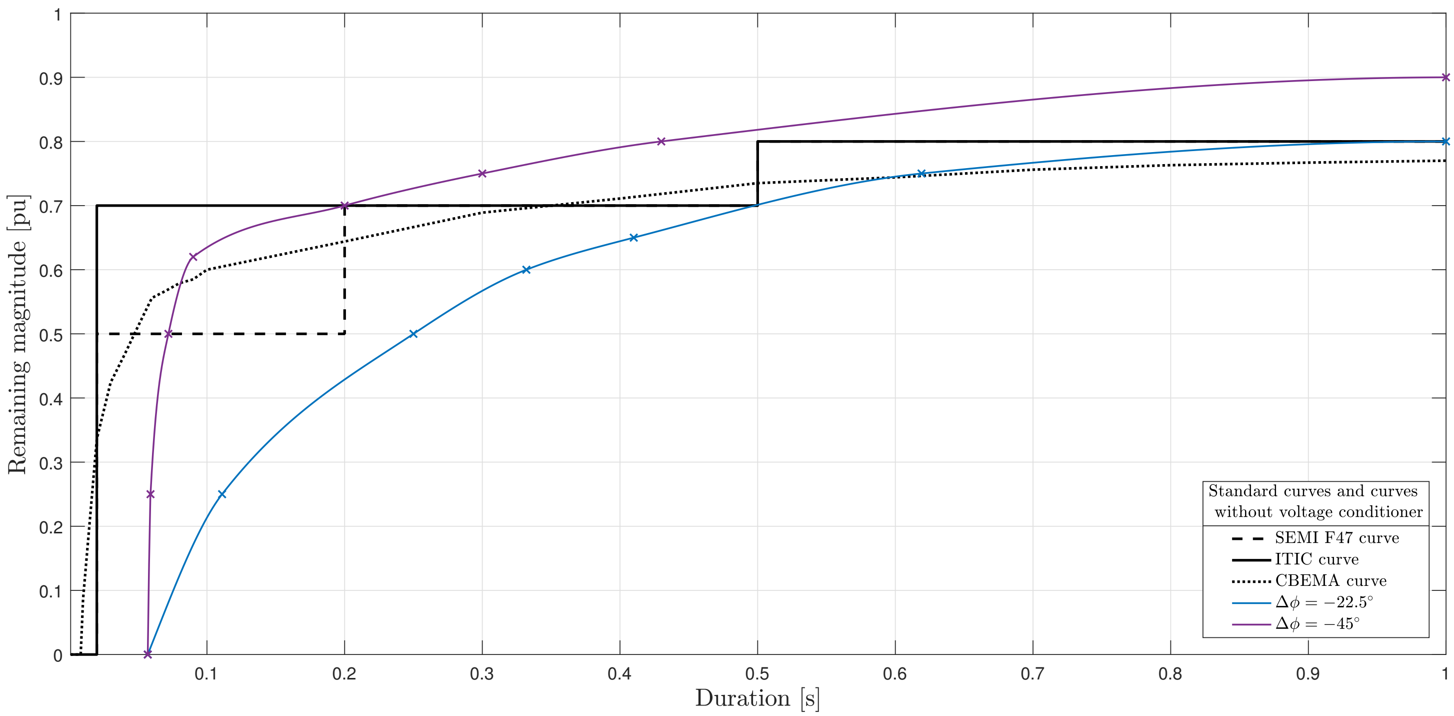

Figure 5.26
New power acceptability curve for single-phase loads (without the equipment)

Line voltages

In this case, the three line voltages are considered. This corresponds to a case where single-phase loads are considered. These are assembled in stars and the line voltage considered for the curve is the lowest remaining one. The analysis is carried on for the two phase angle jumps, with and without the voltage conditioner. The results without the conditioner are assembled in figure 5.26. It shows the dip can be accepted at the entry of the factory (before the *Dyn* transformer). These dips does not yield to a voltage under the CBEMA curve at the load terminal. It shows that the result is not trivial and that the the transformer changes the curve.

For the case with the equipment, figure 5.27 shows the three line voltage magnitudes evolution when phase a is short-circuited (no remaining voltage in phase a). It shows that it does not yield to a voltage sag severe enough to be rejected (according to the CBEMA, the equipment will continue operating). As a short-circuit is the worst case that can be seen, the other dips will never be under the limit. Then, new power acceptability curves, similar to the one obtained with the equipment connected for type A, do not need to be drawn.

The main conclusion is that the machine is able to stay stable whatever the dip in phase a. Then, for studied durations, it can maintain the voltage and this one never goes under the limit when the equipment is present. The over-voltage observed is also acceptable for the equipment according to the CBEMA curve.
Another conclusion is that, more generally, when considering line voltage and a realistic PAJ ($-25°$), the voltage dips observed after the transformer are less severe than the ones before the transformer. In fact, the type B dip (generated before the transformer) is concentrated mainly on one phase. When it propagates, its is divided and the influence is mainly concentrated in two phases. Then, the remaining

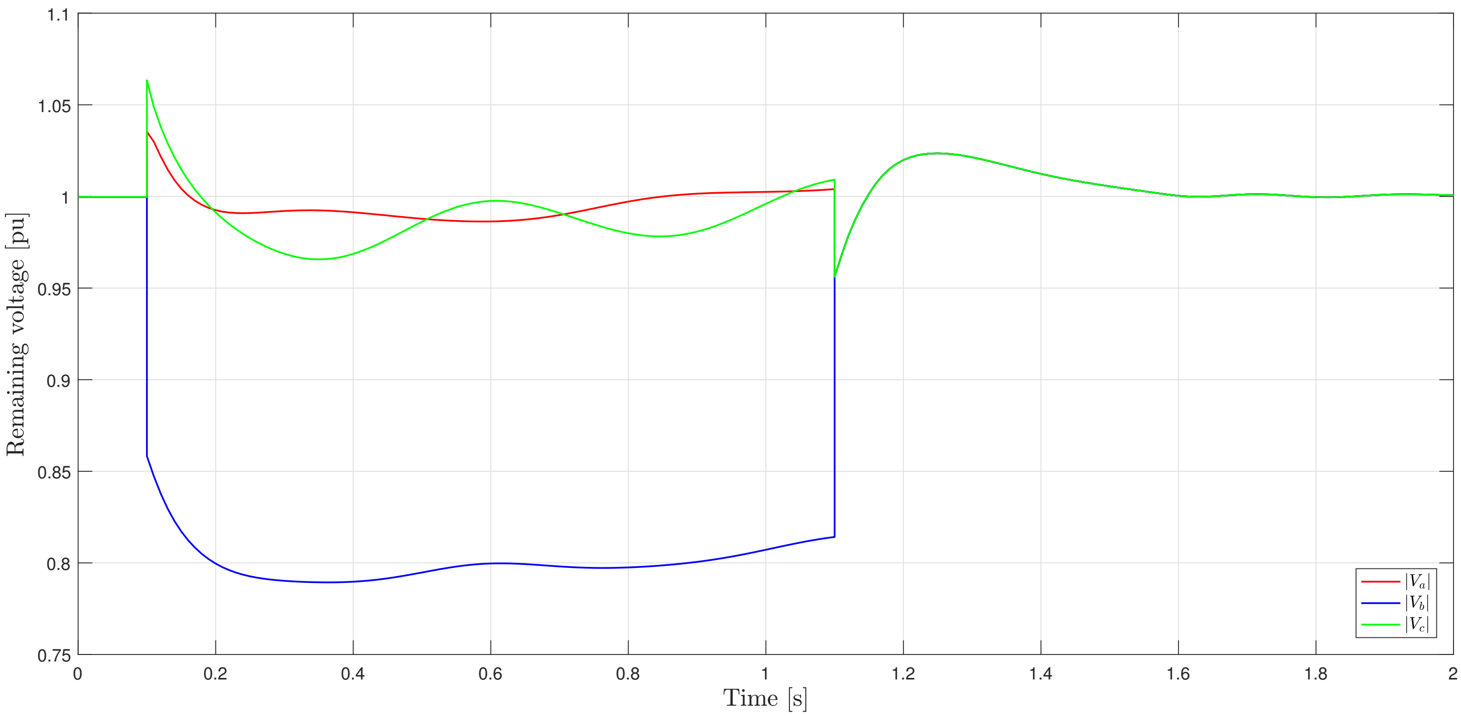

Figure 5.27
Evolution of the three lines voltage magnitudes obtained when the RVC is present

magnitudes in these two are higher.
However, for longer and less severe dips, one can see that the curves is over the CBEMA curve. Then, in this case, the "new curves" are more severe than the CBEMA. This phenomenon is not negligible for the phase angle jump of $-45°$.

Phase voltages

The first thing to remark is the fact that using Δ loads has the same impact as using an ideal *Dyn* transformer with the correct ratio just before a load connected in star. It transforms line voltages in phase voltages. Therefore, a type C dip seen by a Δ load is equivalent as seeing a Type D dip for a star connected load. This can be deduced using figure 1.9 and table 1.2. This gives an overview of the results that could have been obtained with this type. The only difference is that the voltage conditioner is applied at the intermediate stage (when the dip is still of type C) and not when it has been transformed in its final form (Type D). However, the influence of the machine on Type D should not change in term of stability and impact and similar results should be obtained.

In this part, phase voltages are analysed and compared to the standard. This corresponds to a situation where the loads are connected in Δ. The figure 5.28 shows the results without the voltage conditioner. Then, figure 5.29 shows the three phase voltage magnitudes according to time. The analysis principle is the same as the one used for the line voltage case.

Concerning the new power acceptability curves, the same remarks can be emitted and the limit is enlarged. Nevertheless, the same limitation as before (concerning the less severe dips) is not present here.

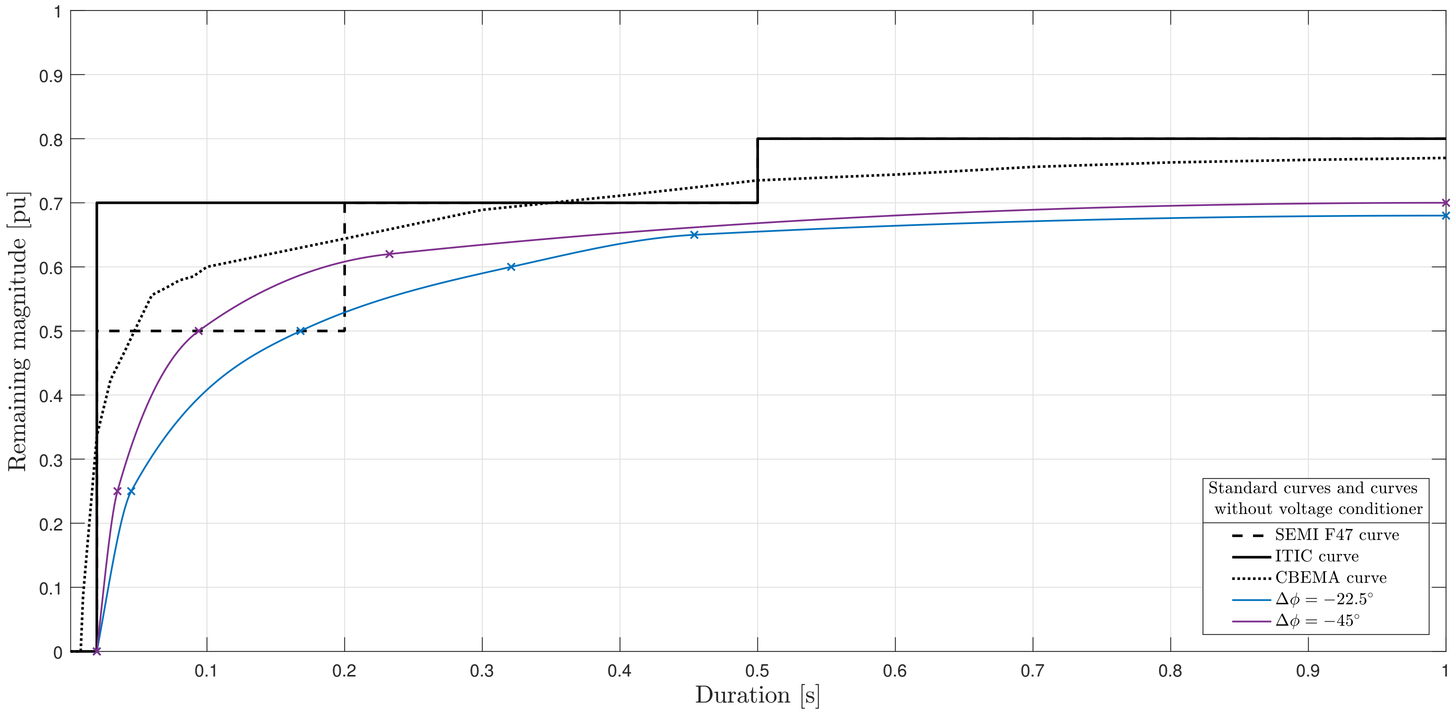

Figure 5.28
New power acceptability curve for loads connected in Δ (without voltage conditioner)

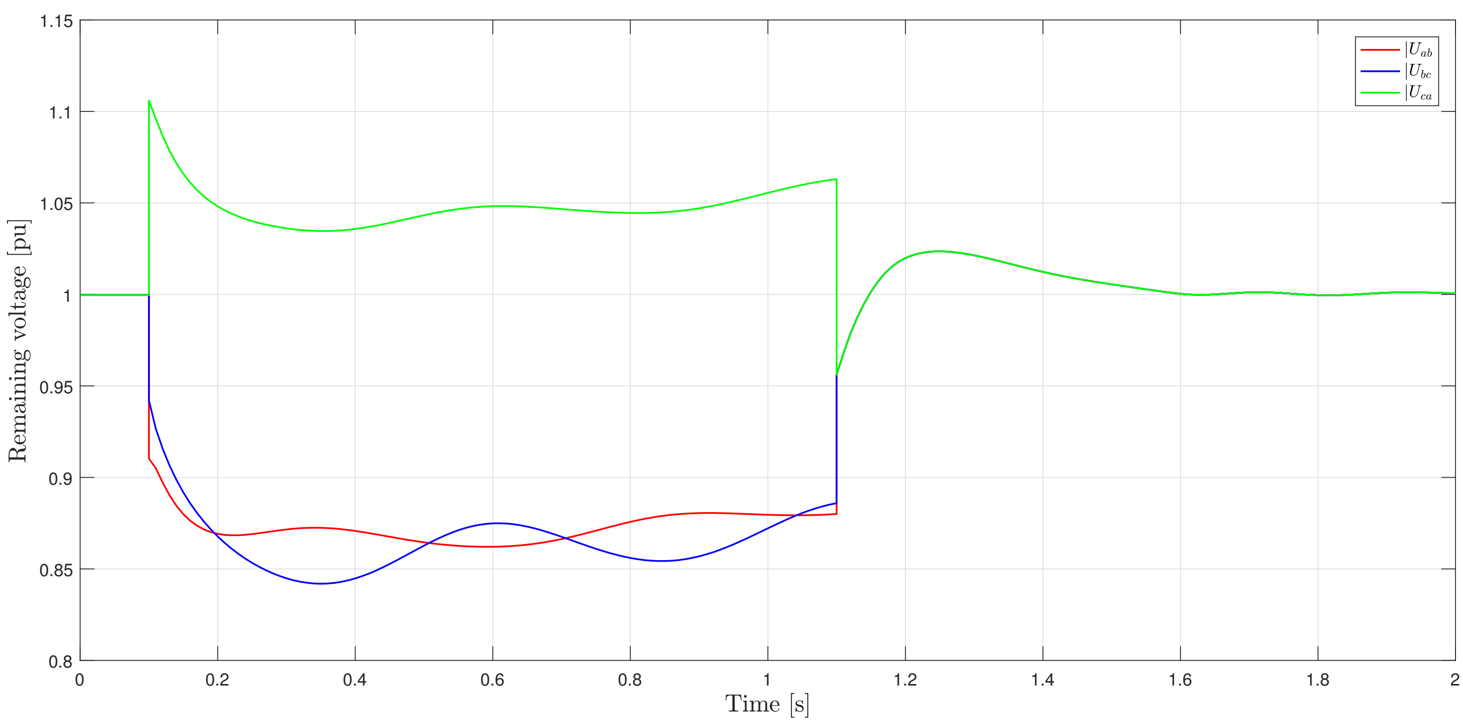

Figure 5.29
Evolution of the three phase voltage magnitude when the conditioner is present

Then, for the case where the voltage conditioner is present, the same results can be observed. The phase voltages remain over the limit for the worst case (short-circuit on one phase). Then, the equipment can deal with all the possible dips.

To conclude, thanks to the transformer, the voltage seen by the load seems a little bit less severe. This enlarges the power acceptability curves even when the voltage conditioner is not present. With the new equipment, the voltage is well maintained and all the dips can be counter.

5.4 Additional inertia

The fact of adding inertia to the machine can greatly increase its capacity. This can be done, for example, by adding additional mass on the rotating shaft of the synchronous machine. In fact, adding this will increase the amount of kinetic energy stored in the machine. It results in an increase of the amount of energy that the machine can release during the dip. Then, the voltage decreases less and the oscillations of the rotor are smaller. To conclude, adding inertia to the machine should improve the behaviour.

In order to analyse the impact of this, three simulations are going to be carried on. The dip is kept the same for all these but the inertia constant of the machine is going to be changed. The first one is obtained using the base value. Then, for the second one, the value is doubled and for the third one, the value is divided by two. The sag characteristics are the following: 25% of remaining magnitude, PAJ of $-15°$ and duration of 150ms. As it has been pointed out previously, the single-phase dips are not very severe. Then, the studied dip is going to be a three-phase one.

The results are shown in figures 5.30, 5.31 and 5.32. These show respectively the active power produced by the machine, the frequency at the load bus and the load voltage.

Concerning the machine active power, it can be seen that the increase of inertia makes the machine able to provide more power. The initial jump of power is more or less the same for all cases but, when the dip duration increases, this power becomes bigger when the inertia constant is increased. After the dip, the oscillations in the active power response are present whatever the constant.
However, it can be observed that the bigger the H, the longer the oscillations. In fact, this is the same principle as a pendulum that oscillates. If its weight increases, it takes more time to stabilise. In this case, the weight is the inertia constant and the pendulum is the rotor. Obviously, the damping of a bigger rotor takes more time.
Nevertheless, an exception can be made for the first peak of power. This one is bigger for smaller inertia constant. This is the inverse as the situation during the dip. In this case, the machine will absorb active power to come back at equilibrium. If the rotor has a small inertia, it is more sensible to this, it is more accelerated and bigger oscillations appear at the beginning.

Afterwards, the frequency can be analysed. As expected, during the dip, it decreases. The frequency at the load terminal is strongly correlated with shaft speed and this one decreases due to the decrease in the kinetic energy of the machine. This one releases this energy and, thus, decelerates. If the machine is smaller (smaller H), it has less energy stored. Then, in order to give the required active power, its speed will decrease more.
The behaviour is similar in the other direction when the dip ends. The machine absorbs active power to come back at equilibrium. This results in an acceleration of the machine and an increase in the frequency. The first peak of frequency is very big in the case of a lower inertia. The frequency is increased by 3Hz (compared to steady state) and this is not acceptable in practice. These peaks are again smaller as the inertia constant increases. Concerning the damping of the oscillations, the behaviour is the same as for

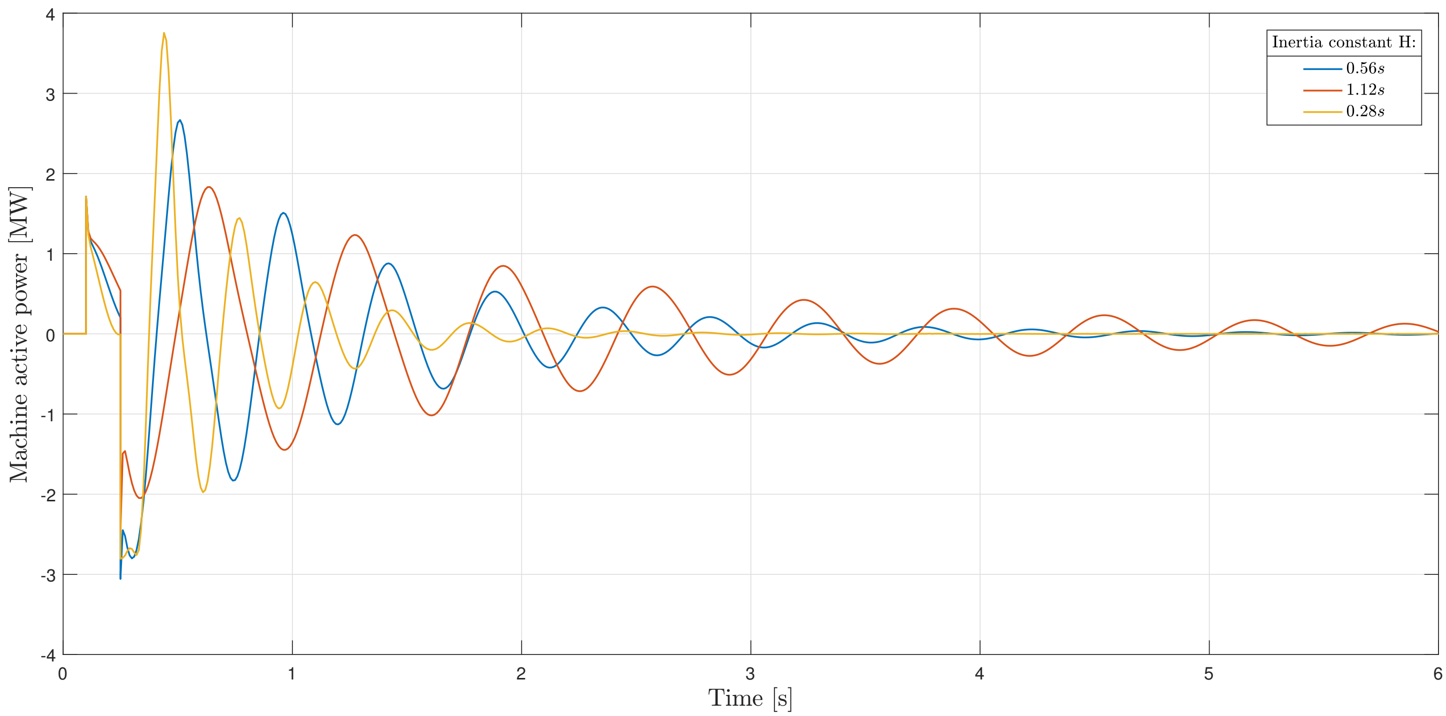

Figure 5.30
Evolution of the active power produced by the machine

the power.

The last thing to analyse is the load voltage. During the dip, this one decreases. It can be observed that it decreases more when the value of this constant decreases. This is due to the fact that the machine does not gives enough active power. In this case, the dip is not severe enough to cause damage or to yield to strong under-voltage but this can have its importance for more severe sags. After the dip, it can be seen that the oscillations have the same behaviour as before. These are more damped when the constant is smaller.

To conclude on the impact of the inertia constant H, it has been observed that increasing or decreasing this value has pros and cons. During the dip, the best behaviour can be obtained with the bigger inertia. However, after the dips, this yields to oscillations that are longer. However, these oscillations do not perturb the general behaviour too much and can be accepted (with limits). Decreasing the inertia yields to bigger problem during the dip and just after (frequency peak) and should be avoided in practice.

The power acceptability curves when H is equal respectively to $0.56s$, $1.12s$, $2.24s$ and "∞" are shown in figure 5.33. The PAJ is set to the value of $-22.5°$. The effect of the inertia constant can be seen and deep dip can be counter for longer time if this constant is doubled. However, for longer but shallower dips, the impact is not significant. In fact, this is due to the fact that the network is still present in this case and can provide active power. Thus, the additional inertia is less useful than for deeper dips (less power needed).
When the inertia constant is again doubled, the results are even better. In fact, increasing the inertia constant gives better results each time. However, it can be seen that even for inertia tending to infinity, all dips can not be countered. In this case, the machine remains stable (the speed does not change) but

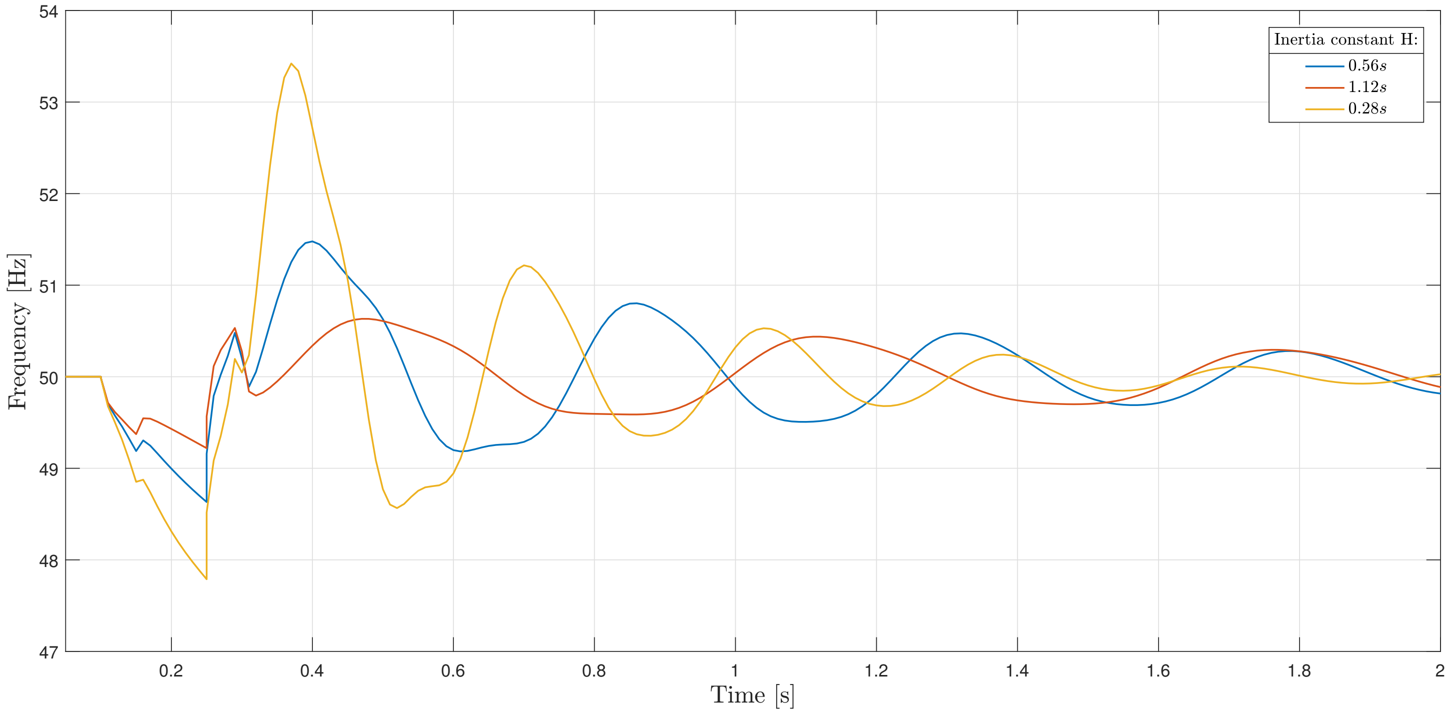

Figure 5.31
Evolution of the frequency at the load terminals

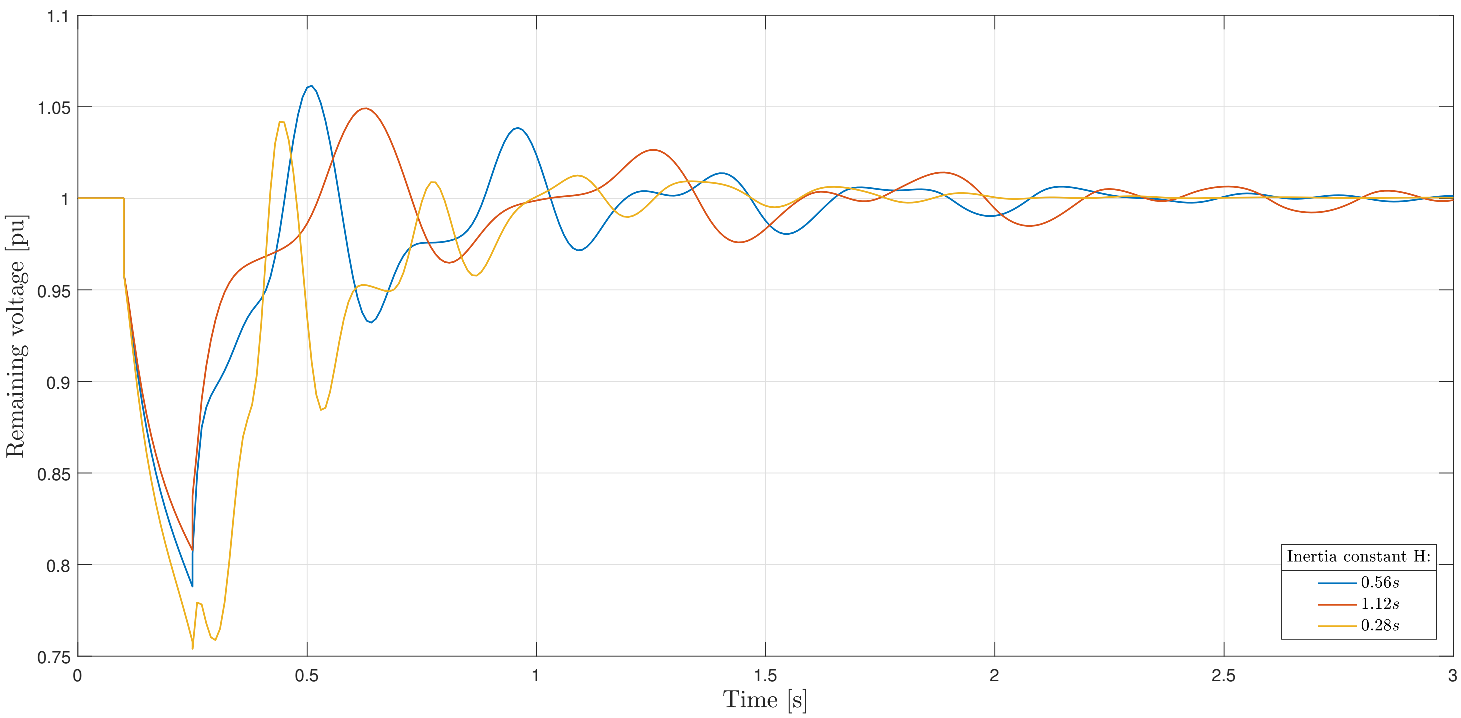

Figure 5.32
Evolution of the load voltages

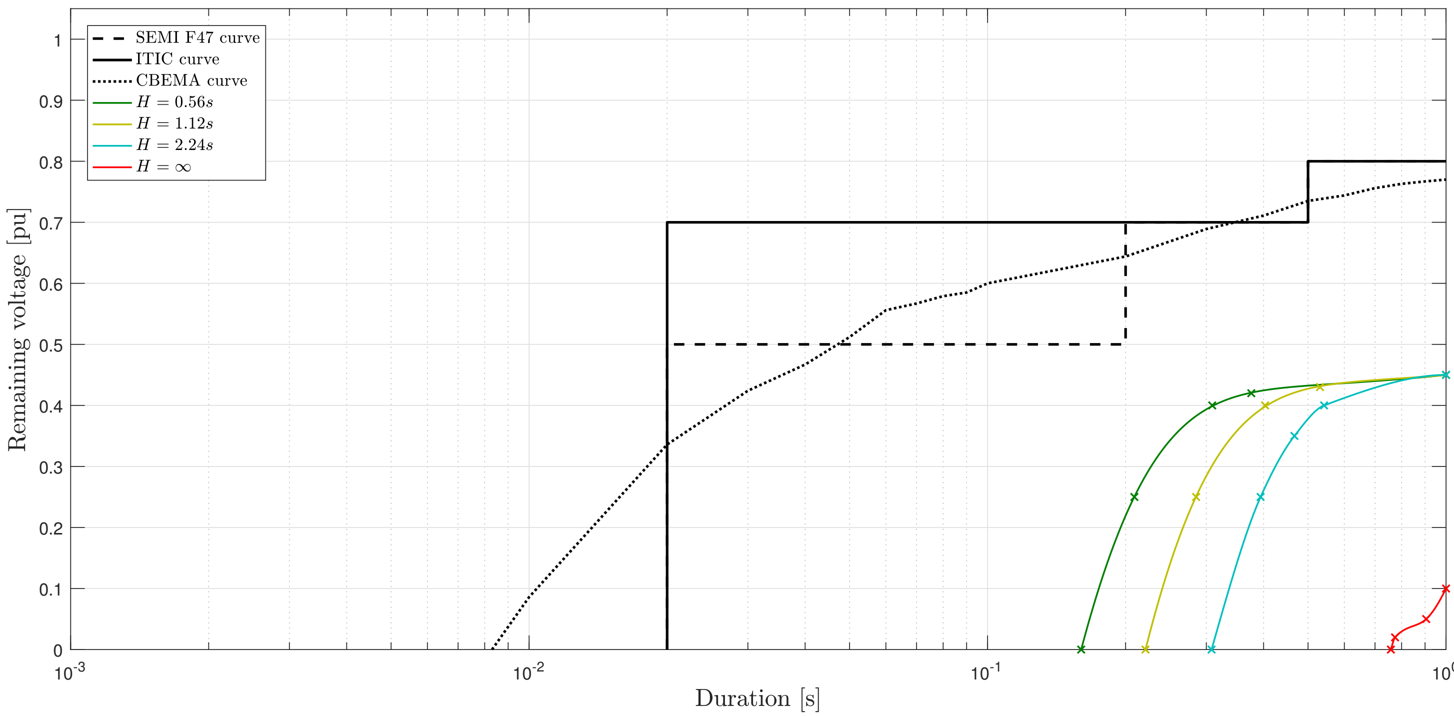

Figure 5.33
Power acceptability curve for $H = 0.56s$, $1.12s$, $2.24s$ and "∞"

the voltage decreases. Then, at a moment it goes under the acceptable limit and the dip can not be encountered. Then, for bigger inertia, the machine is more stable and the main criterion to accept the dip becomes the CBEMA limits.

Chapter 6

Change of load

During all the analysis, the loads were constant power loads and motors. This chapter aims at showing how the behaviour changes when those are changed in another type. In this approach, the same conditioner is used but the loads are changed. ERACS provides us way to model several types of loads. Among these, the following are analysed:

- Base case: 80% of constant power loads and 20% of motor
- All motors
- Real constant power loads

A type of load called "Real constant power loads" is introduced because, in ERACS, the loads labelled "constant power" are modelled as constant admittances in transient. Then, it does not behaves as real constant power loads. It results that another model needs to be find to simulate this behaviour. It is very important to simulate this type of load because it represents the worst loads when studying dips. Indeed, these loads continue to draw the same power during the dip. This is not the case for constant admittance loads because, as the voltage decreases, their will draw less power. Then, the machine has to produce less power. In the case of real constant power loads, the power will remain the same and the machine will have to produce a bigger amount of power, leading to a less stable situation.

6.1 Motors

In this case, the load can be for example a factory using a lot of induction machines for the manufacturing. It is set in order to consume the same active power as the previous load. The same small motors are kept and are assembled in parallel (16 in total). In order to compare to the initial situation, the new power acceptability curve is drawn for a realistic PAJ of $-22.5°$. Then, it can be easily compared to the initial situation.

This new power acceptability curve is shown in figure 6.1. It presents the standard, the curve obtained in the base case and the one obtained when all loads are motors. Two main parts can be extracted and distinguished in the curves.

The first one concerns short but severe dips. It can be seen that the motors help a little bit and that the curve is enlarge in this case. In fact, motors are like spinning reserve with very limited amount of energy in it. At the first moment after the dip, these release this energy to the network. This energy helps mitigating the voltage at the load bus. However, the difference is very small and the results is very

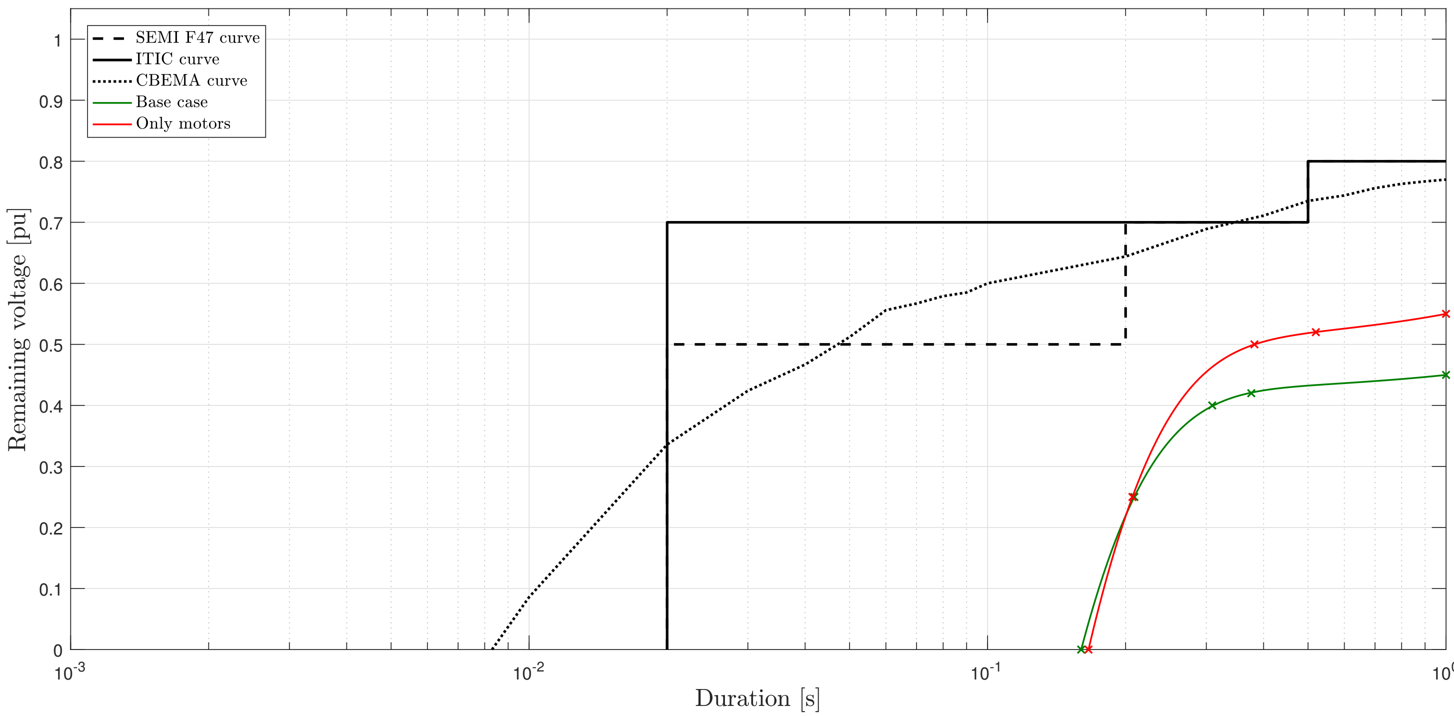

Figure 6.1
Power acceptability curve for phase angle jump in the base case and in full motor case

similar. Then, no significant conclusion can be drawn from this.

For the second part, the longer but less severe dips can be analysed. In this one, the power acceptability curve is worst in the case of full motor loads. This is explained in [27]. If the step decrease of the voltage lasts for too long, the motor has sufficient time to stabilise back at a new equilibrium point. At this point, it requires the same active power as before. In the base case, a majority of the load is constituted by fixed admittances (in ERACS transient module). They do not draw the same power during the dip. As the machine has to produce the bigger part of the active power during the dip, it has to produce more power in the full motor case. As seen before on the $P(\delta)$ curves, the more the production of active power, the less stable the machine. The conclusion is the following, for long dip, the synchronous machine has to produce more active power due to the motor. This results in a worst case compared to before.

This can be observed in figure 6.2. This shows the active power consumed by the load set in the base case and in the case with all motors. It has been obtained simulating a 40% dip (depth) with a PAJ of $-22.5°$ for 1s. This has been chosen so that the dip can be sustained longer enough. Then, the expected behaviour can be observed. It can be seen that, during the dip, the active power required by the motors is bigger than in the base case. This shows that it constitutes a worst case. An exception has to be made concerning the initial part of the power evolution. In this part, the consumed power is bigger in the base case. However, this part is very short and does not matter for longer dip.
After the dip, the oscillations are bigger in the case with all motors. This is due to the fact that this case yields to a worst situation at the end of the dip. Then, the stabilisation of the rotor is more difficult.

At the end, replacing the loads by motors has mainly a negative impact. For short dips, the results are pretty similar for both case. However, for longer dips, the motors restore their power to their pre-fault

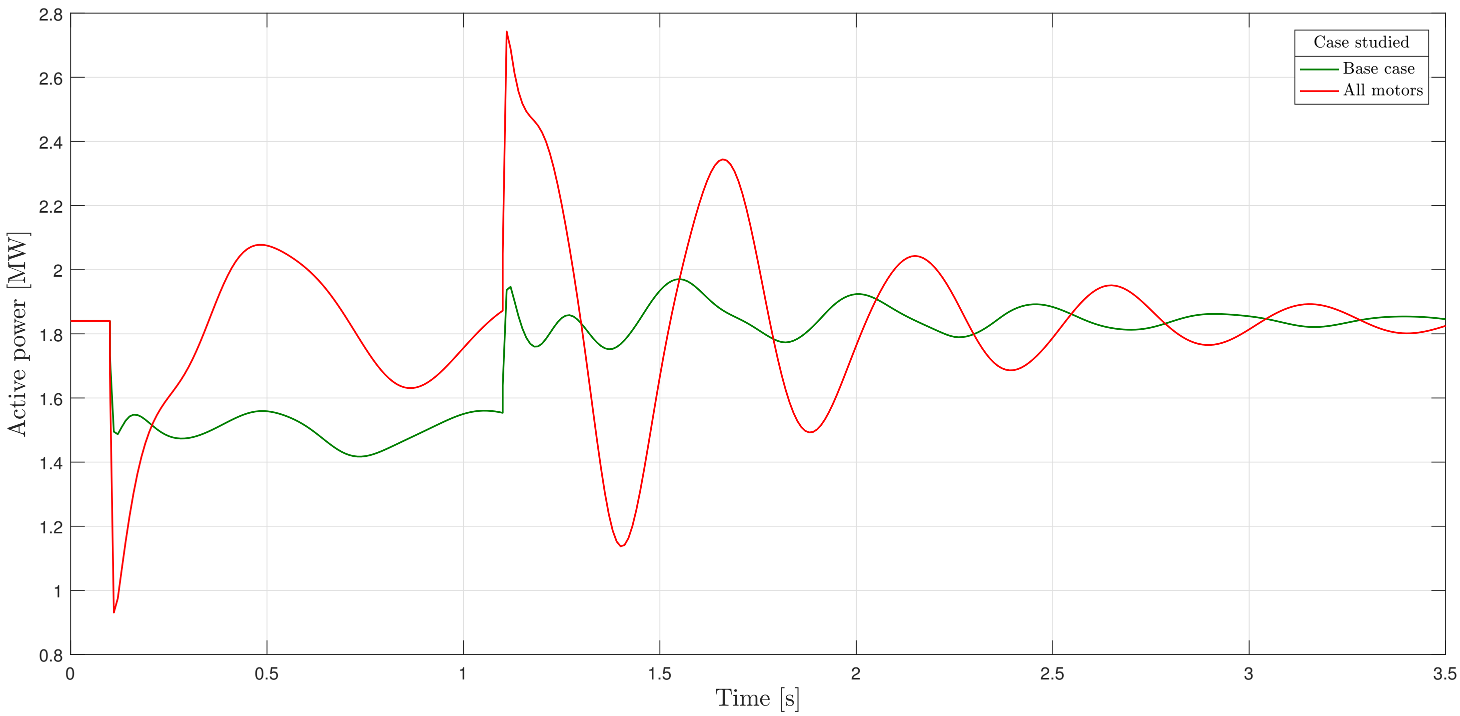

Figure 6.2
Active power consumed by the load in the base case and in the case with all motors

equilibrium. This increases the active power produced by the synchronous machine, yielding to a worst situation.

6.2 Real constant power loads

As explained before, loads called "constant power" are modelled as fixed admittances by ERACS during transient. This gives that the active power drawn by those loads varies with the voltage. During dips, as the voltage decreases, the active power decreases too. It constitutes a better case for the machine because it has to provide less active power. Thus, it is more stable. In the case of real "constant power loads", the active and reactive power consumed are kept constant during the dip, whatever the terminal voltage. Then, the machine has to provide more power and is less stable.

ERACS provides a way to implement such loads. It is further developed in Appendix G. The active and reactive powers consumed by this load during transient are going to be exactly the same as the loadflow values. All the network is the same as before and the new power acceptability curve can be drawn. This one is derived for a phase angle jump of $-22.5°$.

The resulting power acceptability curve is given in figure 6.3. As expected, the case with real constant power loads is worst than the base case. In this case, the curve remains under the CBEMA limits but come closer.

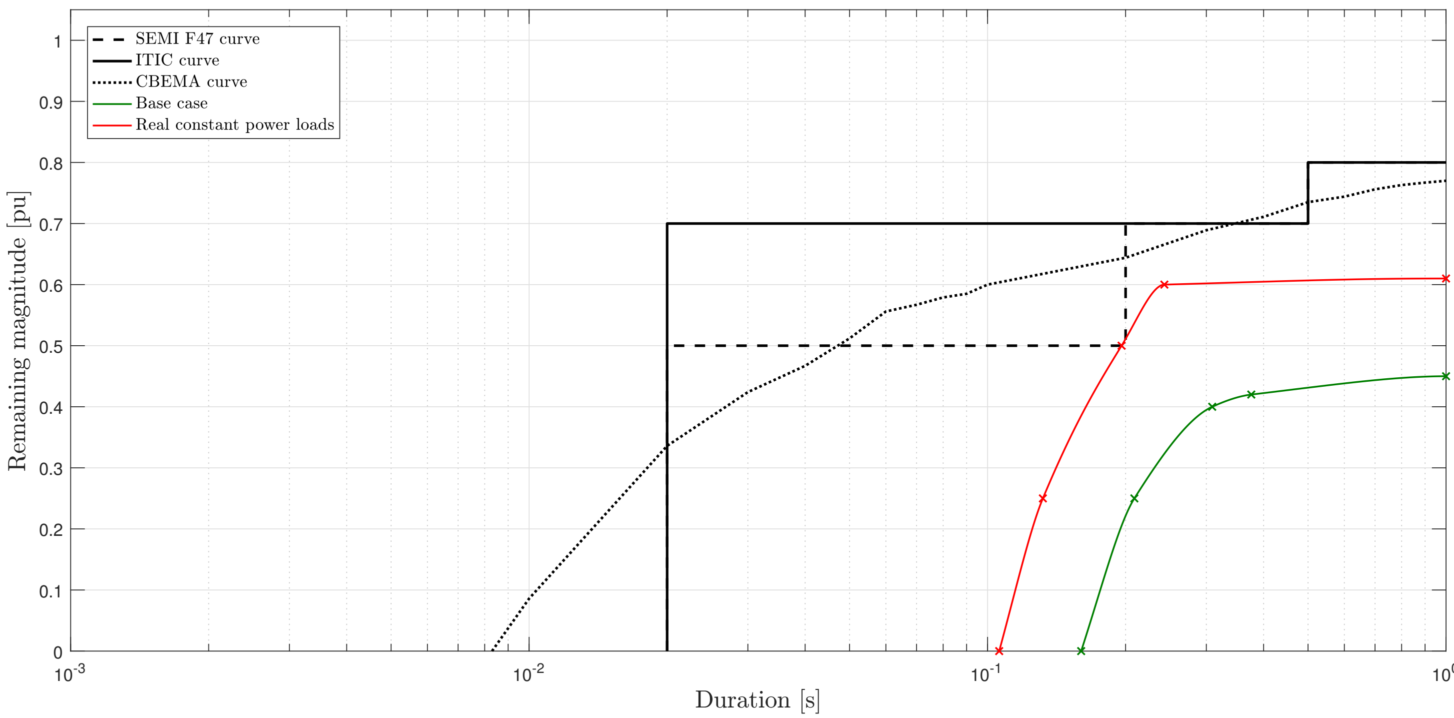

Figure 6.3

Power acceptability curve for the base case and for the case with real constant power loads

Chapter 7

Euro-Diesel products and customers

7.1 Applications

Euro-Diesel sells UPS systems. These ones guaranty a continuous supply of electricity. Therefore, the applications are all the domains that require an uninterrupted power supply. It sells mainly to other companies. This business can be called "Business-to-Business". Among these sectors, one can found:

- Data Centres: This sectors is increasing in importance and represents the main part of the company turnovers (around 55%).
- Infrastructures: It is constituted of airport, tunnel, ...
- Industries: Some fabrication factories require a continuous supply and can not tolerate any shutdown. There are a great number of different type of client (semi-conductors, chemical and automotive industries).
- Hospital: They require this device in order to power all their critical loads (for example: operating room, ...). It represents only a fraction of their total required power (around 20% in general) and therefore, the required machine is smaller.
- Diverse applications: It concerns more original projects. For examples, it can concerns observatory, television tower, ...

As can be seen, lot of sectors are targeted by the company. As a consequence, Euro-Diesel has to provide specialised product to all its customers. Moreover, all the locations are different and have different characteristics in term of space, installations, ... For these reasons, Euro-Diesel provided a particular solution to all its customers.

In terms of power, the company tries to focus on machine between 500 and 3000 kVA. The lower bound of the interval is due to the machine production price per kVA. This one is very high for machines smaller than 500 kVA. Then, for bigger machines, it remains more or less the same. The higher bound is due to technical reasons. In fact, for now this power is the maximal power reachable for the moment.
Machines smaller than 500 kVA can be produced by company but these are uncommon and very specific.

7.2 Targeted market

Euro-Diesel targets a market very limited in terms of size. Therefore, only a few customers are interested by their products. A consequence of this is that, in order to sell enough machines, the company has to target the whole world. For example, if only the Belgian market had been targeted, the number of machine sold would have been very limited and the situation would not been sustainable. This type of market is called a "Niche market".

In this market, two types of UPS can be observed. The first one is constituted of the static UPS. For this one, the main components are power electronics and batteries. More detailed on the functioning can be found previously in section 3.2. The second category is the one in which Euro-Diesel can be placed, the dynamic UPS category. In this one, the energy storage is made of a rotating mass. Moreover, a synchronous machine is there to transform the mechanical power to electrical power. The continuity is guarantied by a diesel engine that starts if the voltage drop is too severe. The two categories are continuously in concurrence. For now, the static UPS are more used and they dominate the market.

In the second category, the main competitors of Euro-Diesel are "Piller/Active power" and "Hitec". These sell a product with similar functions than Euro-Diesel but the storage technology is a little bit different:

- Piller uses as energy storage a big rotating vertical flywheel. This one is separates from the synchronous machine. Their advantage is the fact that it is easier to put their energy storage in parallel and therefore, to reach higher nominal power. Its main drawback is the fact that by multiplying the number of components on their system, the product becomes more complex.

- Hitec sells a product very similar but in their case, the drum is inserted inside the rotating shaft instead of outside. Therefore, it has to rotate quicker in order to have the same kinetic energy (smaller diameter). Then, the bearings are more solicited.

For now, the competitors are in a "race" to who will produce the bigger machine. The reason is that for very high power applications, the number of installed machines can be decreased by using bigger machine. In this scope, Piller has an advantage on the other competitors because, thanks to its energy storage technology, it is easier for him to put them in parallel, and thus increase the power.

These competitors also encounter the same problems as Euro-Diesel and have to target the whole world. The different companies do not share the world in controlled zone and they all sell machines in the whole world. Nevertheless, there are factors that influences the country in which the company sells. For example, Piller is a German company and Germany had always have privileged relations with Russia. For this reason, Piller has been the first to enter on the Russian market. Then, there are external factor influencing but, at the end, all is balancing and everybody target the same customers.

As said before, Euro-Diesel targets the whole world. However, the machines are not sold in the same amount for all parts. Figure 7.1 shows the share of the market in the world. As can be seen in the figure, during the last decade, a sales shift from Europe to the other part of the rest of the world occurs. In general, the increased in the share can be put in relation with the opening of Offices in diverse countries. Each time one is opened, it draws several customers in this region. For now, the main tendency is that the market opens more in the far-east and in South America.

7.3 Sales organisation

As seen before, the company is present all around the world. Then, subsidiaries have been founded all around the world. Each one focuses on its particular zone and sells machines within this one. For example, the Brazilian office is responsible for selling in the whole Latin America (Mexico included). Thanks to this, the company can be closer to their clients.

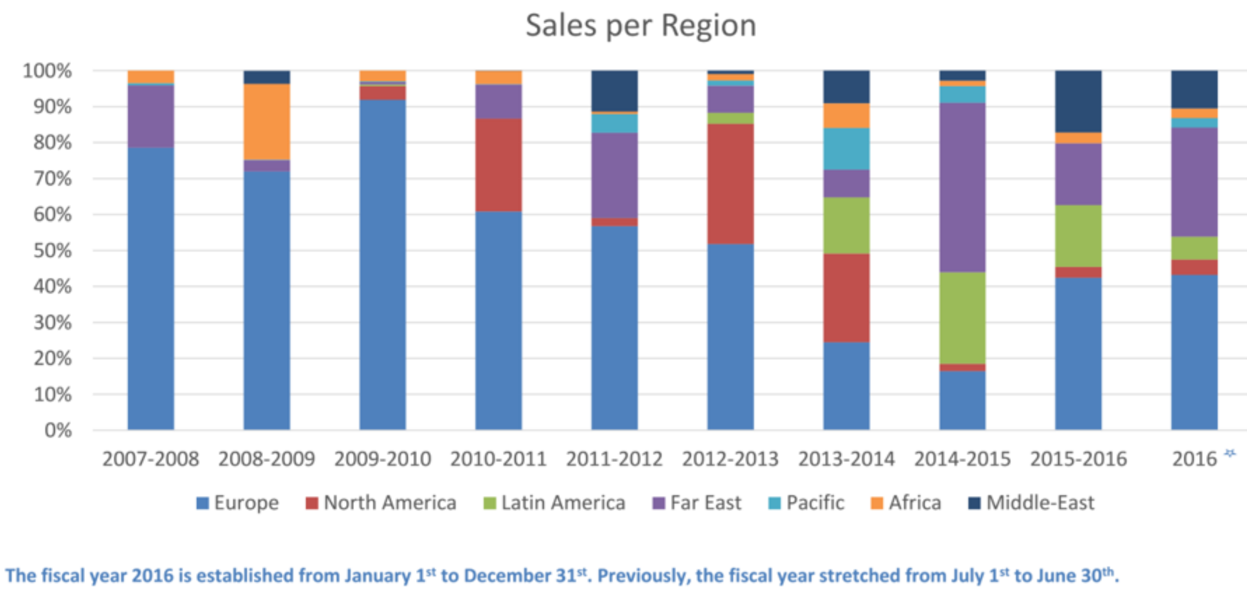

Figure 7.1
Sales share over time

These subsidiaries are located in United-Kingdom, France, United-states, Germany, Singapore, Brazil, Dubai, Doha, Turkey, Russia and Belgium.

These subsidiaries can also include some persons responsible for the maintenance. These are there to do the maintenance in the country in which they are based. In countries where there are no office, an independent employee is formed by the company in order to do the job. The installation of the equipment is not done directly by the company. They subcontract this process to a local company that will be in charge of the cable connections,...

Another way for the company to sales the products is through "Distributors". These are companies all around the world that sells the product. Euro-Diesel trains them and allows them to sell the product. These are independent of Euro-Diesel and are more a collaborator. These takes a marginon the product and do not sell only Euro-Diesel products. A figure showing the locations of the company offices and the distributors is given in figure 7.2.

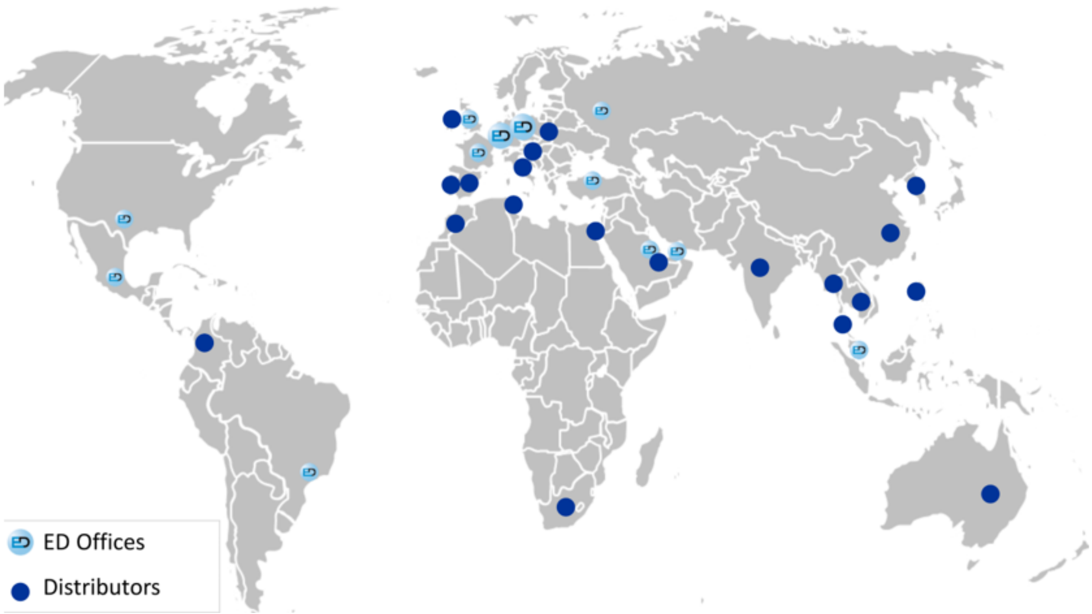

Figure 7.2
Location of Euro-Diesel's office and distributors

Chapter 8

Conclusion

The first conclusion comes from the dip characteristics. These were analysed and detailed in the first part of the thesis. During this part, it has been shown that a voltage dip is more complex than a simple step decrease in the voltage. These can be of several origins like faults, transformer energising,... and they do not have the same time evolutions. Moreover, other parameters are very important when simulating voltage dips. These are phase angle jump, point-on-wave and duration.

Afterwards, two types of dips were analysed. These were simulated using the software ERACS. The focus has been made on two types: the three-phase and the single-phase dips. The first one constitutes the severest one and the second is the most common met in power systems. As a distribution transformer is present at the entry of the equipment, the second type evolves in a type C. Therefore, the dip seen by the load is of type C.

Concerning the first type analysed, the assessment of the synchronous machine stability has been carried on. This one is based on the so-called "equal-area criterion". It has been highlighted that the deepest magnitudes, the longest dips and the biggest phase angle jumps yield to the worst case. Due to the phasor approximation made by the software, the impact of the point-on-wave could not have been observed.

Then, these two types are analysed and simulated in order to obtain new power acceptability curves. The simulations are performed with two phase angle jumps: the biggest encountered in practice ($-45°$) and a more realistic one ($-22.5°$). These can be easily compared to the standard curve. They show the dips at the entry (before the transformer) such that the load voltage stays within limits (the CBEMA). For type A, the main conclusion is that the improvements with the equipment are not negligible. Then, deeper and longer dips can be met.

For type C, a first conclusion can be made about the type of voltage used for the load. It has been shown that, without the equipment, using phase voltage (delta connected load) yields to a situation a little bit better. With the equipment, all dips can be met and the voltage stays within the limits. This is a really big improvement.

Moreover, the impact of a bigger machine inertia constant H has been analysed. It comes from the simulations that, if this one is decreased, higher frequency peaks appear in the response. Nevertheless, if this constant is increased, the results are better. The comparison between several values of this constant has been carried on thanks power acceptability curves. Another conclusion is that, even with an infinite inertia, the load voltage decreases during the dip and some sags are too severe and have to be rejected.

At the end, the impact of two other loads has been investigated. The first one is the case where the whole load is made of motors. In this case, the results are worst than in the base case. Then, the second case is the worst case that can be met: constant power loads. The results obtained with this kind of load are worst.

At the end, there is space for further works on the voltage dip mitigation subject. These can explore ways to improve the results. For example, the AVR can be modified in order to have a more suitable response. An huge improvement can be the addition of an accumulator to the machine. This one has to be modelled in ERACS and should improve the load voltage during dips.

Appendix A

Synchronous machine datasheet

MarelliMotori
Inspired solutions

GENERATORE SINCRONO TRIFASE
THREE - PHASE SYNCHRONOUS
GENERATOR

PRELIMINARY MJB 630 LA 4

CLASSE DI SOVRATEMPERATURA - TEMPERATURE RISE CLASS	F
CLASSE DI ISOLAMENTO – INSULATION CLASS	H
FORMA COSTRUTTIVA – MOUNTING	B20/B14
TEMPERATURA AMBIENTE (℃) – AMBIENT TEMPERATURE (℃)	40
ALTITUDINE MASSIMA (m) - MAX. ALTITUDE (m)	1000
PROTEZIONE - PROTECTION DEGREE	IP 23
FATTORE DI POTENZA - POWER FACTOR	0,80
NUMERO DI POLI - NUMBER OF POLES	4
VELOCITA' NOMINALE (r.p.m.) - RATED SPEED (r.p.m.)	1500
SOVRAVELOCITA' (r.p.m.) - OVERSPEED (r.p.m.)	2250
NUMERO DI TERMINALI - NUMBER OF TERMINALS	6
PASSO DI AVVOLGIMENTO - WINDING PITCH	2/3
RESISTENZA STATORICA @ 20℃ (m Ω) - STATOR RESISTANCE @ 20℃ (m Ω)	0,284
PESO (kg) - WEIGHT (kg)	7500
MOMENTO D'INERZIA (kg*m^2)- INERTIA (kg*m^2)	150

FREQUENZA - FREQUENCY	Hz	50
TENSIONE - VOLTAGE	V	400
CORRENTE NOMINALE - RATED CURRENT	A	4763
POTENZA - RATING	kVA	3300
RENDIMENTO - EFFICIENCY - (%)	4/4	97,2
P.F.= 1	3/4	96,9
	2/4	96,2
	1/4	94,1
RENDIMENTO - EFFICIENCY - (%)	4/4	96,4
P.F.= 0,80	3/4	96,1
	2/4	95,3
	1/4	92,7

PERDITE - LOSSES (kW)	4/5 (80%)	81,1
P.F.= 0	3/5 (60%)	67,7
	2/5 (40%)	57,0
	1/5 (20%)	48,6
	0/5 (0%)	42,5

rapporto di corto circuito - short circuit ratio		SCR	0,48
reattanza - reactance (%)	sincrona diretta - synchronous direct axis	Xd_{uns}	248
	sincrona in quadratura - synchr. quadrature axis	Xq_{uns}	139
	transitoria diretta - transient direct axis	$X'd_{sat}$	24,9
	transitoria in quadratura - transient quadrature axis	$X'q_{uns}$	139
	subtransitoria diretta - subtransient direct axis	$X''d_{sat}$	11,3
	subtransitoria in quad. - subtransient quadr. axis	$X''q_{sat}$	11,6
	di sequenza negativa - negative sequence	$X2_{sat}$	11,4
	di sequenza zero - zero sequence	Xo_{sat}	4,13
costanti di tempo - time constants (s)	a vuoto - open circuit	T'do	4,729
	transitoria - transient	T'd	0,473
	subtransitoria - subtransient	T"d	0,02
	unidirezionale - armature	Ta	0,061
Coppia di corto circuito bifase - Phase to Phase short circuit torque		kN*m	279
Coppia di corto circuito trifase - Three phase short circuit torque		kN*m	186

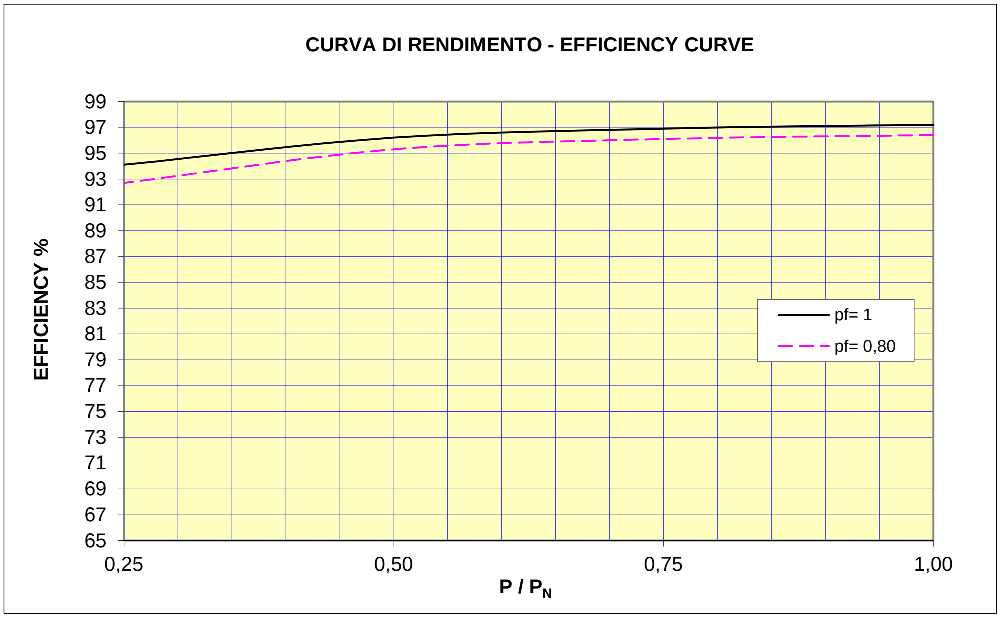
CURVA DI RENDIMENTO - EFFICIENCY CURVE
EFFICIENCY %
99
97
95
93
91
89
87
85
83
81
79
77
75
73
71
69
67
65
0,25
0,50
0,75
1,00
P / P_N
pf= 1
pf= 0,80

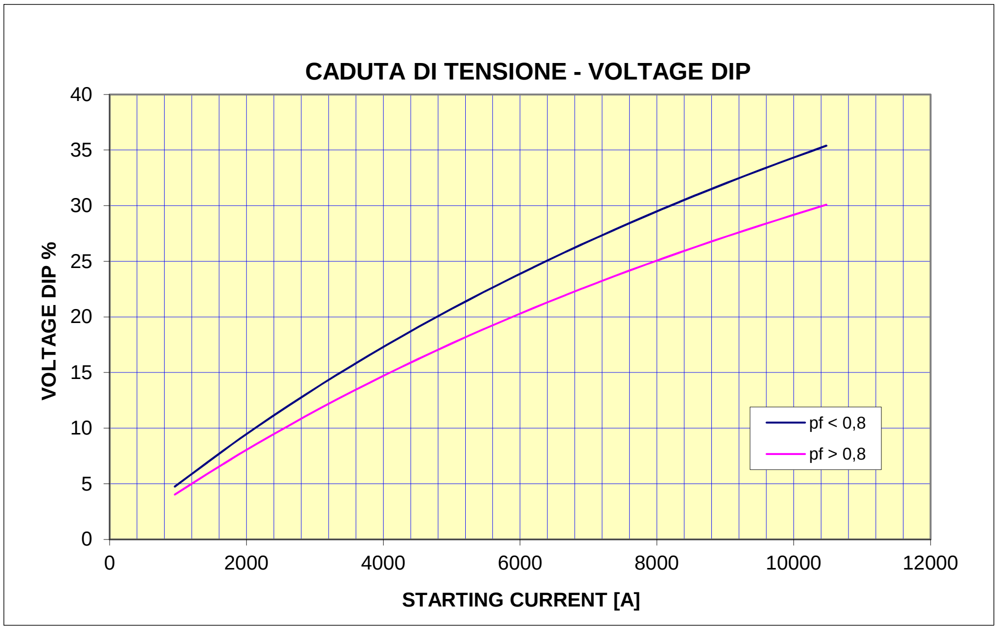
CADUTA DI TENSIONE - VOLTAGE DIP
VOLTAGE DIP %
40
35
30
25
20
15
10
5
0
0
2000
4000
6000
8000
10000
12000
STARTING CURRENT [A]
pf < 0,8
pf > 0,8

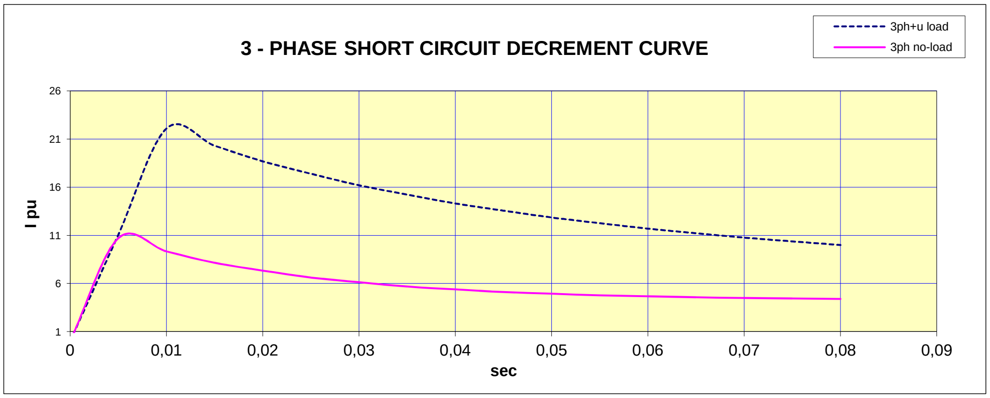

3 - PHASE SHORT CIRCUIT DECREMENT CURVE
3ph+u load
3ph no-load
I pu
26
21
16
11
6
1
0
0,01
0,02
0,03
0,04
0,05
0,06
0,07
0,08
0,09
sec

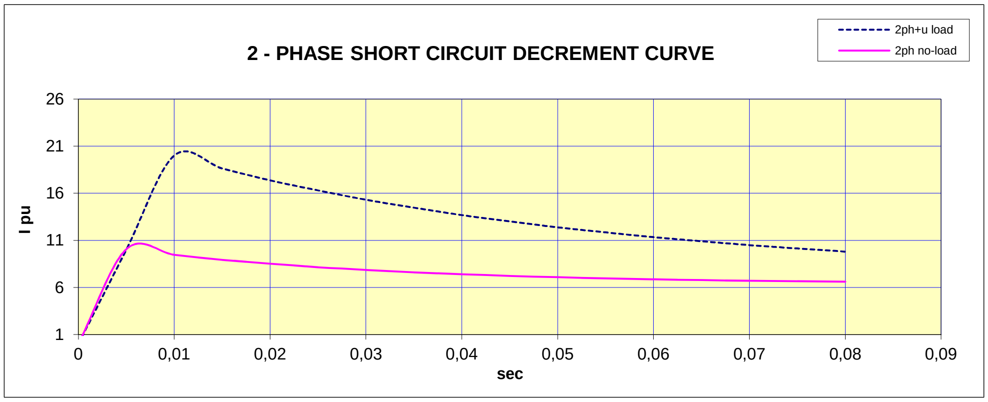

2 - PHASE SHORT CIRCUIT DECREMENT CURVE
2ph+u load
2ph no-load
I pu
26
21
16
11
6
1
0
0,01
0,02
0,03
0,04
0,05
0,06
0,07
0,08
0,09
sec

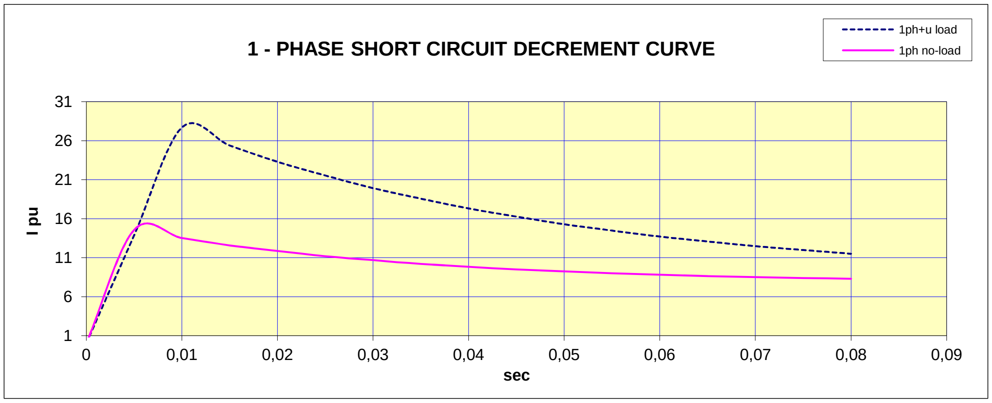

1 - PHASE SHORT CIRCUIT DECREMENT CURVE
1ph+u load
1ph no-load
I pu
31
26
21
16
11
6
1
0
0,01
0,02
0,03
0,04
0,05
0,06
0,07
0,08
0,09
sec

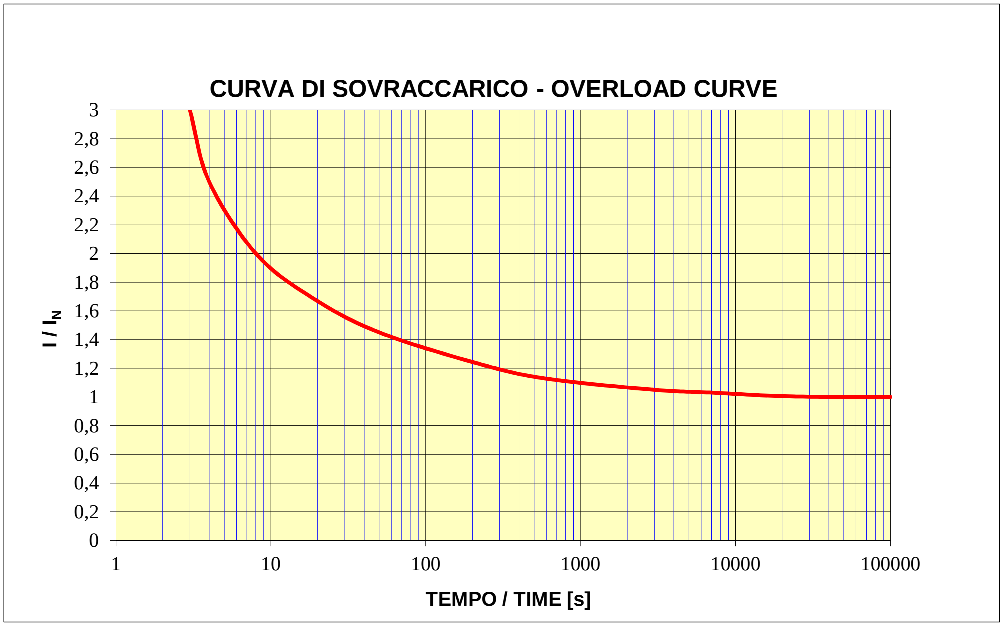

CURVA DI SOVRACCARICO - OVERLOAD CURVE
I / I_N
3
2,8
2,6
2,4
2,2
2
1,8
1,6
1,4
1,2
1
0,8
0,6
0,4
0,2
0
1
10
100
1000
10000
100000
TEMPO / TIME [s]

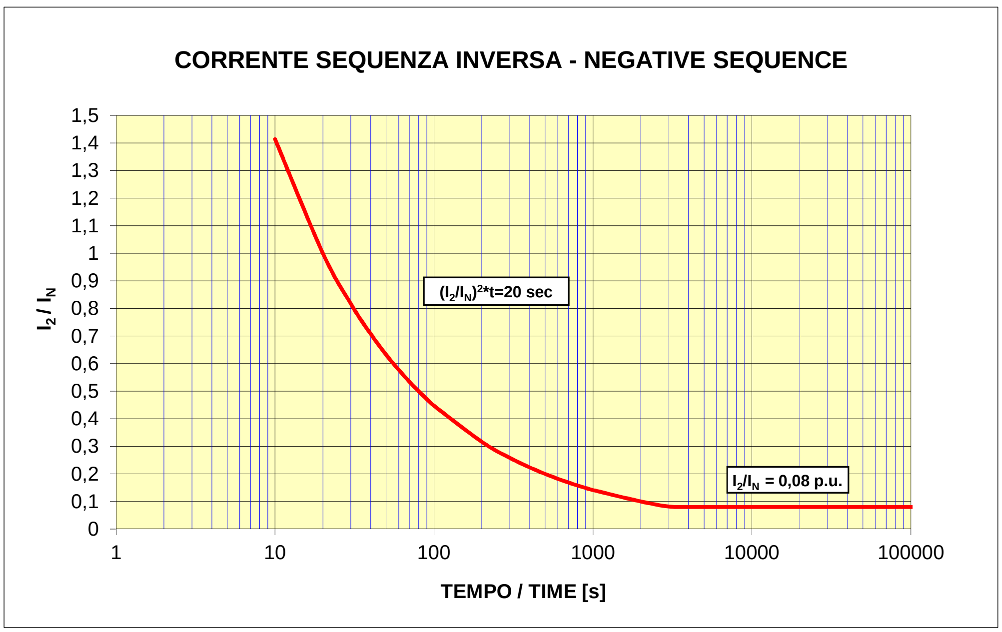

CORRENTE SEQUENZA INVERSA - NEGATIVE SEQUENCE
I2 / IN
1,5
1,4
1,3
1,2
1,1
1
0,9
0,8
0,7
0,6
0,5
0,4
0,3
0,2
0,1
0
(I2/IN)2*t=20 sec
I2/IN = 0,08 p.u.
1
10
100
1000
10000
100000
TEMPO / TIME [s]

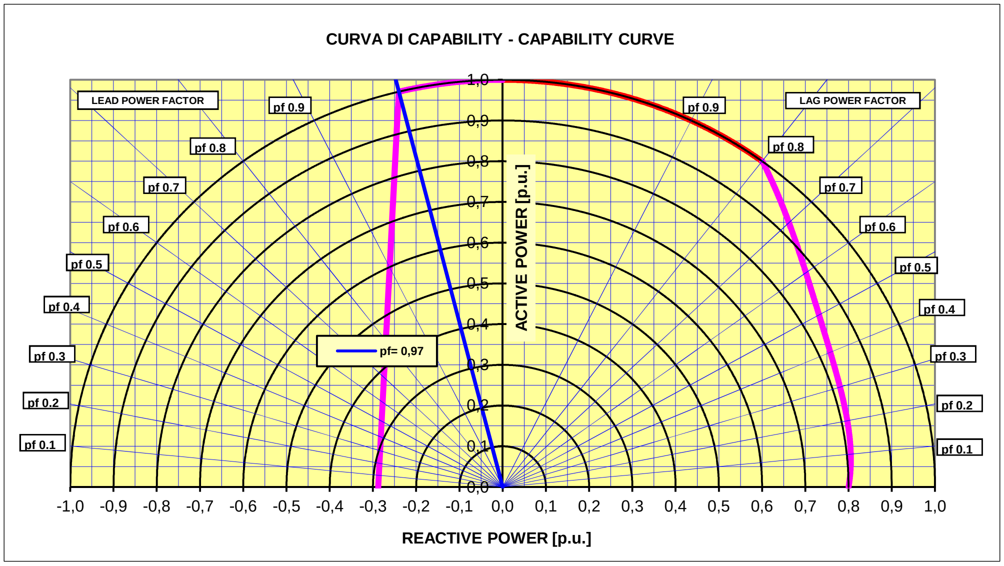
CURVA DI CAPABILITY - CAPABILITY CURVE
LEAD POWER FACTOR
LAG POWER FACTOR
pf 0.9
pf 0.8
pf 0.7
pf 0.6
pf 0.5
pf 0.4
pf 0.3
pf 0.2
pf 0.1
pf= 0,97
ACTIVE POWER [p.u.]
REACTIVE POWER [p.u.]
-1,0 -0,9 -0,8 -0,7 -0,6 -0,5 -0,4 -0,3 -0,2 -0,1 0,0 0,1 0,2 0,3 0,4 0,5 0,6 0,7 0,8 0,9 1,0

Appendix B

Three-point self data

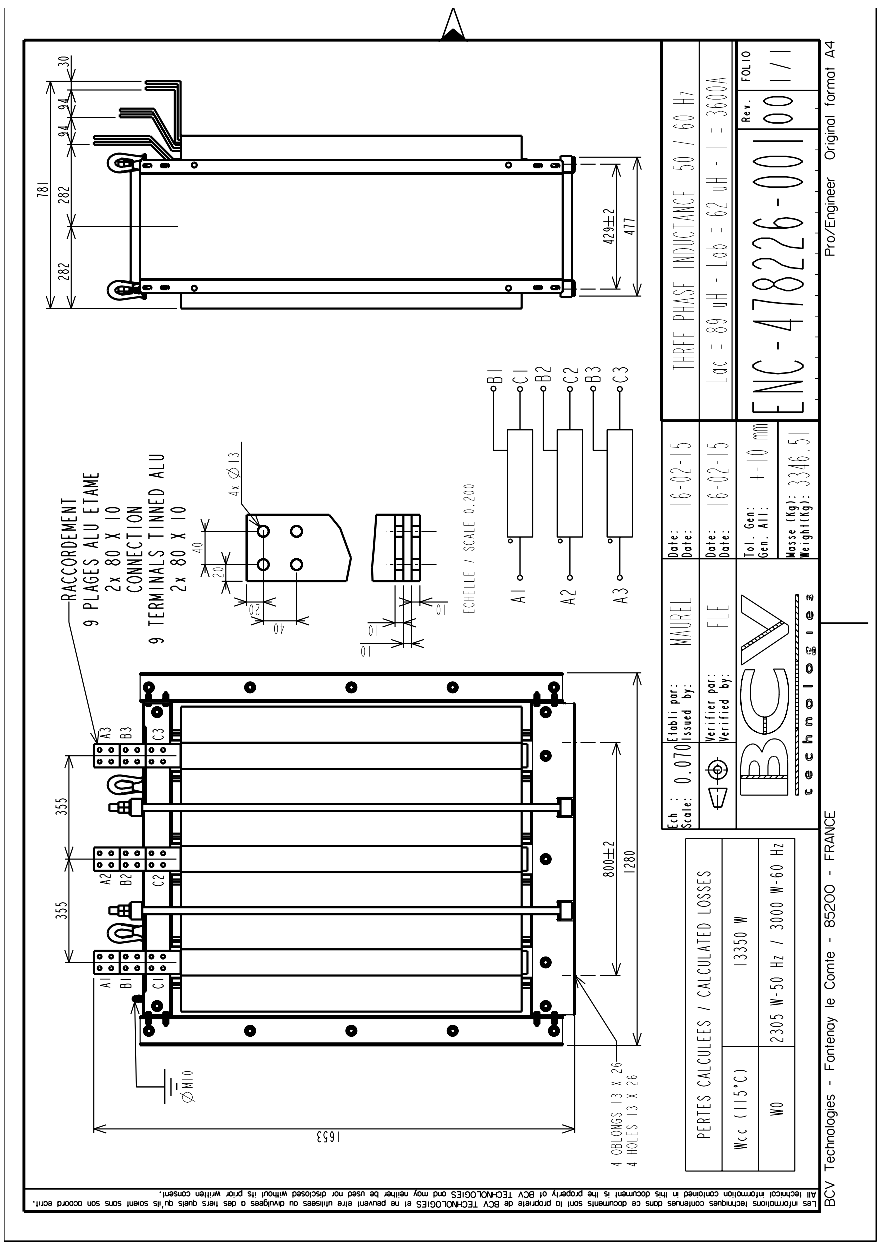

Appendix C

Induction machine data

Name	**modeling**
Address	**base state**

Induction Machine Data:

Identifier:	MI-load
Description:	
Library Key Name:	MA11
Library Key Description:	116kW 0.4kV
Loadflow Data	
Busbar:	BUS-6
Machine Type:	Induction Motor
Number in Parallel:	3
Group Assigned Power (MW):	0,32
Rating (MVA):	0,145
Power Rating (MW):	0,116
Voltage Rating (kV):	0,4
Frequency (Hz):	50
Impedance Units:	pu on rating
Stator Resistance:	0,012
Stator Reactance:	0,121
Magnetising Reactance:	4,091
Rotor Standstill Resistance	0,033
Rotor Standstill Reactance:	0,064
Rotor Running Resistace:	0,021
Rotor Running Reactance:	0,079
Transient Stability Data	
Inertia Units	kW.s / kVA
Inertia:	0,7

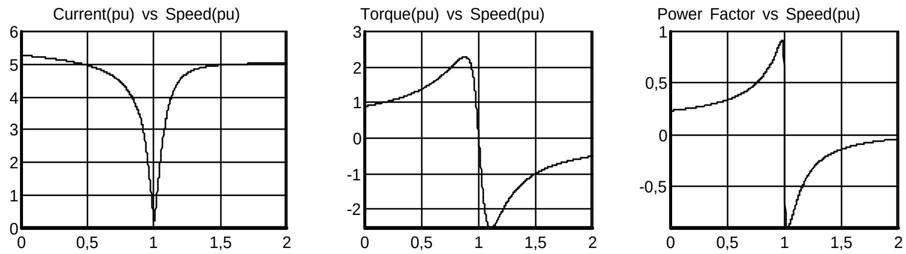

Appendix D

Remaining voltages and fault impedances

In this appendix, the fault impedance expressions are obtained. These ones are used to obtain the expected magnitude and phase angle jump for the remaining voltage during the fault. The developments are made for the three-phase and the single-phase fault as these are the ones studied in this thesis.
In this part, the hypothesis that the grid is the main feeder of the fault is made. This means that the current coming from the load are neglected for the calculation. Indeed, the grid has a short-circuit power very big compared to the device equipment. Moreover, the grid is present just beside the fault. This makes the computation much easier and produces very good results.

Three-phase fault

The simple divider model shown in figure D.1 can be used. $\bar{E}_s$ is the grid equivalent internal voltage, Z_s is the grid equivalent Thévenin impedance and Z_F is the fault impedance. The fault is balanced, then, only the positive sequence is used. This gives a retained voltage at the PCC equal to (load currents are neglected):

$$\bar{V}_{PCC} = \bar{E}_s \frac{Z_F}{Z_F + Z_s} \tag{D.1}$$

Then, knowing the internal equivalent voltage and the Thévenin equivalent impedance of the source, the fault impedance is given by:

$$Z_F = \frac{Z_s \bar{V}_{PCC}}{\bar{E}_s - \bar{V}_{PCC}} \tag{D.2}$$

Thanks to this equation, for every remaining voltage (magnitude and phase), one fault impedance can be computed. The phase angle jump is the difference between the phase of the fault voltage and the pre-fault voltage. As the PCC is used as reference in the circuit, the pre-fault voltage phase is 0° and the PAJ is equal to the faulted voltage phase angle.

Single-phase fault

In this case, not only the positive sequence has to be considered. The negative and the zero sequences have to be assembled together with this sequence. It gives the model shown in figure D.2. Only the elements corresponding to the grid are present due to the assumption explained previously (load currents neglected). In our case, the faulted phase is phase A. The subscripts 1, 2 and 0 describe respectively positive, negative and zero sequences.

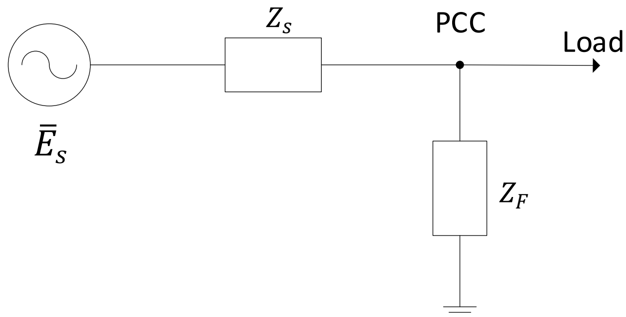

Figure D.1
Model for the three-phase fault

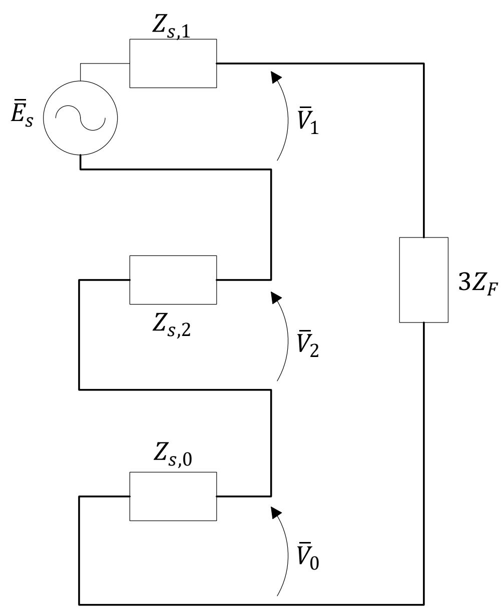

Figure D.2
Model of the sequence network for the single phase fault

Using the definition of the symmetrical components, the voltage in phase A is given by:

$$\bar{V}_a = \bar{V}_1 + \bar{V}_2 + \bar{V}_0 \tag{D.3}$$

It corresponds to the voltage across the impedance $3Z_F$. Using the voltage divider formula, it is equal to:

$$\bar{V}_a = \frac{3Z_F}{3Z_F + Z_{s,1} + Z_{s,2} + Z_{s,0}} \bar{E}_s \tag{D.4}$$

Here, all the three sequences of the source impedance are equal (equal to Z_s). At the end, the faulted impedance can be isolated:

$$\bar{V}_a = \frac{Z_F}{Z_F + Z_s} \bar{E}_s \tag{D.5}$$

At the end, the fault impedance can be isolated as done previously for the three-phase fault case. It can be remark that the result is the same. This is due to the fact that all the sequence impedances of the network are equal.

Appendix E

Extraction of the data and post-processing for type C

This section explains the path followed to retrieve the three voltages at the load terminal. For this, several data are extracted from ERACS. These are: the positive-sequence voltage at the fault location (magnitude and phase), the positive-sequence current flowing in the fault (magnitude and phase) and the positive-sequence current coming from the grid (magnitude and phase). In the case with conditioner, two additional variables are extracted, the magnitude and the phase of the internal EMF used by ERACS to model the motor.
The equivalent general schematic in the case of a single-line-to-ground fault is given in figure E.1. The conventions used for the computation are the ones of the figure. This case describes the way to obtain the load terminal voltages. The way the element are modelled in the software is given in [20].

E.1 Case without the voltage conditioner

The currents are all equal to I_f. This one is extracted from ERACS.
Using Ohm's law, the zero-sequence voltage can be obtained:

$$\bar{V}_0 = -Z_0 \bar{I}_f \tag{E.1}$$

Z_0 is the zero-sequence impedance of the sequence network. In fact, this one is equal to the zero-sequence impedance of the grid equivalent due to the Δy transformer (open-circuit).
The voltage $\bar{V}_a$ is equal to the positive-sequence voltage before and after the dip. During this one, it is equal to $3Z_f\bar{I}_f$ (Ohm's law).
The second Kirchhoff's law gives the negative-sequence voltage:

$$\bar{V}_- = \bar{V}_a - \bar{V}_0 - \bar{V}_+ \tag{E.2}$$

Then, the phasor of the voltages and of the currents at the fault location can be obtained using the transformation matrix $\mathbf{T}$. If $a = e^{j\frac{2\pi}{3}}$, this one is given by:

$$\mathbf{T} = \begin{pmatrix} 1 & 1 & 1 \\ a^2 & a & 1 \\ a & a^2 & 1 \end{pmatrix} \tag{E.3}$$

The relation linking the three voltages and the sequence voltages is used to obtain the voltages at the fault location:

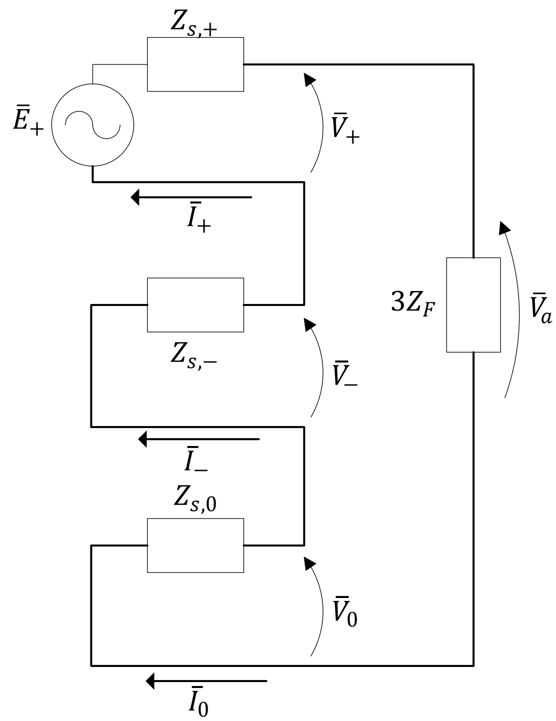

Figure E.1
Model for a single-line-to-ground fault

$$\begin{pmatrix} \bar{V}_a \\ \bar{V}_b \\ \bar{V}_c \end{pmatrix} = \mathbf{T} \begin{pmatrix} \bar{V}_+ \\ \bar{V}_- \\ \bar{V}_0 \end{pmatrix} \tag{E.4}$$

Afterwards, the principle is to come back in the positive- and negative-sequence network in order to obtain the load voltages. The zero-sequence component is not explored as the Δy transformer is an open-circuit in this sequence. Therefore, the zero-sequence current going in the load is equal to zero and the zero-sequence voltage does not propagate to the load. The equivalent positive sequence circuit is modelled by ERACS as shown in figure E.2. For the negative sequence, it is similar but the two EMF are suppressed and the impedances need to be replaced by their equivalent in the negative sequence. In ERACS, these are the same as the positive-sequence impedance for the elements modelled here.
For the grid, the positive-sequence current is directly obtained from ERACS. For the negative sequence, it is found using the Ohm's law. It is equal to $-\bar{V}_-/Z_{s,-}$. The minus sign is due to the convention used. The current in the transformer (modelled by Z_t in figure E.2) is obtained using first Kirchhoff's law. This gives, for the positive sequence, $\bar{I}_{t,+} = \bar{I}_{g,+} - \bar{I}_f$. For the negative sequence, the same equation can be used (with the corresponding element). These flows from BUS-F to BUS-L
The positive- and negative-sequence voltages at the load terminal L are obtained using Ohm's law on Z_t. This gives, for the positive sequence:

$$\bar{V}_{L,+} = \bar{V}_+ - \bar{I}_{t,+} Z_t \tag{E.5}$$

The equation can be used with the corresponding elements in the negative sequence. The three line voltages at L are obtained in the same way as before, using the matrix $\mathbf{T}$ given in E.3 and the equation given in E.4. The last thing to add to obtain the load voltages is the transformation due to the

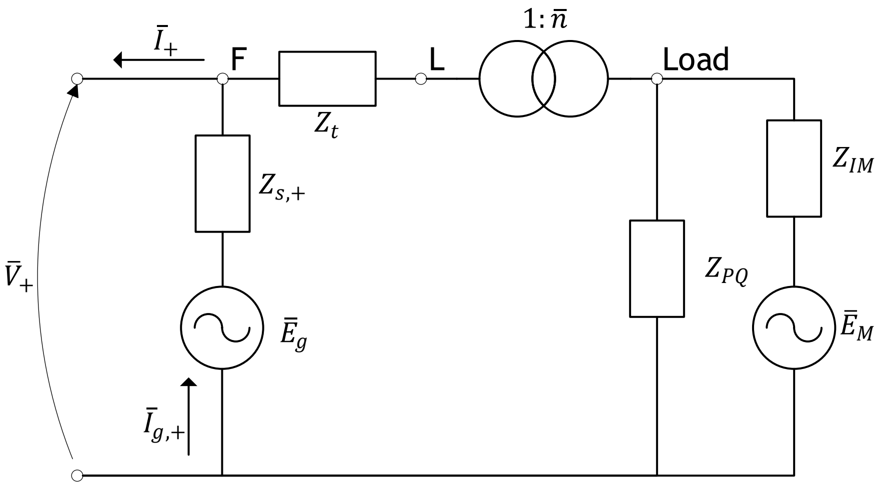

Figure E.2
Equivalent circuit seen from the fault for the positive sequence

transformer. These ones are obtained using a transformation matrix:

$$\mathbf{T}_1 = \frac{j}{\sqrt{3}} \begin{pmatrix} 0 & 1 & -1 \\ -1 & 0 & 1 \\ 1 & -1 & 0 \end{pmatrix} \tag{E.6}$$

This gives load voltages equal to:

$$\begin{pmatrix} \bar{V}_{a,load} \\ \bar{V}_{b,load} \\ \bar{V}_{c,load} \end{pmatrix} = \mathbf{T}_1 \begin{pmatrix} \bar{V}_{a,L} \\ \bar{V}_{b,L} \\ \bar{V}_{c,L} \end{pmatrix} \tag{E.7}$$

The current on this side of the transformer can be obtained in a similar way (using the transformation matrix).

E.2 With the rotary voltage conditioner

In this case, all the previous developments are still valid and are used to obtain the voltages and currents just after the transformer. Figure E.3 shows the equivalent positive-sequence schematic of the whole network (with conditioner). The variables labelled before "load" become the variables with a subscript "A". Remark that, as there are three motors in parallel, Z_{IM} is equal to the impedance of one motor divided by three. $\bar{E}_M$ remains the same as for one motor. The negative-sequence network is the same except concerning the two EMF. These are not present in this sequence. For the zero sequence, the same principle as before holds (open-circuit).
The voltage at the intermediate point is obtained using Ohm's law $\bar{V}_{inter} = \bar{V}_A - Z_{A,+}\bar{I}_A$. In this case $\bar{I}_A$ is the current between "A" and "inter" (obtained as the previous load current).
Afterwards, for the positive sequence, in order to avoid using the part containing the synchronous machine (branch C), the current flowing from BUS "inter" to BUS "Load" is computed using the

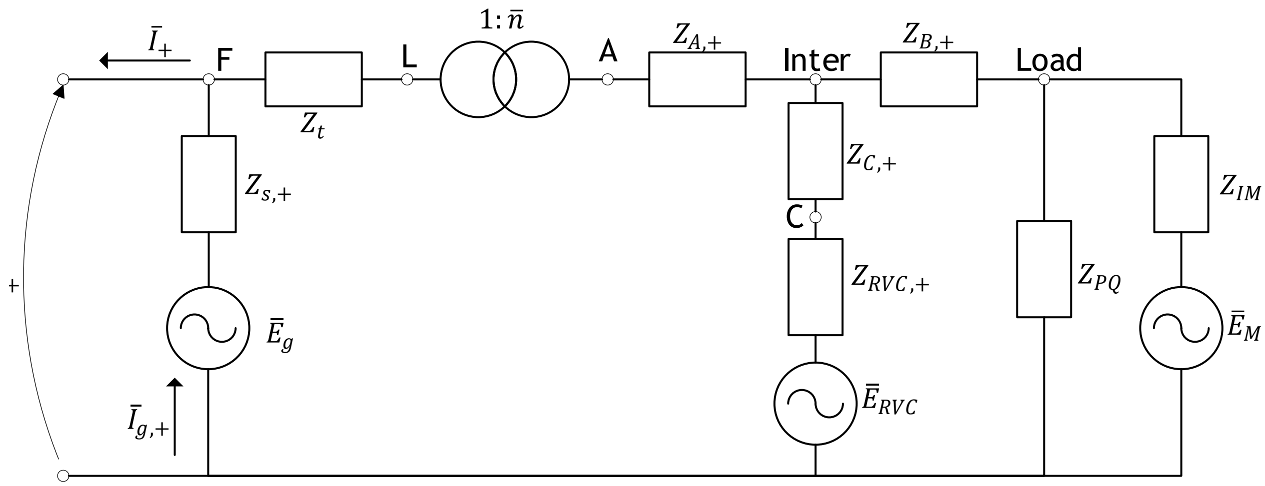

Figure E.3
Equivalent schematic for the positive sequence if the voltage conditioner is present

Thévenin equivalent seen from the BUS "inter". This one does not take the branch C. All calculations made, the equivalent impedance is $Z_{eq} = Z_{B,+} + \frac{Z_{IM}Z_{PQ}}{Z_{IM}+Z_{PQ}}$. The equivalent EMF is given by $\bar{E}_{eq} = \frac{Z_{PQ}\bar{E}_M}{Z_{PQ}+Z_{IM}}$.
Then, the current flowing in the equivalent impedance is given by $\bar{I}_{B,+} = (\bar{E}_{eq} - \bar{V}_{inter})/Z_{eq}$. The load voltage can obtained similarly as before, using Ohm's law:

$$\bar{V}_{load} = \bar{V}_{inter} - \bar{I}_{B,+}Z_{B,+} \tag{E.8}$$

Concerning the negative-sequence voltage, the same principle can be used. In this case, the only difference is that the EMF $\bar{E}_M$ is equal to zero.
At the end, the three voltages are obtained using the transformation matrix $\mathbf{T}$.

Appendix F

AVR Controller

The basic controller of the machine is implemented in a micro-processor. Therefore, it is discreet and it has to be transformed to be modelled in ERACS. The micro-controller has a period of $500\mu s$. The basic diagram of the controller in the z-domain is given in F.1. The values of the parameters are given in table F.1. The principle is the following:

1. The controller computes the square of the three-phase line-to-line voltage (400V). It is done using the sum of the three instantaneous line voltages squared. Then, it is multiplied by a constant.
2. A filter is applied to eliminate the quick variation (noise).
3. The set-point voltage is multiplied by a given constant and squared to obtain the same scale as the voltage to compare to.
4. The error is computed. The one is limited at $[-\Delta U^2_{max}, \Delta U^2_{max}]$.
5. A PI controller is used. The second value is not in volt due to the change of scale. The output of the controller is a value given to a PWM. $v_{f,max}$ corresponds to 100% and 0 to 0% of duty cycle.
6. A power module is used to convert the value of the PWM to the field voltage. This conversion is a simple proportional conversion. The maximal field voltage is equal to 44V (corresponding to 100% of the PWM).

In the controller used, all the voltages are in volt. The inputs $v_a(t)$, $v_b(t)$ and $v_c(t)$ denotes the line voltages and U_0 denotes the phase voltage set-point. The exciter transfer function is not represented here. It will be added to the final block diagram in the s-domain (figure 4.2).
The transformation in the time domain is done using the "bi-linear transformation". This one is the most convenient technique and is widely used in practice. it consists in replacing z in the expression of the discrete transfer function by:

$$z = \frac{1 + sT/2}{1 - sT/2} \tag{F.1}$$

The derivation of this formula is out of the scope of this study. In this case, it is applied respectively to the filter and the PI. After computation, it gives:

SC	ΔU^2_{max}	K_{pz}	K_{iz}	CR	$v_{f,min}$ [V]	$v_{f,max}$ [V]
0.36345	2907	7,32422	0.00149	0.0022	0	44

Table F.1
Parameters of the discrete controller

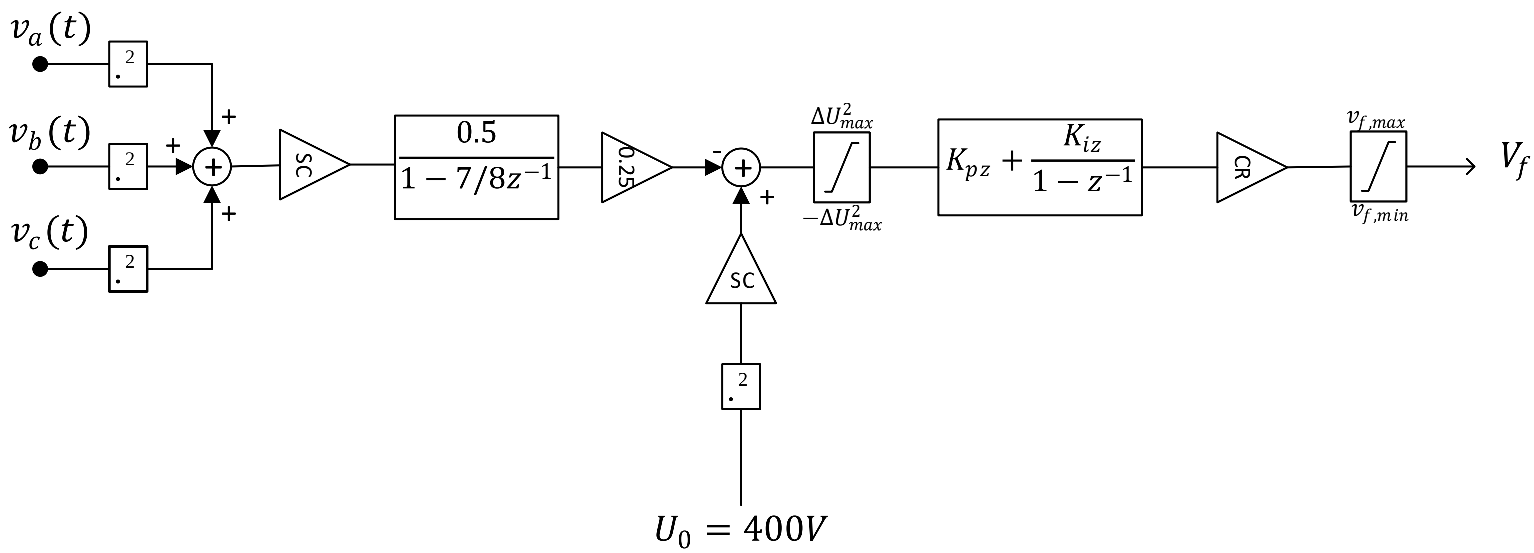

Figure F.1
Discrete controller of the AVR

$$H_f(s) = \frac{1 + sT/2}{1 + 15sT/2} \tag{F.2}$$

$$H_{PID}(s) = K_{p,s} + \frac{K_{i,s}}{s} \tag{F.3}$$

One can remark that both transfer functions have changed. Indeed, The filter has gained a zero. However, this one is very small and does not influence much.

The new parameters are given in the table 4.2. The block diagram is the same as the discrete controller except for the two transfer functions that are replaced using equations F.2 and F.3. The block diagram could have been simplified furthermore, by putting all the gains together,... but it is kept as that. This is done to keep a controller close to the real discrete controller. Then, the intermediate variable of this one can be computed and can be compared to the real one.

Appendix G

Real constant power loads

As explained, another model needs to be found for the constant power loads during transient. This can be done in ERACS using what is called a "controlled shunt". This allows to work with shunts that are controlled depending on inputs. Then, a controller adjusts the admittance of this load in time.
In this case, the controlled shunt is expected to consume a constant active and reactive power. This one is function of the voltage and of the admittance as shown by the formula (for the apparent power):

$$S = Y^*|V|^2 = P + jQ \tag{G.1}$$

This equation can be inverted and real and imaginary parts can be extracted in order to obtain the required susceptance and conductance to apply to consume the required active and reactive power. It gives:

$$G = \frac{P_0}{V^2} \tag{G.2}$$

$$B = \frac{-Q_0}{V^2} \tag{G.3}$$

In these equations, V is the norm of the load terminal voltage and P_0 and Q_0 are the targeted active and reactive power.
In ERACS, the controlled is designed in the same way as the AVR. The schematic is shown in figure G.1.

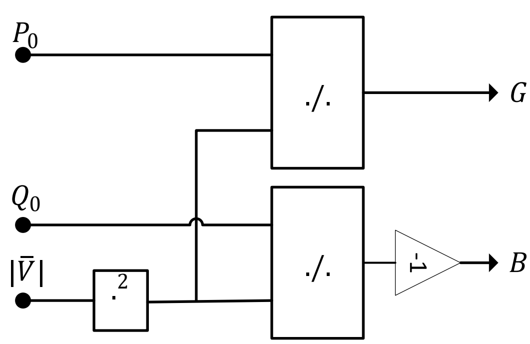

Figure G.1
Schematic of the controlled shunt used to model a constant power load

Bibliography

[1] TI0001: Harmonics Mitigation. Technical report, EURO-DIESEL SA. rev02.

[2] TI0007: Voltage Control and Power Factor. Technical report, EURO-DIESEL SA. rev00.

[3] Ieee recommended practice for monitoring electric power quality. IEEE Std 1159-2009 (Revision of IEEE Std 1159-1995), pages c1–81, June 2009.

[4] D. Aguilar, A. Rolan, G. Vazquez, F. Corcoles, and P. Rodriguez. Symmetrical and unsymmetrical voltage sag effects on the three-phase synchronous machine stability. In 2009 13th European Conference on Power Electronics and Applications, pages 1–7, Sep. 2009.

[5] Jaber Alipoor, Aref Doroudi, and Seyed Hossein Hosseinian. Identification of the critical characteristics of different types of voltage sags for synchronous machine torque oscillations. Electric Power Components and Systems, 42(13):1347–1355, 2014.

[6] Azam Bagheri, Math HJ Bollen, and Irene YH Gu. Improved characterization of multi-stage voltage dips based on the space phasor model. Electric Power Systems Research, 154:319–328, 2018.

[7] M. H. J. Bollen and E. Styvaktakis. Tutorial on voltage sag analysis. In Ninth International Conference on Harmonics and Quality of Power. Proceedings (Cat. No.00EX441), volume 1, pages 193–194 vol.1, Oct 2000.

[8] Math Bollen. Voltage sags in three-phase systems. Power Engineering Review, IEEE, 21:8 – 15, 10 2001.

[9] Math HJ Bollen. Voltage recovery after unbalanced and balanced voltage dips in three-phase systems. IEEE Transactions on Power Delivery, 18(4):1376–1381, 2003.

[10] Math HJ Bollen and E Styvaktakis. Characterization of three-phase unbalanced dips (as easy as one-two-three?). In Harmonics and Quality of Power, 2000. Proceedings. Ninth International Conference on, volume 1, pages 81–86. IEEE, 2000.

[11] Math HJ Bollen and LD Zhang. Different methods for classification of three-phase unbalanced voltage dips due to faults. Electric power systems research, 66(1):59–69, 2003.

[12] Herivelto Bronzeado, S O. Pinto, Per Jonsson, Jose Oliveira, and Marcelo Lynce Chaves. Controlled energizing of three-phase transformer: Analysis of test results. 01 2007.

[13] Joaquín Caicedo, Felipe Navarro, Edwin Rivas, and Francisco Santamaría. The state of the art and new developments in voltage sag immunity. Ingeniería e investigación, 31:81–87, 2011.

[14] Fredrik Carlsson. Behavior of synchronous machines subjected to transient overvoltages. In Harmonics and Quality of Power, 2002. 10th International Conference on, volume 2, pages 724–729. IEEE, 2002.

[15] RM Gnativ and JV Milanovic. Advanced characterization of voltage sags and assessment of equipment sensitivity. International Journal of Power and Energy Systems, 29(1), 2009.

[16] A Honrubia-Escribano, E Gómez-Lázaro, A Molina-García, and JA Fuentes. Influence of voltage dips on industrial equipment: Analysis and assessment. International Journal of Electrical Power & Energy Systems, 41(1):87–95, 2012.

[17] Electromagnetic compatibility (EMC) – Part 4-11: Testing and measurement techniques – Voltage dips, short interruptions and voltage variations immunity tests . Standard, International Electrotechnical Commission, Geneva, CH, March 2004.

[18] Vanya Ignatova, Pierre Granjon, and Seddik Bacha. Space vector method for voltage dips and swells analysis. IEEE Transactions on Power Delivery, 24(4):2054–2061, 2009.

[19] Vanya Ignatova, Pierre Granjon, Seddik Bacha, and Frederic Dumas. Classification and characterization of three phase voltage dips by space vector methodology. In Future Power Systems, 2005 International Conference on, pages 6–pp. IEEE, 2005.

[20] RINA Consulting Ltd. ERACS : Technical manual, 10 edition, Jan. 2018.

[21] M. F. McGranaghan, D. R. Mueller, and M. J. Samotyj. Voltage sags in industrial systems. IEEE Transactions on Industry Applications, 29(2):397–403, March 1993.

[22] Wang Ping M.H.J. Bollen and N. Jenkins. Analysis and consequences of the phase jump associated with a voltage sag. In 12th Power systems Computation Conference, pages 316–322, Aug 1996.

[23] Rahul Omar and Nasrudin Abd Rahim. Modeling and simulation for voltage sags/swells mitigation using dynamic voltage restorer (dvr). pages 1 – 5, 01 2009.

[24] Nicolás Louzán Pérez and Manuel Pérez Donsión. Technical methods for the prevention and correction of voltage sags and short interruptions inside the industrial plants and in the distribution networks. In International Conference on Renewable Energy and Power Quality (ICREPQ'03), 2003.

[25] M. S. Sezgin, Ö. Polat, K. Yumak, Ö. Gul, and N. E. Atilla. Simulation of voltage sag events in distribution networks and utility-side mitigation methods. In 2017 10th International Conference on Electrical and Electronics Engineering (ELECO), pages 211–215, Nov 2017.

[26] Ramesh Sinha, Ritesh Kumar, Ramesh Lekshmana, and M Venmathi. analysis of voltage sag with different dg for various faulty condition. IJJCET,IJCNS, 1:189–195, 01 2010.

[27] Van Cutsem T.

[28] Van Cutsem T. Introduction to balanced fault analysis. University Lecture, 2017.

[29] Van Cutsem T. The phasor approximation explained with an example. University Lecture, 2017.

[30] Van Cutsem T. Transient stability analysis and improvement. University Lecture, 2018.

[31] Rodney HG Tan and Vigna K Ramachandaramurthy. A comprehensive modeling and simulation of power quality disturbances using matlab/simulink. In Power Quality Issues in Distributed Generation. InTech, 2015.

[32] D. V. Tien, R. Gono, and Z. Leonowicz. Analysis and simulation of causes of voltage sags using emtp. In 2017 IEEE International Conference on Environment and Electrical Engineering and 2017 IEEE Industrial and Commercial Power Systems Europe (EEEIC / I CPS Europe), pages 1–5, June 2017.

[33] Dirk Van Hertem, Marcel Didden, Johan Driesen, and Ronnie Belmans. Choosing the correct mitigation method against voltage dips and interruptions: A customer-based approach. Power Delivery, IEEE Transactions on, 22:331 – 339, 02 2007.

[34] Lidong Zhan and Math HJ Bollen. Characteristic of voltage dips (sags) in power systems. IEEE transactions on power Delivery, 15(2):827–832, 2000.